UNIVERSITY OF PIRAEUS
DEPARTMENT OF MARITIME STUDIES

HELLENIC NAVAL ACADEMY
DEPARTMENT OF NAVAL SCIENCES

INTERINSTITUTIONAL POSTGRADUATE PROGRAM IN MARINE SCIENCE AND TECHNOLOGY MANAGEMENT

Thesis

REVIEW OF TECHNOLOGIES FOR THE USE OF NATURAL GAS IN DUAL FUEL MARINE ENGINES AND TECHNO ECONOMIC STUDY OF MARINE DIESEL ENGINES RETROFIT TO DUAL FUEL ENGINES

Sotirios Kostopoulos
MNSND 23061
Ioannis Chronopoulos
MNSND 23056

Supervisor: Professor
Mr. Zannis Theodoros, Associate Professor HNA

Piraeus
March 2026

DECLARATION OF AUTHENTICITY

The person who is conducting the Thesis bears the entire responsibility of determining the fair use of the material, which is defined based on the following factors: the purpose and character of the use (commercial, non-profit or educational), the nature of the material used (part of the text, tables, figures, images, or maps), the percentage and significance of section, which it uses in relation to the entire copyrighted text, and the possible consequences of this use on the market or the overall value of the copyright text

«This Diploma Thesis was unanimously approved by the three-member Examination Committee appointed by the Board of Directors of the MSc in accordance with the Regulations of the MSc 'Management in Maritime Science and Technology'.
The members of the Committee were:

- MEMBER A': Mr. Zannis Theodoros, Associate Professor HNA
- MEMBER B': Mr. Pariotis Efthimios, Associate Professor HNA
- MEMBER C': Mr. Katsanis Ioannis, Associate Professor HNA

The approval of the thesis by the Department of Maritime Studies of the University of Piraeus does not imply acceptance of the author's views. »

Abstract

In recent years, the International Maritime Organization (IMO) has introduced stringent regulations to reduce gaseous emissions from marine diesel engines, targeting sulfur oxides (SOx), nitrogen oxides (NOx), and carbon dioxide (CO_2). Compliance measures include limits on fuel sulfur content, NOx emission standards, and energy efficiency frameworks such as the Energy Efficiency Design Index (EEDI) and Ship Energy Efficiency Management Plan (SEEMP). Within this regulatory context, natural gas has emerged as a promising alternative marine fuel.

This thesis evaluates the technological, environmental, and economic feasibility of using natural gas in four-stroke marine compression ignition engines operating in dual-fuel mode. Natural gas combustion enables significant reductions in NOx, CO_2, and particulate matter emissions, while effectively eliminating SOx emissions. However, challenges such as increased unburned hydrocarbon emissions and methane slip—due to methane's high global warming potential—must be considered.

The study combines thermodynamic analysis, experimental data from the literature, and a techno-economic assessment of retrofitting existing vessels. Results indicate that dual-fuel operation is a technically viable and environmentally beneficial solution, although its economic feasibility is highly dependent on fuel price dynamics and retrofit costs.

Keywords: Diesel; Natural gas; Performance characteristics ; Pollutant emissions

Table of Contents

1 Introduction

1.1 General information on diesel engines

The Diesel engine is an internal combustion engine that converts the thermal power released from the combustion of fuel oil into effective mechanical power, while it is also the most efficient thermal engine, providing propulsion for many ground and marine transport vehicles, generating electrical power and contributing to many agricultural, construction and industrial activities [1-3].

The Diesel engine has low maintenance requirements, has a long service life and has the lowest specific fuel consumption compared to any other marine engine. The latter characteristic is the main criterion for the selection of diesel engines as a means of propulsion for transport and power generation. At the same time, relative older diesel engines had low power concentration, i.e. they showed low values of real power per unit of engine capacity, were noisy and had vibration problems, especially during the cold start process [4,5]. In recent years, however, very significant steps have been taken in the development of diesel engine technology. This has been helped by the application of the following techniques [4,5]:

- Electronic control of the engine
- Increased injection pressure
- Innovative injection technology (common rail injection technology with multiple pulses, common pump-injector unit)
- Improved turbocharging technology (variable geometry turbines, use of an intercooler or a charge air cooler, development of rotors for turbines with low inertia torque, improved turbine efficiency).

Nevertheless, the diesel engine continues to be a source of pollution and interest in the relative impact of diesel engine pollution on human health and the general quality of human life has been growing in recent years. Towards this aim, important technological developments are nowadays available which can dramatically reduce pollutant emissions, thus minimizing the negative impact of diesel engines on the environment. In its present form, the diesel engine has both advantages and disadvantages:

- To maintain the high-pressure values of the diesel cycle (typically 2 to 2.5 times higher than those of petrol engines of comparable power), the materials used in the construction of the various engine parts need to be more durable, which makes them more expensive.
- The lean combustion characteristics (with excess oxygen) of the naturally aspirated diesel engine cause it to produce less power per unit of cylinder volume than the Otto engine produces.
- Finally, the diffusion combustion process of the diesel engine is slower than the premixed combustion of a typical gasoline engine, limiting the operation of diesel engines to lower maximum rotational speeds [1-6].

However, these limitations are balanced by the advantages of diesel, which are:

- At full load, the diesel engine uses no more than 70% of the amount of fuel that a comparable petrol engine uses to produce the same power. For operation at part load, the advantage of this engine over that of a petrol engine is even greater. It should be mentioned that modern supercharged diesel engines achieve thermodynamic efficiencies of up to 50% [2-6].
- The higher fuel economy of the diesel engine also means lower specific CO_2 emissions compared to other means of propulsion and consequently lower greenhouse gas emissions [3-6].

Depending on the times in which a full cycle is carried out, diesel engines are divided into two-stroke (2-S) and four-stroke (4-S) engines. For four-stroke diesel engines, the operating cycle consists of the following phases [1,2]:

- Suction of atmospheric air (for naturally aspirated engines) or supercharged intake air to fill the cylinder.
- Compression of the inlet air after closing the intake valve, injection of fuel into the hot air of the combustion chamber close to the end of the compression and progressive combustion of the heterogeneous mixture.
- Expansion of the combustion-released gases and production of useful work.
- Extraction of the exhaust gases from the cylinders to the exhaust duct.

The times and the corresponding operating phases of a 4-S diesel engine are shown in Figure 1-1.

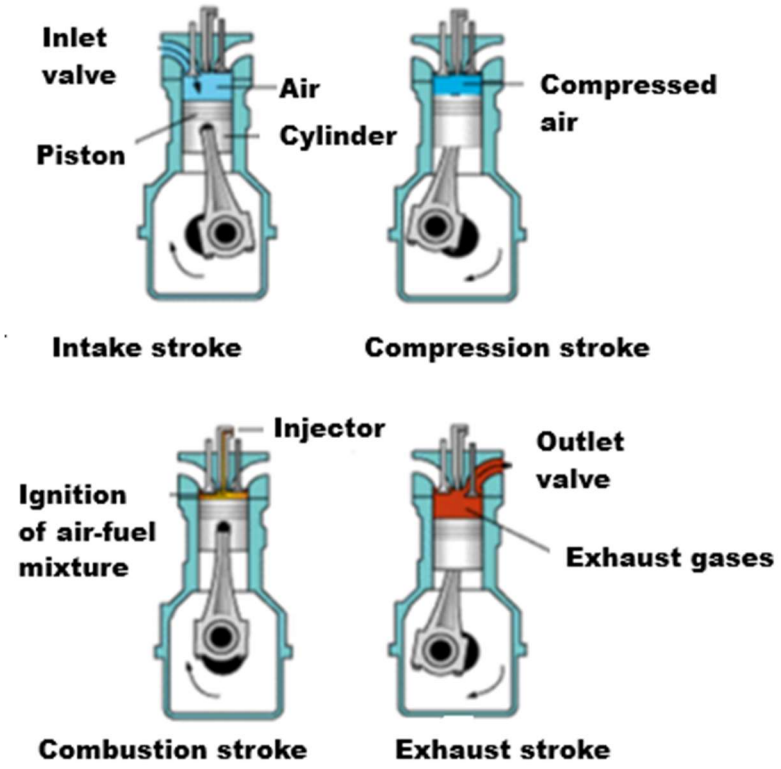

Figure 1-1. Operating times and phases of the 4-X diesel engine [7]

1.2 Basic operating characteristics of 4-S diesel engines

This paragraph discusses the basic operating characteristics of 4-S diesel engines. The definitions of the key operating parameters that characterize the efficiency and performance of a 4-stroke diesel engine are fundamental to a further deeper understanding of the variation in the corresponding variables of 4-S dual-fuel (gas - diesel) compression ignition engines.

1.2.1 Cylinder Pressure vs. Crank Angle Diagram (Indicator Diagram) – Peak Cylinder Pressure – Indicated Power – Indicated Mean Effective Pressure (imep) – Indicated Specific Fuel Consumption (isfc)

The most common measurement that can be made inside the combustion chamber during the operation of a diesel engine is to take the Cylinder Pressure profile diagram. The dynamometer diagram provides the instant value of cylinder pressure versus crank angle (cylinder pressure diagram p - crank angle φ) or versus instant piston displacement (cylinder pressure p - instant piston displacement within the cylinder x). Observation of the cylinder pressure profile provides immediately useful information on the stages of compression, ignition, combustion and expansion of the working

medium [1,2,8]. Figure 1-2 shows a typical cylinder pressure profile of the closed cycle of a 4-S diesel engine in which the compression phase, the start of fuel injection, the period of ignition delay, the period of cylinder pressure rise to its maximum value (maximum combustion pressure) and the phase of cylinder pressure decrease in the expansion phase are depicted. In particular, it should be noted that the maximum combustion pressure, which usually occurs after the Top Dead Centre (TDC), is a particularly useful parameter that characterizes the operation of a diesel engine because it is for this value that the engine manufacturer usually gives a maximum critical value, which the engine must not be allowed to exceed during operation in order to avoid engine problems caused by excessive mechanical and thermal stress.

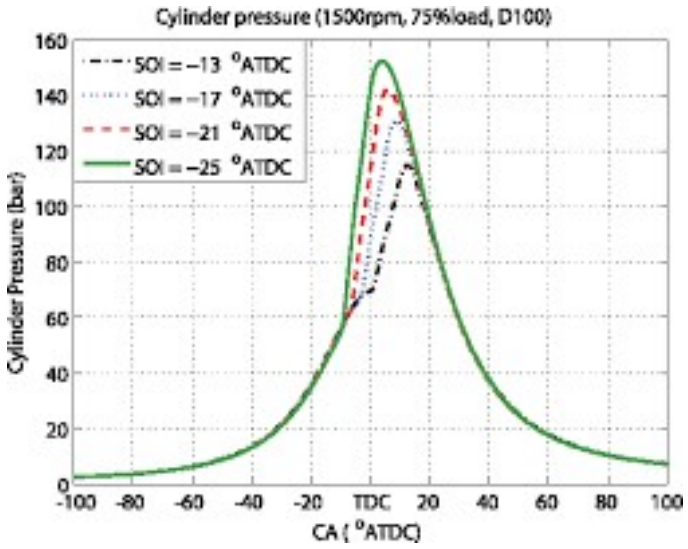

Figure 1-2. Typical cylinder pressure versus crank angle power diagram of a 4-S diesel engine [9]

There are two basic techniques for measuring cylinder pressure: The use of a mechanical indicator and the use of a piezoelectric transducer (electronic indicator). Due to the mechanical inertia of the moving parts of this system, the use of a mechanical indicator is only recommended for measuring cylinder pressure in slow-speed engines and is not recommended for use in high-speed and medium – speed diesel engines due to errors in the recording of pressure variations within the cylinder. Therefore, for the measurement of cylinder pressure in four-stroke high-speed or medium-speed diesel engines, piezoelectric transducers are used almost exclusively, each of which is located either in the pressure-indication valve located at the head of each cylinder or, if the

former is not possible, in the bleed valve of each cylinder. The principle of operation of the piezoelectric transducer is based on the recording of the instantaneous variation of the pressure inside the cylinder by the piezoelectric transducer and its appropriate conversion into a potential difference [1,3,8-10].

Each piezoelectric transducer has a constant for converting voltage to pressure (constant expressed in bar/Volt). Because the output signal of the piezo crystal is usually weak, the use of an amplifier is required for amplifying the signal. The signal of the piezoelectric transducer after amplification can be recorded on a PC via an Analog to Digital Converter (ADC) card. The advantage of the electronic indicator is the absence of mechanical inertia which allows measurement to be taken on high-speed engines [1,3,8-10].

The disadvantage of the electronic indicator is the difficulty in determining the TDC and the BDC due to the use of the crank angle as a variable. This is corrected by using a magnetic sensor of the TDC (by creating a suitable notch in the flywheel of the engine). Figure 1-3 shows the installation of a magnetic pick-up sensor (magnetic pick-up) to record the position of the TDC in the 4-S diesel engine flywheel. The TDC sensor is activated whenever the plastic "blade", which is located at the zero-degree position of the flywheel, is aligned with the sensor thereby generating an electrical signal after a change in the magnetic field is induced. This signal is fed to the amplifier for amplification and simultaneously fed to the ADC recording system where it is recorded [1,3,8-10]. At this point it should be mentioned that usually in diesel engines cylinder pressure measurement is taken in consecutive operating cycles (200 - 300 consecutive operating cycles) so that the sample size is statistically satisfactory with a corresponding effect on the statistical reliability of the measurement.

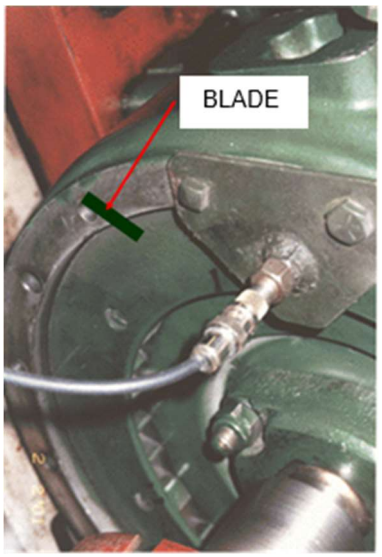

Figure 1-3. Arrangement for recording the position of the TDC in the flywheel of a 4-S diesel engine [3,10]

Having at our availability, after appropriate processing of all received operating cycles, the "average" per cycle cylinder pressure profile, we can start the process of calculating the basic operating parameters that characterize the performance of a diesel engine. In particular, the calculations start with the determination of the indicated work and correspondingly the indicated power. Given the principles of thermodynamics according to which the calculation of the net power produced by the expansion of the combustion gases on the piston of a cylinder (indicated power) is based on the calculation of the corresponding volumetric displacement power or, in other words, on the area measurement of the pressure - volume diagram. It is therefore necessary to convert the cylinder pressure diagram p - crank angle φ into a cylinder pressure diagram p - instantaneous cylinder volume V. This conversion is based on the calculation of the instantaneous cylinder volume as a function of the crank angle φ and the basic geometric characteristics of the cylinder (cylinder diameter, piston stroke, crank radius and dead volume). The relation for calculating the instantaneous piston displacement x(φ) and through it the instantaneous cylinder volume V(φ) is as follows [1,2,8-10]:

Instantaneous piston displacement from the TDC:

$$x(\varphi) = r \cdot (1 - \cos\varphi) + \ell_{rod} \cdot \left[1 - \sqrt{(1 - \lambda^2 \cdot \sin^2\varphi)}\right] \quad (m) \quad (1.1)$$

Instantaneous cylinder volume:

$$V(\varphi) = V_c + \frac{\pi D^2}{4} x(\varphi) \quad (m^3) \tag{1.2}$$

Figure 1-4 schematically illustrates the conversion of the cylinder pressure - crank angle dynamometer diagram into a cylinder pressure - instantaneous cylinder volume diagram.

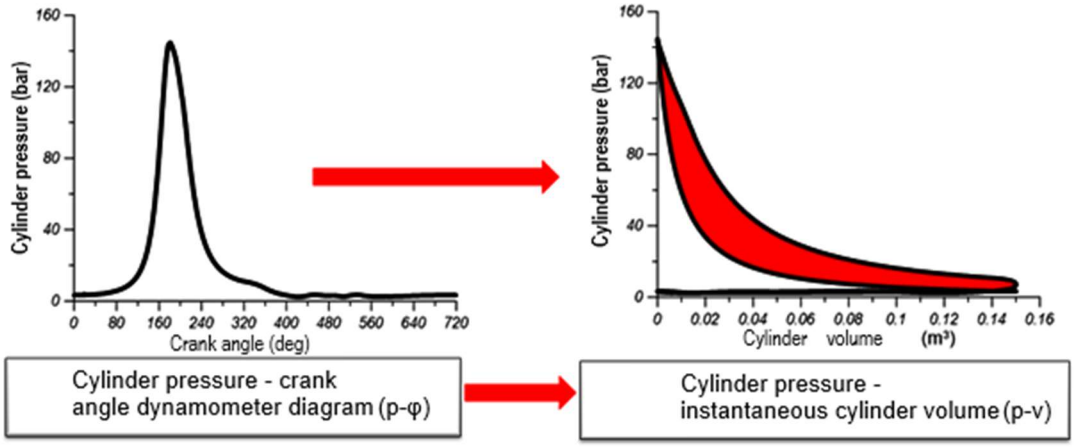

Having thus calculated the cylinder pressure - instantaneous cylinder volume diagram, we can calculate the corresponding integral to determine the indicated work and through this the indicated power of each cylinder of a piston engine:

Indicated work:

$$W_i(Joule) = \int_{\varphi=1}^{720\ \eta\ 360} p_{\kappa\upsilon\lambda.}\, dV \tag{1.3}$$

In the above calculation formula, the integration is done as 720 degrees of crank angle for a 4-S engine or 360 degrees of crank angle for a 2-S engine.

Indicated power:

$$P_i(W) = \frac{W_i(J) \cdot n(RPM)}{30k\,(k = 4\ \gamma\iota\alpha\ 4\text{-}X\ \eta\ k{=}2\ \gamma\iota\alpha\ 2\text{-}X)} \tag{1.4}$$

After the indicated work and indicated power, an important operating parameter that characterizes the engine load and constitutes a parameter for quantifying the power concentration is the Average Indicated Pressure, which is usually calculated in bar by means of the following equation:

$$imep(bar) = \left[\frac{\text{Indicated work } W_i(J)}{\text{Engine capacity } (m^3)} \right] \times 10^{-5} \quad \acute{\eta}$$

$$imep(bar) = \left[\frac{\text{Indicated power } P_i(W)}{\text{Engine capacity } (m^3)\, x \dfrac{n(\text{rpm})}{120(4-X)\, \acute{\eta}\, 60(2-X)}} \right] x10^{-5}$$

(1.5)

The average indicated pressure is a measure of the power concentration of a piston engine since it indicates how much useful power can be produced by the expansion of combustion gases on the pistons of an engine per unit volume (engine size). Furthermore, the indicated mean effective pressure is a measure of the cylinder load of an engine since it is intrinsically related to the variation of the cylinder pressure power curve which changes substantially when there is a change in the load of a cylinder of a piston engine [1,2,8,9].

A performance parameter may then be defined that quantifies the rate of conversion of the thermal energy released from the combustion of the fuel within a piston engine into useful work (indicated work). This performance measure of a piston engine is called the indicated efficiency and is defined as follows [1,2,8,9]:

$$\eta_i = \frac{\text{Indicated Work} \quad W_i(J)}{\text{Fuel Heating Power} \quad Q_B(J)} = \frac{W_i(J)}{m_B LHV} \Leftrightarrow$$
$$\eta_i = \frac{\text{Indicated Power} \quad P_i(W)}{\text{Fuel Heating Power} \quad \dot{Q}_B(W)} = \frac{P_i(W)}{\dot{m}_B LHV}$$

(1.6)

where mB is the fuel consumption in kg per cycle, is the fuel consumption in kg/sec and LHV is the lower heating value of the fuel. Finally, instead of the indicated efficiency, an alternative efficiency parameter can be defined, which quantifies the amount of fuel that must be burned in a piston engine to produce one kWh of useful energy from the exhaust gas expulsion in the engine pistons. This quantity is the Indicated Specific Fuel Consumption (ISFC) and is defined as follows [1,2,8,9]:

$$isfc\left(gr/kWh\right) = \frac{\dot{m}_B\left(kg/sec\right)\cdot 1000\left(gr/kg\right)\cdot 3600\left(sec/h\right)}{P_i\left(kW\right)}$$

(1.7)

1.2.2 Brake Power – Brake Mean Effective Pressure – Brake thermal efficiency - Brake specific fuel consumption

Unfortunately, not all of the work generated by the exhaust gas expansion on the pistons of an internal combustion engine is 100% transferred to the engine crankshaft because of mechanical losses. The mechanical losses of an internal combustion engine consist of two main parts: Frictional losses in the mechanical parts of the engine that cooperate with each other during engine operation, e.g. friction between piston rings and cylinder liners, and the mechanical power losses due to the operation of the engine's auxiliary devices (fuel pump, coolant pump and lubricating oil pump), which receive motion from the crankshaft (dependent components). Therefore, the Brake - as it is called – Work $\mathbf{W_e}$ that "reaches" the crankshaft of a piston engine will be equal to the Indicated Work $\mathbf{W_i}$ produced in the engine pistons minus the Work of Mechanical Losses $\mathbf{W_r}$ [1,2,8,9]:

$$W_e = W_i - W_r \tag{1.8}$$

The Brake Power $\mathbf{P_e}$ delivered to the crankshaft by an engine with z cylinders when operating at rotational speed n(RPM) will be:

$$P_e(W) = z(\text{ cyl }) \cdot W_e\left(\frac{J}{\text{cycle . cyl}}\right) \cdot \frac{n(RPM)}{30 \cdot k(=2 \text{ for 2-S or } =4 \text{ for 4-S })}$$

(1.9)

By multiplying the actual useful work of an ICE to its total capacity or its brake power to its theoretical volumetric flow rate, the Brake Mean Effective Pressure - bmep is obtained:

$$bmep\left(\frac{Nt}{m^2}\right) = \overline{p}_e\left(\frac{Nt}{m^2}\right) = \frac{W_e(J)}{V_H\left(m^3\right)} = \frac{W_i(J) - W_r(J)}{V_H\left(m^3\right)} \Leftrightarrow$$

$$bmep\left(\frac{Nt}{m^2}\right) = \frac{P_e(W)}{V_H\left(m^3\right)\frac{n(RPM)}{30k}} = \frac{P_i - P_r}{V_H\left(m^3\right)\frac{n(RPM)}{30k}} \Leftrightarrow$$

$$bmep\left(\frac{Nt}{m^2}\right) = imep\left(\frac{Nt}{m^2}\right) - mmep\left(\frac{Nt}{m^2}\right) = \overline{p}_i\left(\frac{Nt}{m^2}\right) - \overline{p}_r\left(\frac{Nt}{m^2}\right)$$

(1.10)

The bmep is one of the most commonly used engine performance parameters used to quantify the power concentration of an internal combustion engine because it expresses the actual work reaching the crankshaft of an engine per unit volume (engine size) [1,2,8-10].

The two basic quantities that characterize the actual performance of a piston engine are the Brake Thermal Efficiency - BTE $\mathbf{n_e}$ and the Brake Specific Fuel Consumption (BSFC), which are defined as follows:

$$\eta_e = \frac{\text{Brake Work} \quad W_e(J)}{\text{Fuel Thermal Energy} \quad Q_B(J)} = \frac{\text{Brake Power} \quad P_e(W)}{\text{Fuel Heating Power} \quad \dot{Q}_B(W)} \Leftrightarrow$$

$$\eta_e = \frac{W_e}{W_i} \cdot \frac{W_i}{W_{th}} \cdot \frac{W_{th}}{Q_B} = \eta_M \cdot \eta_g \cdot \eta_{th} = \eta_M \cdot \eta_i$$

(1.11)

where n_M is the mechanical efficiency of the engine, n_i is the indicated engine efficiency and n_g is the ratio of the indicated work with respect to work of the corresponding ideal cycle.

$$bsfc\left(gr/kWh\right)=\frac{\dot{m}_B\left(kg/sec\right)\cdot 1000\left(gr/kg\right)\cdot 3600\left(sec/h\right)}{P_e\left(kW\right)}$$

(1.12)

The brake specific fuel consumption BSFC is related to the brake thermal efficiency through the following relationship:

$$bsfc\left(gr/kWh\right)=\frac{3.6x10^6}{\eta_e\cdot LHV\left(kJ/kg\right)} \qquad (1.13)$$

1.3 Combustion mechanism in diesel engines

1.3.1 General combustion principles

The term combustion is applied to a process of mass and energy exchange in which the chemical energy of the fuel bonds is converted into thermal energy. Combustion is a rapid exothermic chemical reaction between the fuel and the oxygen in the air (oxidation), which results in the release of thermal energy and an increase in pressure and temperature [1-3,7-10]. The main objective in piston internal combustion engines is to achieve perfect combustion with the ultimate goal of maximizing the heat released and limiting the emissions of pollutants. Combustion generally depends on the developing temperatures, turbulence levels and available time [1,7,8]. The stoichiometric combustion of a hydrocarbon fuel (C_nH_m) with oxygen is given by the following equation:

$$C_nH_m+\left(n+\frac{m}{4}\right)O_2+3.76\left(n+\frac{m}{4}\right)N_2\rightarrow nCO_2+\frac{m}{2}H_2O+3.76\left(n+\frac{m}{4}\right)N_2$$

(1.14)

In reality, however, perfect combustion requires a much larger mass of air than the mass of fuel. The excess air relative to the fuel mass is defined by the air equivalence ratio given by the following relationship:

$$\lambda_a=\frac{m_{air}}{AF_{st}\cdot m_f} \qquad (1.15)$$

where m_{air} s the mass of air involved in combustion, m_f is the mass of air involved in combustion, AF_{st} is the stoichiometric air requirement for complete combustion of one kg of fuel. For standard liquid fuels used in internal combustion engines the stoichiometric air requirement is about 15 times the mass of the fuel. It should also be noted that diesel engines operate with excess air (air equivalence ratio values greater than unity) in order to limit smoke emissions [1,2,8-10].

1.3.2 Description of the stages of combustion in diesel engines

Combustion inside the cylinder of a diesel engine takes place in three characteristic stages in which complex alternations of chemical and physical processes take place, the separation of which depends on the design and operation of the engine. These three stages can be distinguished in the following typical diagram of the heat release rate of a diesel engine [2,8].

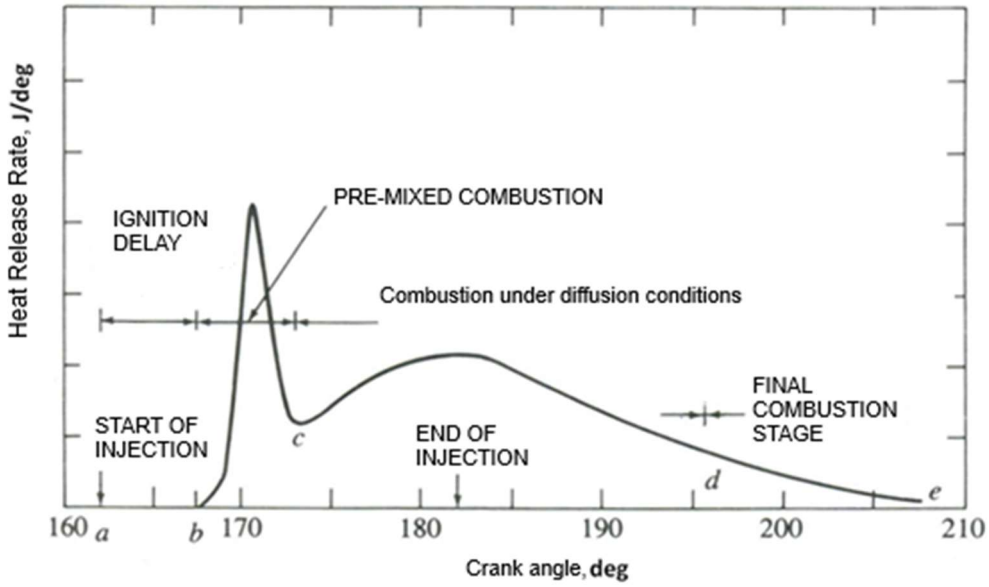

Figure 1-5. Illustration of the stages of combustion in a typical diesel engine heat release rate diagram [2]

1.3.2.1 Ignition delay

Towards the end of the compression stroke the fuel is injected into the combustion chamber in the form of droplets at high pressure and mixed with the cylinder contents. During this period of pre-mixing of the fuel with the cylinder gas mixture, combustion does not take place because any fuel requires a certain amount of time for the physical (mixing) and chemical (kinetic reactions) preparation of the mixture. This period is completed, as shown in the heat release rate diagram above

(figure 1-5), by the sudden increase in the rate of heat release due to the spontaneous combustion of the premixed cylinder mixture. This time between fuel injection and auto-ignition is called the Ignition Delay Period and is inversely proportional to the auto-ignition temperature θz which demonstrates the importance of having a high degree of compression [2,8-10].

The physical preparation of the fuel/air mixture that takes place inside the cylinder during the ignition delay period is based on the dispersion of the fuel bundle into fine droplets, the vaporization of the fuel droplets and the mixing of the fuel vapor with the hot cylinder air (figure 1-6). By applying a large pressure differential across the injector nozzle, the liquid fuel enters the combustion chamber at sufficient velocity to disperse into small droplets for vaporization and mixing with the compressed air in the cylinder [2,3,7-10]. In addition to the high-pressure differential, the size of the holes and the viscosity of the fuel play an important role in achieving the smallest possible droplets. The resulting conical fuel bundle travels into the combustion chamber at a decelerated speed because it encounters an air environment with a much lower momentum than the momentum of the injected fuel bundle (figure 1-7 and figure 1-8). Furthermore, the fuel beam is slowed down due to its mixing with the air, resulting in a swelling of the beam [2,3,8-10].

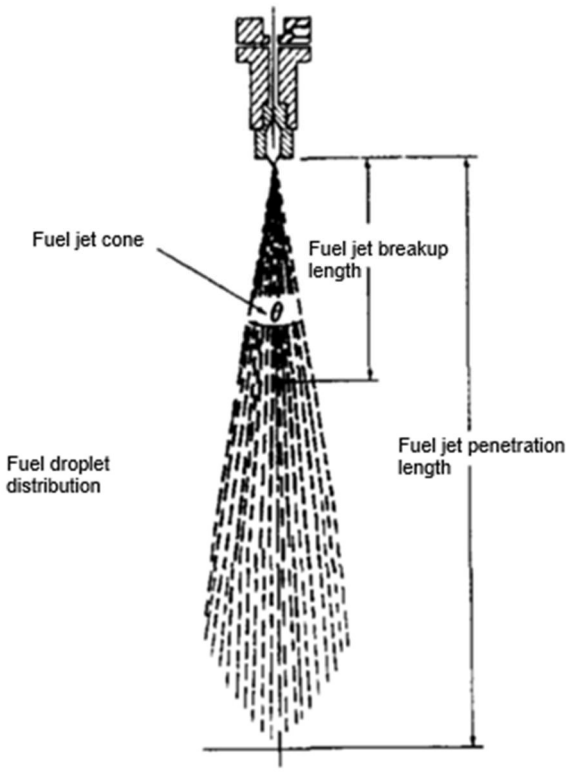

Figure 1-6. Typical conical fuel beam shape [2]

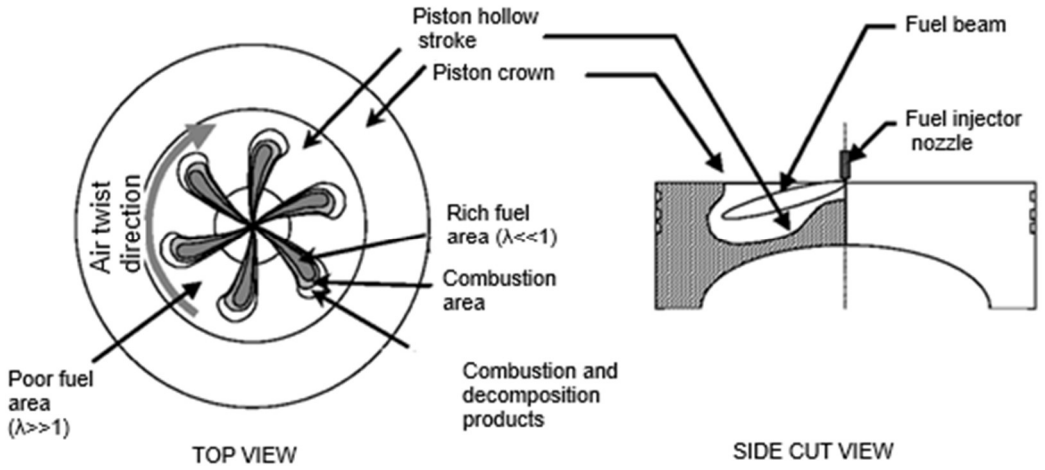

Figure 1-7. Schematic illustration of fuel injection and fuel bond formation inside the combustion chamber. It is characteristic that the fuel bundles are dragged by the twisting of the intake air which indicates the improvement of fuel-air mixing [2]

The effect of mixing the fuel jet with the air is particularly enhanced if there is a twisting of the air within the combustion chamber (see Figure 1-8 and Figure 1-9). The fuel droplets within the bundle begin to vaporize as it penetrates the combustion chamber and continues to entrain the air. This creates areas within the beam with less or more liquid or vaporized fuel (more vaporized fuel and air at the periphery and more liquid fuel at the beam axis) [2,3,8-10].

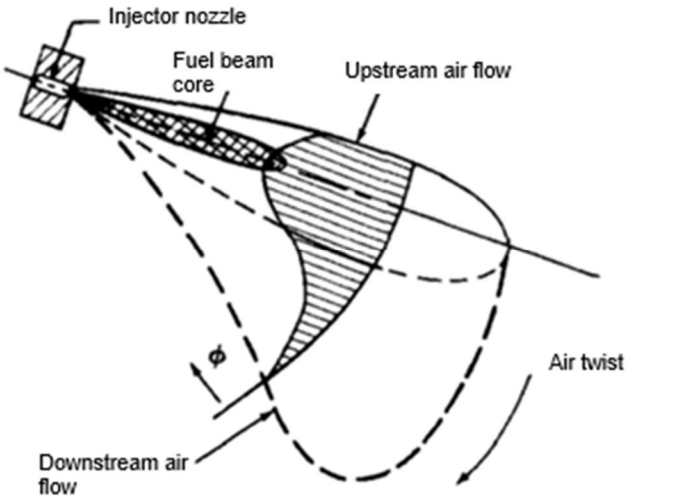

Figure 1-8. Shape of a fuel beam injected into air by twisting and distribution of the fuel equivalence ratio Φ transversely across the beam [2,8]

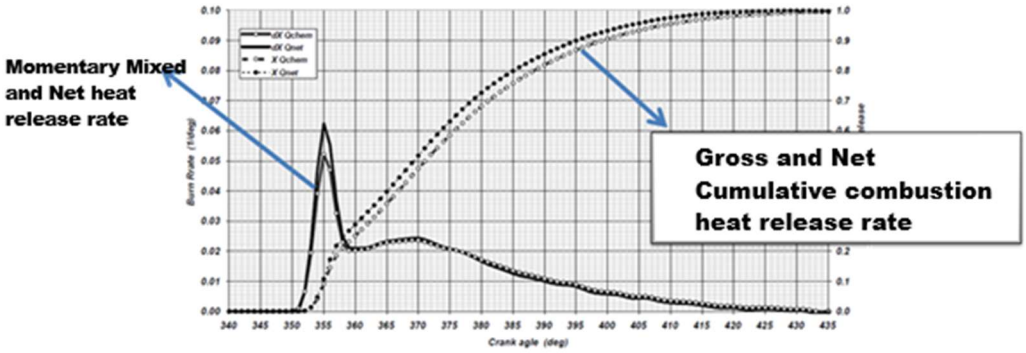

Figure 1-9. Schematic representation in a common diagram of the instantaneous gross and net heat release rate and the corresponding cumulative heat release rates. Results of processing experimental measurements from a 4-X cylinder diesel engine are shown [2,8,9].

$$P_e(W) = z(\text{ cyl }) \cdot W_e\left(\frac{J}{\text{cycle . cyl}}\right) \cdot \frac{n(RPM)}{30 \cdot k(=2 \text{ for 2-S or} =4 \text{ for 4-S})}$$

The vaporization of the fuel is more intense the smaller the droplet size, the higher the air temperature and the higher the beam speed. When the jet has penetrated to the boundary of the combustion chamber, it strikes the walls of the cylinder or piston and is forced to flow along the wall until it reacts with another jet (for multi-hole injectors), which is undesirable. We therefore conclude that we are interested in optimizing the length and speed of the beam to obtain the desired results [2,7-9].

The chemical preparation of the mixture focuses on the fuel reactions that precede the combustion reaction. After vaporization of the droplets, the heavier and generally more inert hydrocarbons are broken down into lighter and more reactive hydrocarbons, which can be auto-ignited. This chemical process depends on the composition of the fuel, the temperature and pressure of the cylinder filling, and the physical preparation mentioned earlier. It can therefore be concluded that spontaneous combustion of the fuel is achieved by the right combination of physical and chemical preparation of the fuel [2,3,7-9].

The main property of a diesel fuel is Ignition Quality, which must be high to ensure smooth combustion and is determined by the cetane number. For smooth combustion and desired results, especially for high-speed engines, fuels with a relatively high cetane number (CN>45) are needed, while slow-speed diesel engines can also run on fuel with a lower cetane number (CN>30) [2,8,9].

It is obvious that the ignition delay time must be short to avoid intense pre-mixed combustion and its negative consequences (irregular operation, emissions, noise, stress on engine components). Various factors affecting the ignition delay time are as follows [2,8]:

- The timing of fuel injection (pre-injection timing) because this determines the timing of the start of the ignition delay.
- Injection pressure which has a direct effect on the faster dispersion of the fuel into fine droplets and their faster vaporization. These effects lead to a reduction in ignition delay.
- The pressure and temperature of the intake air. For a given compression ratio, an increase in intake air pressure leads to higher values of pressure and temperature at the end of compression. Therefore, the fuel is injected into a warmer environment within the cylinder resulting in faster physical and chemical preparation of the fuel and therefore a reduction in ignition delay.
- Wall temperature.
- The twisting of the air. As already mentioned, air twisting helps to improve and speed up the physical preparation of the air-fuel mixture.
- The oxygen concentration with an inversely proportional effect on the ignition delay time.

1.3.2.2 Premixed or uncontrolled combustion

The fuel preparation period ends when the premixed cylinder mixture is spontaneously ignited due to the high pressure and temperature, which are the result of the compression of a homogeneous mixture, in a short period of time. Ignition takes place at various locations in the combustion chamber where the air-fuel mixture is within the limits of ignitability. Fuel injection continues until the desired fuel supply enters the cylinder, but this is not the cause of the sudden increase in pressure, rather it is the ignition of the ignited flames [2,8].

As the dispersion of the injected fuel, the vaporization of the droplets and the mixing of the air with the fuel continue to take place, the ignition sources expand throughout the combustion chamber area creating the conditions for combustion of the continuously forming mixture. This sudden ignition may result in shock combustion

and the generation of a pressure wave that produces a sharp sound (combustion noise). The short ignition delay time helps to avoid such negative effects [2,8].

1.3.2.3 Controlled or diffusion combustion

Immediately after premixed combustion, fuel combustion is mainly heterogeneous and controlled by diffusion (the rate of combustion is determined by the rate of fuel/air mixing). This phase is called controlled because the pressure, quantity and rate of injection, as well as the air swirl can be adjusted to achieve good air-fuel mixing. The injected fuel finds ideal conditions for combustion, which takes place with the minimum possible ignition delay. Combustion continues until the end of the expansion phase in the so-called tail section of the entire combustion period [2,8].

The individual stages of diesel engine combustion are shown in Figure 1-10 where a common diagram shows typical variations for injector needle lift, cylinder pressure and heat release rate. Also shown schematically are the various forms that the fuel takes from the moment of injection and during the combustion phases [11].

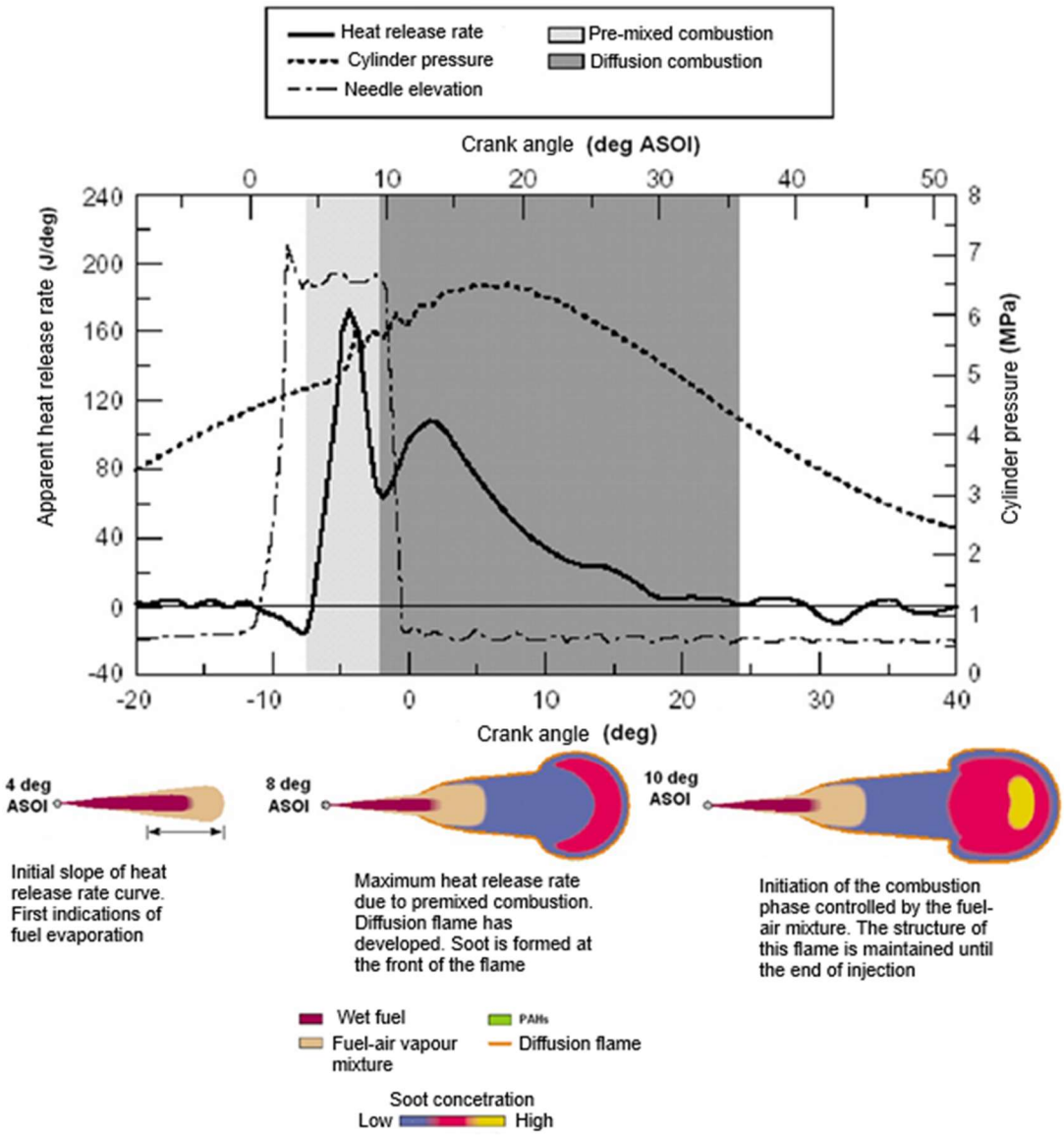

Figure 1-10. Typical variations for injector needle lift, cylinder pressure dynamometer diagram and combustion heat release rate. The stages of vaporization, ignition and combustion and soot formation in the fuel bundle are even distinguished [11]

1.3.3 Calculation of heat release rate and combustion characteristics of diesel engine

As it became clear from the preceding analysis, the in-cylinder heat release rate diagram is, after the cylinder pressure dynamometer diagram, perhaps the most important diagram for visualizing and studying the combustion taking place within a cylinder of a piston engine. It is therefore particularly useful to describe the process of processing the dynamometer diagram to calculate the instantaneous heat release rate.

Applying the 1st Law of Thermodynamics and the constitutive equation for perfect gas (assuming the gas mixture of the combustion chamber) in differential form and assuming that during the closed cycle (intake and exhaust valves closed) the thermodynamic system of the gas cylinder is a closed system with a constant total working fluid mass (negligible mass loss through the springs) gives [2,8]:

Expression of the 1st Law of Thermodynamics for a closed system in differential form:

$$\frac{dQ_B}{d\varphi} - \frac{dQ_L}{d\varphi} = p\frac{dV}{d\varphi} + mc_V\frac{dT}{d\varphi} \tag{1.16}$$

Differential expression of the gas end-gas constitutive equation:

$$d\left(pV\right) = d\left(mRT\right) \Rightarrow p\frac{dV}{d\varphi} + V\frac{dp}{d\varphi} = mR\frac{dT}{d\varphi} \tag{1.17}$$

After working out the last two equations, it follows that:

$$\frac{dQ_{net}}{d\varphi} = \frac{dQ_B}{d\varphi} - \frac{dQ_L}{d\varphi} = (1 + \frac{c_V}{R})p\frac{dV}{d\varphi} + \frac{c_V}{R}V\frac{dp}{d\varphi} \tag{1.18}$$

Where:

- $\frac{dQ_{net}}{d\varphi}$ is the **Net Heat Release inside the cylinder, which is usually expressed per degree of crank angle** (J/deg)
- $\frac{dQ_B}{d\varphi}$ is the **Gross Heat Release Rate inside the cylinder, which is usually expressed per degree of crank angle** (J/deg).
- c_v is the specific heat capacity of the cylinder gas mixture, calculated by calculating the specific heat capacity of each gas from corresponding polynomials as a function of the instantaneous cylinder gas temperature and by calculating the instantaneous composition of the cylinder gas mixture before and after combustion.
- p is the measured instantaneous value of cylinder pressure in Pa
- V is the instantaneous cylinder volume, which is calculated at each degree of crank angle
- R is the cylinder gas mixture constant, obtained by applying the law of mixtures to the gaseous components within the cylinder before and after combustion

- $\frac{dQ_L}{d\varphi}$ is Instantaneous Heat Loss Rate of the cylinder gas mixture, usually expressed per degree of crank angle (J/deg). Various empirical and semi-empirical models have been proposed in the bibliography [2,8] to calculate the heat loss rate. One of the most widely used semi-empirical models to determine the heat loss rate is Annand's model [2], which takes into account both heat transfer mechanisms (convection due to gas flow within the cylinder and radiation after the start of combustion due to the presence of a flame). According to Annand's semi-empirical model [2,8] the heat loss rate per unit cylinder surface area will be:

$$\dot{q} = a_c \frac{\lambda_g}{D} Re^{0.7}(T_g - T_w) + c_{rad}\sigma(T_g^4 - T_w^4) \qquad (1.19)$$

where:

- T_g is the average temperature of the gas inside the cylinder at each degree of crank angle. Its instantaneous value is calculated during the operating cycle with the help of the measured combustion pressure and instantaneous cylinder volume by applying the constitutive equation [2,8].
- T_w is the average temperature of the combustion chamber walls (depends on the type and application of the engine). Typical average engine combustion chamber wall temperature values [2,8]:
  - ✓ Cylinder liner: 150 to 200ºC
  - ✓ Cylinder head: 200 to 250ºC.
  - ✓ Upper piston head: 250 to 350ºC.
- σ is Stephan- Boltzmann constant (5.67×10^{-8} W/m^{2}K^4) [2,8].
- c_{rad} is the radiation coefficient [2,8]. Indicative value for Diesel engines (combustion and exhaust): 0.576.
- λ_g is the coefficient of thermal conductivity of the cylinder gas, calculated from appropriate polynomial correlations as a function of cylinder gas temperature.
- Re is the dimensionless Reynolds number, which is equal to $Dsn/30\nu_g$ where s the cylinder diameter, s is the piston stroke, n is the engine speed and $_{ng}$ is the kinematic consistency of the gas mixture [2,8].
- α_c is a constant which takes values between 0.25-0.8 [2,8]. This can be calculated so that the ratio of the total gross heat released within the cylinder in

one cycle to the lower heating value of the fuel is equal to the fuel consumption in kg/cycle, which has been recorded experimentally during cylinder pressure measurement tests:

$$m_f = \frac{Q_{B,tot}}{LHV} \tag{1.20}$$

Therefore, the instantaneous heat loss rate per degree of crank angle is calculated from the following relationship:

$$\frac{dQ_L}{d\varphi} = \frac{1}{6 \cdot n\left(RPM\right)} \cdot A_{cyl}\left(\varphi\right) \cdot \dot{q} \tag{1.21}$$

where $A_{cyl}(\varphi)$ is the heat exchange surface of the cylinder (lateral sleeve surface, piston head surface and cylinder head surface) at each degree of crank angle.

During experimental measurements carried out mainly in laboratory test beds of diesel engines, in addition to the cylinder pressure dynamometer diagram, the fuel injection pressure signal in the high-pressure pipe connecting the fuel pump to the injector is obtained via a corresponding sensor. For the fuel injection pressure signal, too, successive measurements are taken for 200 to 300 operating cycles in parallel with the corresponding measurement of the dynamometer diagram and finally - after processing - the 'average' fuel injection pressure diagram per operating cycle is obtained. Figure 1-11 shows the cylinder pressure dynamometer diagram, the measured fuel injection pressure diagram and the in-cylinder heat release rate diagram in a common diagram. Each manufacturer shall provide as information a given pressure in the fuel depression tube for which the injector needle is raised and fuel injection into the cylinder is initiated. The experimental results shown in Figure 1-11 have been obtained for a single-cylinder 4S high-speed diesel engine in which the injector needle is raised for a pressure equal to 180 bar. By going to the fuel injection pressure diagram, we can assign a specific crank angle e.g. 165 degrees crank angle to the starting pressure of fuel injection inside the cylinder. The distance of the in-cylinder fuel injection starting angle relative to the TDC (180 degrees crank angle starting from the BDC) corresponds to the so-called Dynamic Injection Timing or Start of Injection (SOI).

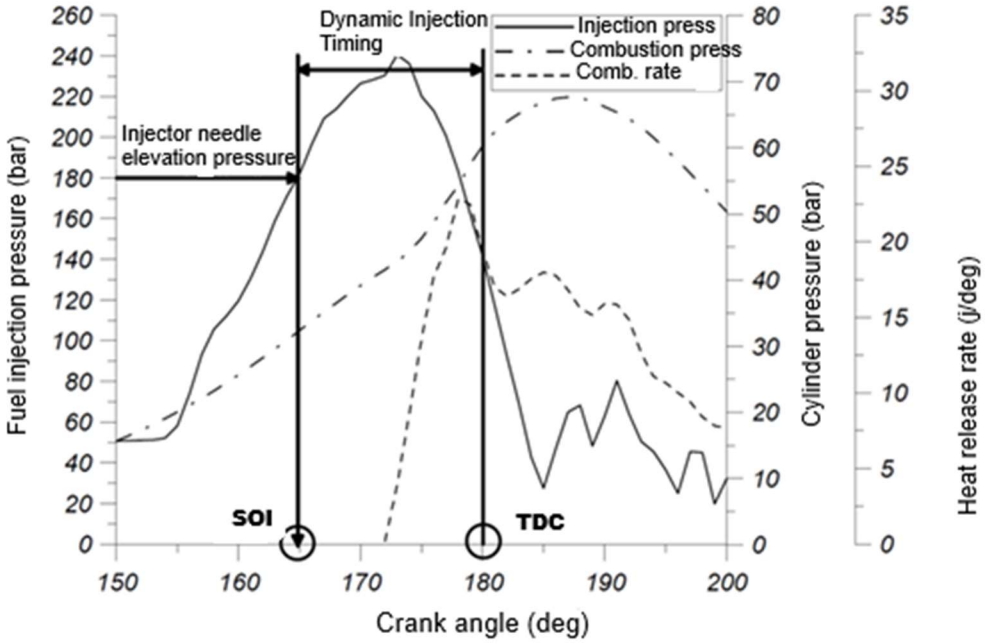

Figure 1-11. Schematic determination of fuel injection advance dynamics (in-cylinder fuel** injection **timing) by plotting cylinder pressure and fuel injection pressure as a function of crank angle on a common graph [3]

As shown in Figure 1-12, the measured cylinder pressure dynamometer diagram, the measured fuel injection pressure diagram and the net heat release rate diagram are again presented in a common diagram. Having determined the time of initiation of fuel injection into the cylinder, we can experimentally determine the ignition delay time, which corresponds to the time interval between the ignition or initiation point and the injection advance. The ignition point is determined from the net heat release rate plot and corresponds to the time, expressed in degrees of crank angle, at which the heat release rate first starts to become positive and non-zero.

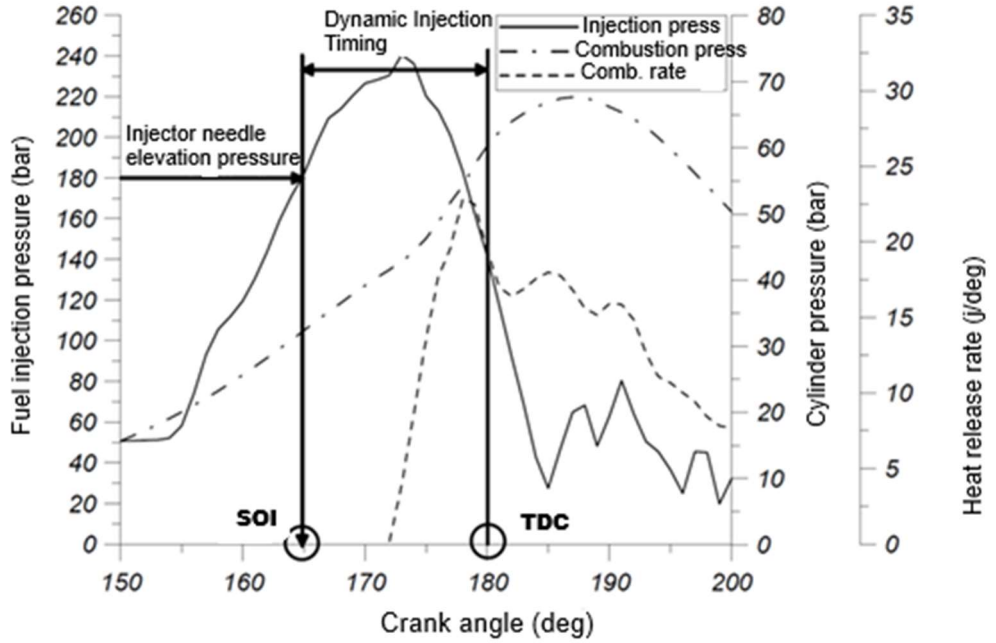

Figure 1-12. Schematic determination of ignition delay by correlation on a common graph of measured fuel injection pressure and heat release rate [3]

Finally, a particularly important characteristic of combustion in diesel engines is Combustion Duration, which expresses the time in degrees of crank angle that corresponds to the complete combustion of the fuel injected per cycle. Accurate calculation of the combustion duration during an operating cycle is not straightforward since it is difficult to determine the exact duration of combustion. This is because the heat release rate diagram shows several anomalies (fluctuations of limited range) during the expansion phase, so that the exact point at which combustion ends is not clearly defined. What is usually done is to calculate the time - in degrees of crank angle - between the start of combustion (ignition point) and the point in time at which combustion of a preselected percentage (e.g. 50% or 95%) of the amount of fuel injected per cycle has been completed. The process of calculating the burn time is greatly facilitated by plotting the **Cumulative Heat Release Rate** versus crank angle. The total amount of heat theoretically expected to be released if all the fuel injected were burned is:

$$\dot{Q}_{b,tot,th}\left(\frac{Joule}{sec}\right)=\dot{m}_f\left(\frac{kg}{sec}\right)LHV\left(\frac{Joule}{kg}\right) \qquad (1.22)$$

The cumulative amount of heat released by summing the elementary amounts of the gross heat release rate at each degree of crank angle will be:

$$Q_{b,tot,exp} = \sum_{\varphi=SOI}^{EVO} \frac{dQ_B}{d\varphi} \Delta\varphi \tag{1.23}$$

where SOI is the starting point of in-cylinder fuel injection and EVO is the time of opening of the exhaust valves after the TDC. Thus, by combining the last two relationships, the corresponding combustion duration in degrees of crank angle can be calculated for all or a predetermined percentage of the fuel injected per cycle:

$$Q_{b,tot,exp}(J) = \dot{Q}_{b,tot,th}\left(\frac{Joule}{sec}\right) \cdot \Delta t(sec) = \dot{Q}_{b,tot,th}\left(\frac{Joule}{sec}\right) \cdot \frac{\Delta\varphi_{tot}}{6 \cdot n(RPM)} \Rightarrow$$

$$\Delta\varphi_{tot} = \frac{Q_{b,tot,exp}(J) \cdot 6 \cdot n(RPM)}{\dot{Q}_{b,tot,th}\left(\frac{Joule}{sec}\right)} \tag{1.24}$$

1.4 Formation of pollutants in diesel engines

Despite its many advantages, the diesel engine is still polluting. Engine exhaust gases consist of hundreds of gaseous, semi-volatile and particulate organic compounds produced through the combustion of oil. The exact composition of exhaust gases depends on operating parameters such as rotational speed, engine load, engine type, fuel composition, ambient air temperature and relative humidity [2-6,8].

As mentioned in the analysis of the combustion mechanism in diesel engines, the distribution of the fuel within the combustion chamber, its mixing with air, ignition and combustion are phenomena that are local in nature and consequently have a significant influence on the formation of pollutants. The chemical dimensioning effect that takes place during combustion, which is strongly dependent on temperature and fuel-air ratio, is pronounced due to the heterogeneous nature of the mixture. For example, soot, which occurs for very high fuel/air mass ratios, is formed in specific local areas (bundle core) which are fuel-rich because complete mixing has not been achieved. A brief description of the main atmospheric pollutants and the contribution of the diesel engine to their formation is given below, as well as their formation inside the engine combustion chamber [2-8].

1.4.1 Nitrogen oxides (Nox)

The nitrogen oxides that are considered air pollutants are nitrous oxide (NO), nitrogen dioxide (NO_2) and nitrous oxide (N_2O). The first two of these compounds are collectively referred to as NOx, but NO is the dominant oxide of nitrogen produced by internal combustion engines [2-6,8,9]. Almost all of the NOx (94%) emitted to the atmosphere comes from anthropogenic activities. Diesel engines are responsible for 27% of the total NOx emissions released into the environment from anthropogenic activities [2-8].

Nitrogen oxides (NOx) play an important role in photochemical reaction cycles, leading to the formation of smog (photochemical smog) in the urban troposphere. Under the influence of solar radiation (ultraviolet sunlight), they participate in certain chemical reactions under the interaction of volatile organic compounds (VOCs) that result in the conversion of unburnt hydrocarbons into so-called photochemical oxidants and the production of ozone, which is also toxic to the respiratory system and causes losses in agricultural production [2-8]. With the help of ozone and atmospheric oxygen, nitrogen oxides then create a cycle of secondary pollution, which results in the formation of photochemical smog and airborne toxicants. Nitrogen oxides also lead to the depletion of stratospheric ozone, which is valuable for absorbing ultraviolet radiation, as well as to acid rain.

Nitrogen monoxide (NO) is formed in diesel engines over the entire range of the high temperature range occupied by the combustion products around the flame. The main source of formation is the oxidation of nitrogen (N_2) in the cylinder filling air. The highest rates of NO formation are observed in areas close to the stoichiometry, thus mainly during the uncontrolled combustion phase where a premixing flame is present. Nitrogen dioxide (NO_2) is formed from NO in the flame region [2-9].
Nitrogen in atmospheric air is normally an inert gas. At the combustion temperatures of the vaporized fuel, quantities of nitrogen combine with oxygen to form nitrogen oxides. For this reason, the formation of NOx depends mainly on the in-cylinder temperatures (strong exponential correlation) during combustion and on the amount of oxygen available [2-9].

We therefore conclude that the critical period of NOx formation is between the start of combustion and shortly after reaching maximum pressure. This is true because shortly afterwards (i.e. during controlled combustion), due to the penetration and

decomposition of the beam and mixing with cold air, there is a drop in temperature and a "freeze" of the chemical formation reactions [2,3,8].

Any interventions in the design or operation of the engine that cause a reduction in the maximum temperature and combustion, the partial pressures of nitrogen and oxygen resulting from the dimensioning, or the residence time of the fuel mixture at very high temperatures, may result in a reduction in NOx emissions.

The main operating parameters affecting the formation of nitrous oxides are [2,3,8]:

- The adjustment of the engine load, i.e. the adjustment of the fuel flow, with an increase in fuel flow, there is an increase in temperature in the reaction zone, one of the two parameters responsible for the formation of NOx
- The injection advance, the reduction of which helps to reduce the duration of premixed (uncontrolled) combustion, thus contributing to the reduction of NOx emissions
- The percentage of residual gas in the combustion chamber, an increase in which causes a significant reduction in NOx, mainly due to its high specific heat capacity which helps to reduce the temperature level (development of the exhaust gas recirculation technique).

1.4.2 Carbon monoxide (CO)

Carbon monoxide (CO) is mainly produced by the combustion of solid, gaseous and liquid fuels. The US Environmental Protection Agency estimates that diesel engines are responsible for about 5% of CO emissions from anthropogenic activities (mainly from gasoline engines). The toxicity of CO is due to its ability to reduce the oxygen carrying capacity of the blood and causes headaches and circulatory problems [2,3,8].

Carbon monoxide (CO) is the result of incomplete combustion of hydrocarbons (and carbon in general) and is formed mainly in the fuel-rich areas of the combustion chamber. If temperatures are high enough, carbon monoxide can react further with oxygen to form CO2. In general, CO emissions from internal combustion engines increase when the available oxygen is not sufficient for stoichiometric combustion of the mixture, so they are mainly controlled by the fuel equivalence ratio. Because diesel engines always operate with excess air, CO emissions are generally low [2,3,8].

1.4.3 Unburned hydrocarbons (HC)

All hydrocarbons in the atmosphere are considered volatile organic compounds and are not counted as pollutants as a whole, although some specific components are classified as toxic. Most hydrocarbons are not toxic at low concentrations, while some compounds are carcinogenic or suspected carcinogens (particularly benzene). Their importance arises from their involvement in ozone formation and hence photochemical cloud formation. Diesel engines are estimated to contribute only 5% of the total emissions of VOCs from anthropogenic activities [2,3,8].

Emissions of crude hydrocarbons from diesel engines are a consequence of incomplete combustion of the hydrocarbon fuel. They are mainly due to the entrapment of fuel and lubricant in the gaps between the piston and cylinder walls, which prevents sufficient mixing with the air to achieve complete combustion. Under some cold start conditions, the unburned hydrocarbons associated with the fuel are emitted as a mist of liquid unburned fuel particles ('white smoke') [2,8].

The main causes of hydrocarbon emissions, for normal operating conditions of a diesel engine, are the overmixing effect during the ignition delay and undermixing. The unburned hydrocarbons can be controlled during their formation in the combustion chamber by reducing the size and number of gaps and also reducing the ignition delay [2,8].

Overmixing is a condition in which, in certain areas of the beam, the fuel is mixed with the air stream beyond the poor flammability limit (heterogeneous air-fuel mixture), resulting in incomplete combustion of the mixture in that area. The duration of the ignition delay and the mixing rate have a direct influence on this phenomenon. Undermixing is the condition in which there is low mixing of the fuel with the air. This is mainly due to the fuel leaving the injector at a very low velocity at the end of the combustion process, but may also occur in the event of engine overload or secondary injection. Finally, the temperature of the combustion chamber walls also has a significant effect, which can lead to flame extinction or even ignition failure [2-4,7,8].

1.4.4 Soot

The high concentration of soot formed by combustion is noticeable in the form of black smoke during extraction. The term 'soot' refers to the carbon particles formed

during combustion, which takes place in the gaseous phase at high temperature. When viewed under an electron microscope, soot takes the form of a chain of solid aggregates consisting of collections of smaller primary particles. These are spherical or nearly spherical (primary soot particles) [2-4,8] clustered in aggregates (assemblies or chains) called particles, which are emitted from diesel engines, vary in size from 10 to 80 nm [2,4,8] and contain a small amount of hydrogen. In the following figure, a soot particle generated during diesel combustion is distinguished, showing it as an aggregate of spherical particles with a diameter of 20 nm. [2-4,8].

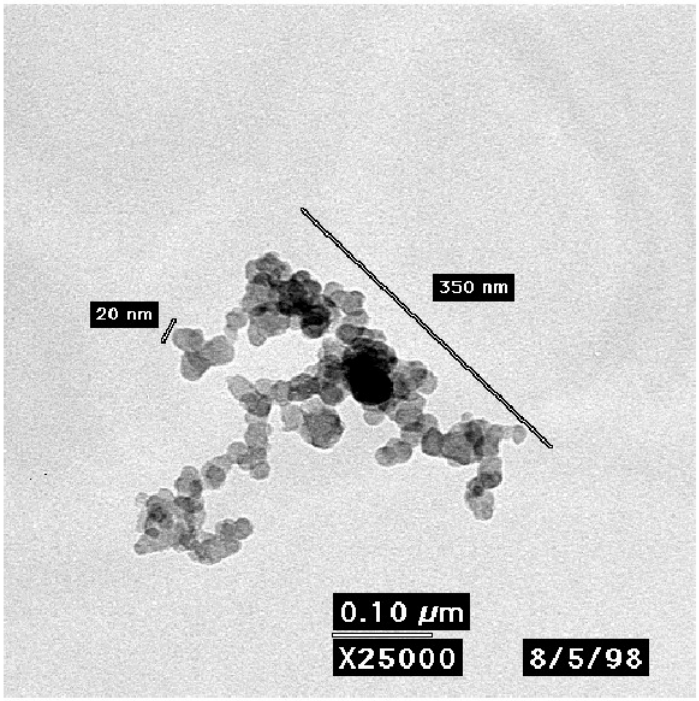

Figure 1-13. Photomicrograph of a soot particle generated during diesel combustion, showing it to be an aggregate of spherical particles with a diameter of about 20 nm

A primary particle contains 10^5 to 10^6 carbon atoms [7]. As shown in the following figure, the carbon atoms of carbon black primary particles are arranged on hexagonal surfaces called "platelets". These platelets are arranged in planes to form crystallites, each of which contains 2-5 platelets. For diesel engine soot particles, typically 15-30% of the particle mass can be extracted using strong solvents.

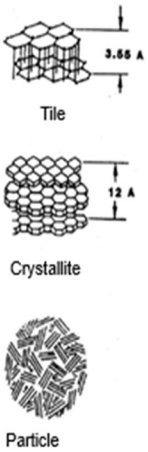

Figure 1-14. Soot particle microstructure [3]

Soot emissions are associated with serious respiratory problems and are suspected of causing cancer. Particularly important is their size distribution, because particles smaller than 2.5 μm, i.e. 90% of the total mass of particles in the exhaust, are respirable and end up directly in the lungs. In addition, the emission of particulate matter also causes problems in engine operation due to its deposition.

The solid particulate matter emitted by diesel engines consists mainly of carbon. At temperatures above 1300 K, the fuel components in the bundle core, where the mixture is extremely rich, can be pyrolyzed to form carbon particles (the highest concentrations of soot are observed in this region) [2,3,8].

Pyrolysis is the chemical preparation of hydrocarbons, i.e. the splitting of heavier hydrocarbons into other lighter and more reactive ones. These first particles are very small because the rate of formation is very high. Later they undergo surface expansion, contraction and aggregation due to chemical chain reactions that take place until the temperature of the exhaust gas decreases [2,3,8].

Thus, soot concentrations increase rapidly at the start of combustion and decrease sharply after the end of fuel injection, when the core is mixed with air in poorer proportions [2,3,7,8]. Figure 1-15 schematically depicts the soot formation and oxidation regions, as well as the nitric oxide formation zone around the flame.

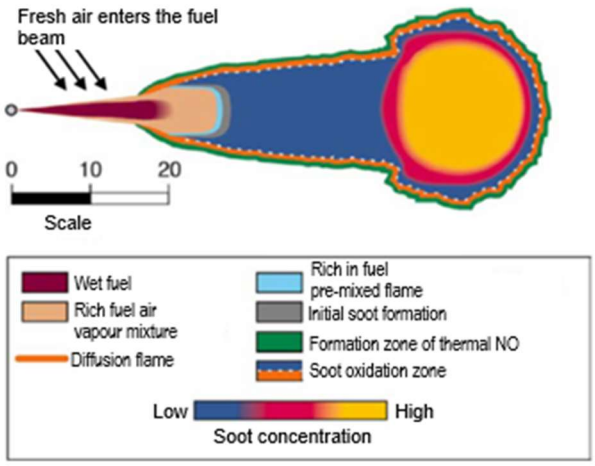

Figure 1-15. Schematic representation of the fuel bundle inside the diesel engine based on Dec's model [11]

Most of the elemental carbon formed (80-98%) is oxidized during the last stages of combustion. The remaining elemental carbon accumulates in a complex soot particle chain and exits the engine as a component of the particulate matter emissions. The emitted soot is then subjected to an additional process of mass increase, following cooling and mixing of the exhaust gas with ambient air [2-4,8,11].

From this description, the formation of soot during combustion and its subsequent emission from the engine in the form of solid particles depends on three main factors [2-4,6,8,11]:

- Temperature
- operation time with intensely rich mixtures
- Availability of oxidants

Therefore, the control of soot particle formation inside the combustion chamber is achieved by varying various parameters that affect these variables, such as load (soot load limit), injection advance, engine rotation speed, fuel injection pressure and rate, and air twist, while balancing the resulting effects on NOx emissions and fuel consumption [2-4,8,11].

1.5 Use of natural gas as a fuel in shipping

1.5.1 Basic characteristics of natural gas

Natural gas is a gaseous mixture of hydrocarbons consisting mainly of methane (CH_4), usually with a content of more than 80% by volume (usually in Greece it ranges from 70 to 90%) and in lower concentrations of ethane (C_2H_6), propane (C_3H_8), butane (C_4H_{10}) and pentane (C_5H_{12}), while its chemical composition also includes small amounts of carbon dioxide (CO_2), hydrogen sulphide (H_2S) and nitrogen (N_2). Natural gas is light, colorless, odorless and non-toxic. After production, it is enriched with odorants to give it a characteristic odor and to make it detectable in the event of a leak. Also, because it is lighter than air in the event of escape, it rises to a great height, becomes diluted and becomes non-hazardous [23-27]. Not every underground source of natural gas produces a gas of the same composition as another, since its composition depends on the origin and type of organic matter from which it was formed [23-27]. Natural gas is formed by the thermal degradation of high molecular weight primary organic matter derived from organic sediments (terrestrial or marine) under high pressure and temperature conditions at a depth of several kilometers in the subsurface. The methane produced is trapped in impermeable geological formations, creating reservoirs, at the base of which oil is usually trapped [23-27].

The mixture of gases that make up natural gas varies considerably depending on the source and the corresponding field [23-27]. Natural gas contains mainly methane (CH_4), ethane (C_2H_6), propane (C_3H_8) and butane (C_4H_{10}). Ethane, propane and butane have a higher calorific value than methane [23-27]. Natural gas cannot be liquefied under pressure. For this reason, it must be cooled to a temperature of about -160 ºC. So, in this state its volume is reduced to 1/600, making it possible to transport it by sea in an economical way [23-27]. Table 1-5 contains typical thermodynamic properties of various gases transported in liquefied form by sea while Table 1-6 shows a typical gas composition of natural gas [23-27]. Figure 1-16 shows a schematic illustration of a typical liquefied natural gas transport vessel [23-27].

Table 1-5. Typical thermodynamic properties of methane, ethane, propane, ammonia and butane [23 - 27]

Properties	Methane CH_4	Ethane C_2H_4	Propane C_3H_8	Ammonia NH_3	Butane C_4H_{10}
Storage temperature (ºC)	-161	-104	-43	-34	-1

Load transfer pressure (kg/cm^2)	1.04	1.04	1.04	1.04	1.04
Liquid specific gravity	0.474	0.570	0.583	0.683	0.602
Ignition temperature (ºC)	595	450	470	652	472
Gasification heat (Kcal/Kg)	124	115	101	326	91

Table 1-6. Typical composition of LNG [23 - 27]

Methane	95.23
Ethane	4.41
Propane	0.30
Butane	0.04
Isobutane	0.02
N- Butane	0.00
Isopentane	0.00
Hexane	0.00
Heptane	0.00
Octane	0.00
Carbon dioxide	0.00
Nitrogen	0.00
TOTAL	**100.00 %**

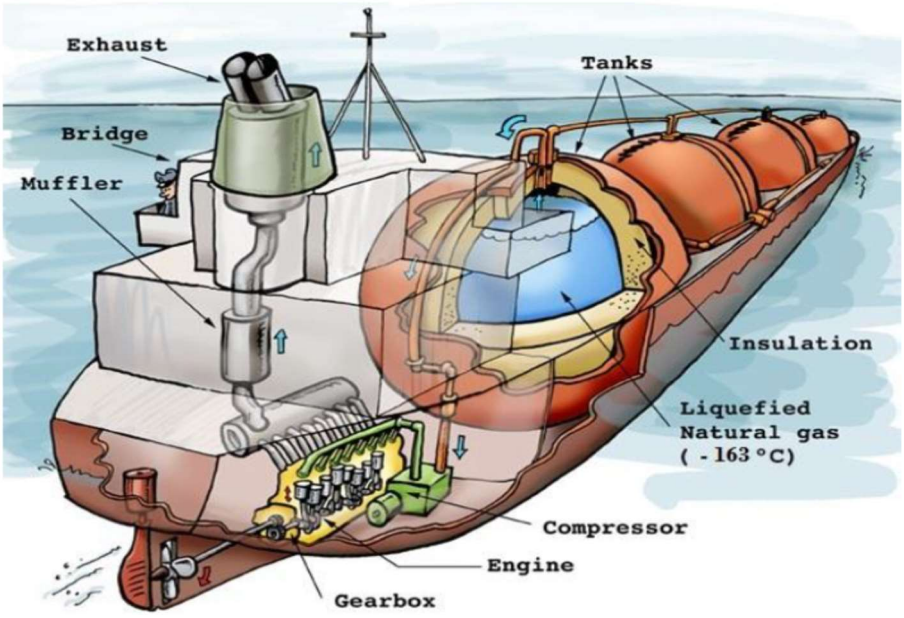

Figure 1-16. Schematic representation of a LNG carrier [23 - 27]

Natural gas is often characterised by the presence or absence of specific components. Thus, we have the following characterizations of gas [23 - 27]:

- **Wet Gas**: Usually, the unprocessed gas containing condensable hydrocarbons (propane, butane, etc.).
- **Dry Gas:** when it does not contain condensable hydrocarbons

- **Sour Gas:** when it contains carbon dioxide (>2%), hydrogen sulphide and other sulphur compounds in concentrations exceeding certain limits.
- **Sweet Gas:** when it contains carbon dioxide (<2%) and the concentrations of hydrogen sulphide and other compounds are below certain limits.

1.6 Advantages and disadvantages of using natural gas in shipping

The use of natural gas as a fuel in shipping has both specific advantages over other fuels and specific disadvantages. The advantages of using natural gas in shipping are as follows [36]:

- The large availability of natural gas from underground reserves: The recent discovery of huge available marine underground gas reserves, for example off East Africa and in the Caspian Sea, guarantee uninterrupted global supply for many years to come [36].
- The competitive cost of supplying natural gas compared to heavy oil fractions and light fractional distillation products: Natural gas is expected to have competitive costs relative to heavy refinery residues and light fractional distillation products by 2035 (see Figure 1-17). Currently, natural gas has about 70% lower supply costs relative to heavy refinery residues and 85% lower supply costs relative to light fractional distillation products [36].
- Lower CO_2, PM, NOx and SOx emissions compared to liquid fuels: In particular, combustion of natural gas in internal combustion engines results in significant reductions in CO_2 emissions (20-30%) and NOx emissions (by about 80%). Still, combustion of natural gas in internal combustion engines produces virtually no Sox emissions, has extremely low particulate matter emissions and still leaves no heavy residues such as heavy refinery fractions [36].
- The rules for the construction of gas carriers by various classification societies such as DNV/GL and Lloyd's Register.
- The wide availability of gas-fuelled marine internal combustion engines: Nowadays there are various versions of two-stroke and four-stroke compression ignition (dual-fuel) and four-stroke spark ignition natural gas fueled marine engines available on the commercial market. Dual-fuel engines can be used either as main propulsion engines (2-S and 4-S) or as electric motors (4-S) while 4-S gas engines with spark ignition can be used either as

main propulsion engines in passenger ships and coasters or as electric locomotives [36]. Examples of gas engine manufacturers are Wartsila, MAN B&W, Rolls Royce (Bergen Engines), Caterpillar [36].

- Many years of technological experience in the management of natural gas in commercial ships carrying gas and using it as fuel in their main and auxiliary engines [36].

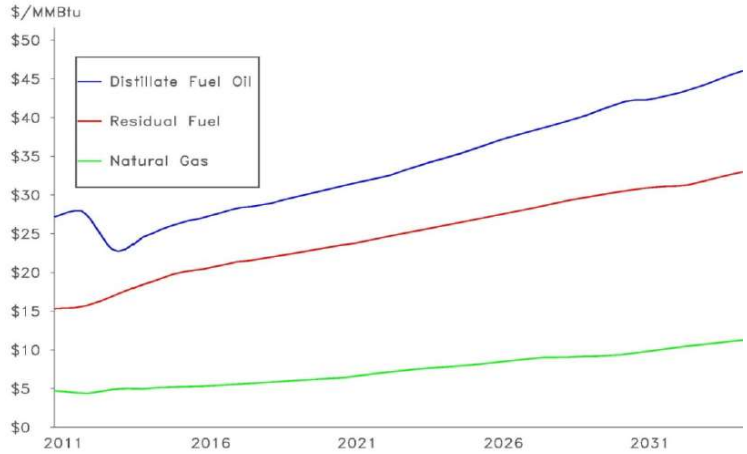

Figure 1-17. Price evolution over time for natural gas, heavy oil and light distillate oil [36]

The main disadvantages of using natural gas on ships are as follows [36]:

- The higher emissions of gross hydrocarbons and methane leakage associated with the combustion of natural gas in piston engines compared to liquid fuel combustion: In particular, the combustion of natural gas in piston engines with either dual fuel or spark ignition results in a 70 to 75% deterioration of gross hydrocarbon emissions compared to conventional operation [36]. Furthermore, natural gas combustion in piston engines results in methane slip from the engines. Considering that methane is considered 20 to 25 times more dangerous greenhouse gas than carbon dioxide, the use of natural gas in shipping raises strong skepticism regarding methane emissions. For this reason, it is expected that methane will be included in the calculation of greenhouse gases and on this basis, it is expected that high operating costs for ships using natural gas as fuel will be incurred by the potential imposition of a CO_2 tax on shipping [36].
- Natural gas is not directly compatible with the existing ICEs and the corresponding fuel supply systems of the marine ICEs: In particular, the use of natural gas as a fuel in shipping requires structural modifications to existing marine ICEs and/or additions to the fuel supply systems of a ship's main and auxiliary engines. Additional modifications to the ship's networks are also required for safety reasons regarding the handling of natural gas on board ships. Of particular interest are the results of a comprehensive study carried out in 2013 [36], in which the cost of converting the main and auxiliary engines of three different ships to run on natural gas as fuel was calculated. Furthermore, the corresponding cost of converting the main and auxiliary

engine supply networks to gas was calculated in this study [36]. Table 1-7 summarises the results of this analytical study [36].

- The higher cost of building a ship carrying natural gas compared to a conventional ship: In particular, a new ship carrying natural gas and using it as fuel for its engines has higher construction costs than a conventional ship. The higher cost of a gas carrier is due to the higher cost of the gas combustion engines, the gas supply system for the engines and the cost of building LNG storage tanks. According to a study by DNV/GL [36], the cost of building an LNG carrier is about 25% higher than the cost of building a new tanker [36]. Furthermore, according to a second study by DNV/GL [36], if a ship spends more than 30% of its operating time in areas where NOx and SOx emissions are controlled, the cost of purchasing the gas engines for that ship can be justified.
- The increased on-board requirements for the storage of natural gas: In particular, increased availability of on-board space is required to store the necessary volume of natural gas for ship autonomy similar to that of a conventional liquid-fuelled ship [36]. A given weight of natural gas stored as LNG requires only about 40% of the corresponding weight of natural gas stored as LPG at a pressure of 3,600 psi (≈ 250 bar). Therefore, LNG requires much less storage space than LPG and for this reason it has been the preferred method of storing natural gas on board ships in recent years. When natural gas is stored as LPG it requires twice as much space as the corresponding space required to store a liquid fuel, while when stored as LNG it requires 5 times as much space as the space required to store a liquid fuel [36]. Table 1-8 shows examples of a comparison of the minimum storage capacity and onboard storage volume for transporting light or heavy oil, LNG and CNG with three different types of ships while Figure 1-18 shows the comparison of fuel weight per light oil equivalent gallon for light oil, for heavy refinery residue, LNG and CNG@3,600 psi and the comparison of fuel storage volume per gallon equivalent of light oil for light oil, heavy refinery residue, LNG and CNG@3,600 psi [36].
- The increased time to supply a ship with gas: In particular, the duration of time to fuel a ship with natural gas is longer than the duration of time to fuel a ship with liquid fuel. In particular, as regards on-board storage of gas in the form of LNG, it can be argued that this solution is not considered to be viable in the main because of:

    - ✓ The higher delivery times of the ship compared to the transport of LNG in the form of LNG.
    - ✓ The additional storage requirements for the storage tanks of the LNG storage tanks.
    - ✓ The limited transport volume, which leads to limited autonomy of the LNG carrier.

For the above reasons, LNG is considered as a viable solution for ships making short voyages and having sufficient return time for refueling. The main disadvantages of LNG are the following:

  - The liquefaction of natural gas requires, as already mentioned, cooling of the gas to a temperature of about -160 degC. Nowadays this deep cooling is possible by means of technically complex and expensive onshore installations.
  - LNG carriers should be equipped with technical deep-freezing systems to enable them to maintain LNG at a temperature of -160 degC.

- The additional safety requirements of a gas carrier: The transportation of natural gas from a ship requires additional safety facilities and arrangements and leads to construction interventions that result in higher construction costs for the gas carrier [36].
- The limited onshore infrastructure for supplying gas to ships: In particular, in order to make it attractive to transport LNG and use it as a fuel for the majority of ships, an international network of LNG onshore transshipment terminals will have to be built. At present, the transshipment of LNG from onshore terminals is more expensive and technically more complex than the transshipment of liquid fuels on board ships. Furthermore, LNG transshipment to ships can be carried out at a limited number of terminals around the world [36].

Table 1-7. Conversion costs of specific types of ships for operation with natural gas as fuel [36]

Vessel type	Displacement (tonnes)	Engines	Engines Conversion cost (mil. $)	Cost of engine fuel supply system conversion (mil. $)	Total conversion costs (mil. $)
Tug	**150**	**2 x 1500 HP**	**1.2**	**6.0**	**7.2**
Ferry	**1,000**	**2 x 3,000 HP**	**1.8**	**9.0**	**10.8**
Great Lakes Bulk	**19,000**	**2 x 5,000 HP**	**4.0**	**20**	**24**

Carrier					

Table 1-8. Examples of comparison of minimum storage capacity and on-board storage volume for the transport of light or heavy oil, LNG and CNG with three different types of vessels [36]

				Standard minimum on-board storage capacity		Storage volume on board		
Vessel	**Fuel type**	**HP**	**Daily fuel consumption (gal)**	**[days]**	**[gal]**	**Light or heavy fuel oil [ft^3]**	**LNG [ft^3]**	**CNG [ft^3]**
Towing tug	Light fuel oil	3,000	1,417	14	20,000	2,674	4,830	12,178
100-car Ferry	Light fuel oil	6,000	2,268	7	16,000	2,139	3,864	9,742
Great Lakes Ore Carrier	Heavy fuel oil	10,000	6,934	21	145,000	19,385	38,183	92,264

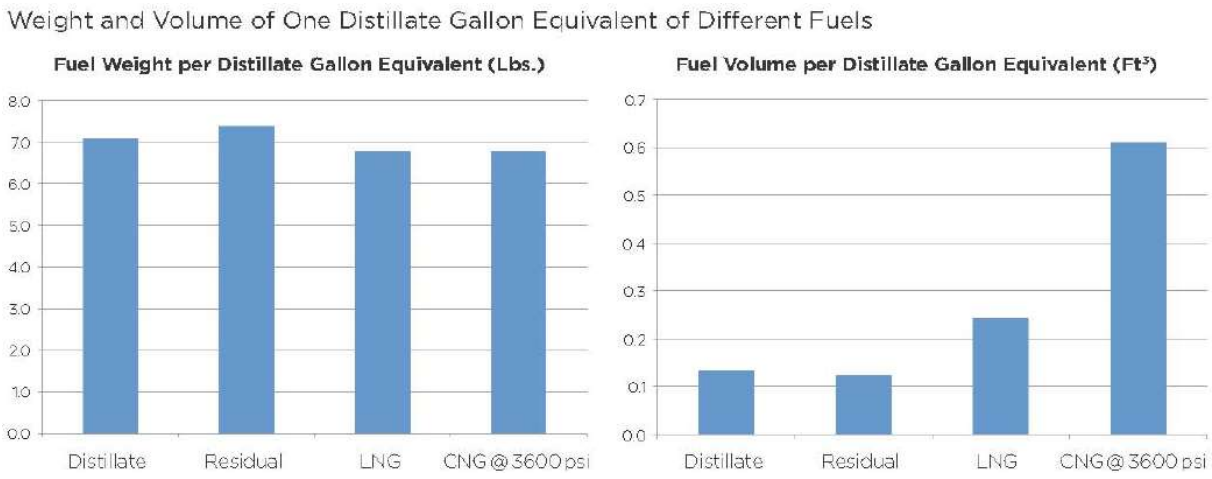

Figure 1-18. (Left figure) Comparison of fuel weight per gallon equivalent of light oil for light oil, heavy refinery residue, LNG and LNG@3,600 psi (Right figure) Comparison of fuel storage volume per gallon equivalent of light oil for light oil, heavy refinery residue, LNG and LNG@3,600 psi [36]

1.7 4-S dual fuel (gas/diesel) compression-ignition engines (dual fuel engines)

Dual fuel engines are an attractive alternative for use as marine engines to meet international air pollutant restrictions as they significantly reduce NOx losses and SOx emissions. However, they are not widely installed in modern ships due to the phenomenon of shock combustion and, in addition, in diesel operation the efficiency of these engines is low [23-34].

Dual fuel engines generally have high efficiencies, low gas pressure and low losses due to the high efficiencies and purity of the fuel used. In addition, they provide flexibility in the fuel used since they can run on either gas or diesel. This chapter presents the main characteristics of these engines and their advantages over conventional two-stroke and four-stroke marine engines [23-34].

1.7.1 Description of natural gas combustion in 4-s spark ignition engines – Principles of operation

Dual-fuel (gas-oil) marine compression ignition engines are two-stroke main or four-stroke main and auxiliary engines. They can run on natural gas (LNG), marine diesel oil (MDO) and heavy fuel oil (HFO). One of the key features of dual fuel engine technology is that - in most cases - the engine can switch between oil and gas operation and vice versa. During the short-duration switching, the oil fuel is gradually replaced by gas [23-37]. If the gas supply is momentarily interrupted the engine switches from gas operation to oil operation at any load instantaneously and automatically. In addition, the separate liquid fuel system with which these engines are equipped makes it possible to switch from MDO to HFO and vice versa without power interruption [23-37].

Figures 1-19(a) and 1-19(b) show the two modern ways of designing combustion chambers for dual-fuel (gas-oil) compression-ignition engines recently proposed by the engine developer AVL in a related publication [37]. In particular, Figure 1-19(a) shows the open chamber combustion chamber design of a dual-fuel compression ignition engine. In this combustion chamber design, a gas-air mixture is introduced into the combustion chamber through the intake valves. The gas-air mixture

is ignited by pilot injection and oil ignition. The pilot quantity of oil is injected by a corresponding injector, which as shown in Figure 1-19(a) is centrally located in the engine cylinder. This type of dual fuel auto-ignition engine design can be operated either as described previously as a pilot injected dual fuel engine or purely as a marine main or auxiliary diesel engine with various types of liquid fuels providing a choice of operation depending on the sailing and operating conditions of a ship [37]. Pilot injection and ignition of oil helps reduce the likelihood of gas ignition failure and increases the speed of flame front transmission [37]. The disadvantages of this system include the maintenance of combustion stability under various operating conditions and the limited ability to meet NOx emission limits in NOx controlled areas [37]. Figure 1-19(b) shows the second combustion chamber design of a dual-fuel compression-ignition engine, which includes a pre-chamber and main combustion chamber as well as a pilot oil injector [37]. In this case, a mixture of gas and air is reintroduced through the intake valves into the main combustion chamber. The pilot oil injector is mounted in the antechamber through which a very small amount of oil is injected, which is ignited in the antechamber. The flame that develops in the antechamber is transmitted to the main combustion chamber resulting in the ignition and combustion of the gas mixture in the main combustion chamber [37]. This combustion chamber design offers improved ignition stability compared to the previous type of combustion chamber at low NOx emission levels since the stability of the liquid fuel is not substantially affected by the high air/fuel ratio in the antechamber. This system offers a higher efficiency and more stable and complete combustion and thus lower NOx emissions than the previous system. The major disadvantage of this system compared to the previous system is that it is more complex in terms of construction [37].

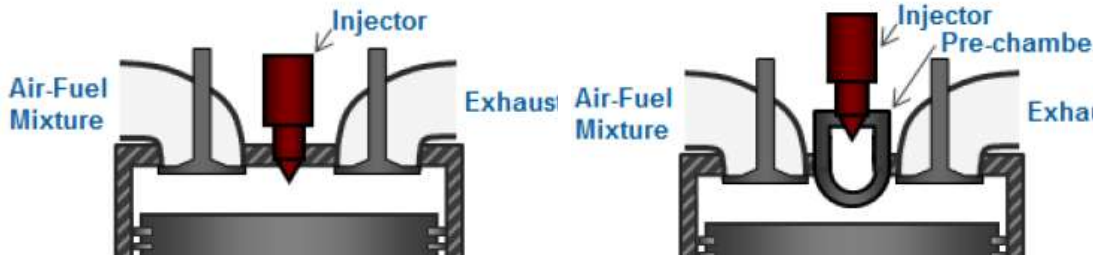

Figure 1-19. Modern combustion chamber and gas feed chamber designs of four-stroke dual-fuel (gas-oil) compression ignition four-stroke engines [37]

The gas is supplied to the engine through suitable valves in which the gas is filtered and through which the gas supply pressure is controlled. The gas supply system

of a compression-ignition engine includes the necessary switches and ventilation valves to ensure a safe and trouble-free gas supply. In the engine, the gas is supplied through a large common system of pipes running the length of the engine. Each cylinder then has a self-contained piping system to the gas supply valve on the cylinder. The piping of the engine gas supply system is double-walled for safety reasons. When the engine is running on gas, the air/gas mixture is ignited with a small amount of pilot oil (approximately 1 - 5% of the corresponding liquid fuel consumption at a given load and rpm) [23-37].

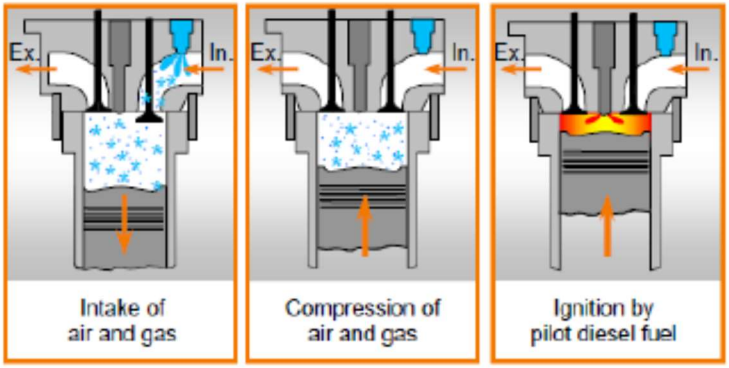

Figure 1-20. Operating phases of the dual-fuel engine during operation with natural gas [23-34]

In the operating mode of the diesel engine, the operating principle is based on the diesel engine and the injection of diesel into the engine.

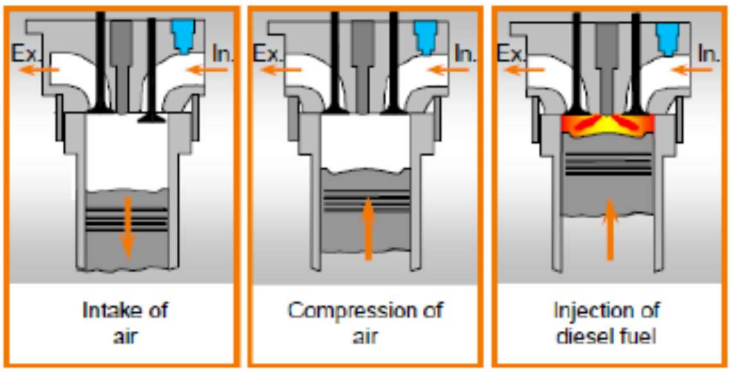

Figure 1-21. Operating phases of the dual-fuel engine when running on oil [23-34]

The amount of pilot fuel is optimized for better combustion by integrating the engine speed and load into the control and monitoring system. The automation system used in these engines, which will be presented below, provides a safety and monitoring system [23-37].

The elements of the double-wall piping system are shown in Figure 1-22. The components that make it up are the gas valve and oil injector electrical connections, gas manifolds, gas blowers, gas valve, gas nozzle, inlet valve, dual injection valve nozzle, main fuel injection pipe, and main fuel injection pump [28-34].

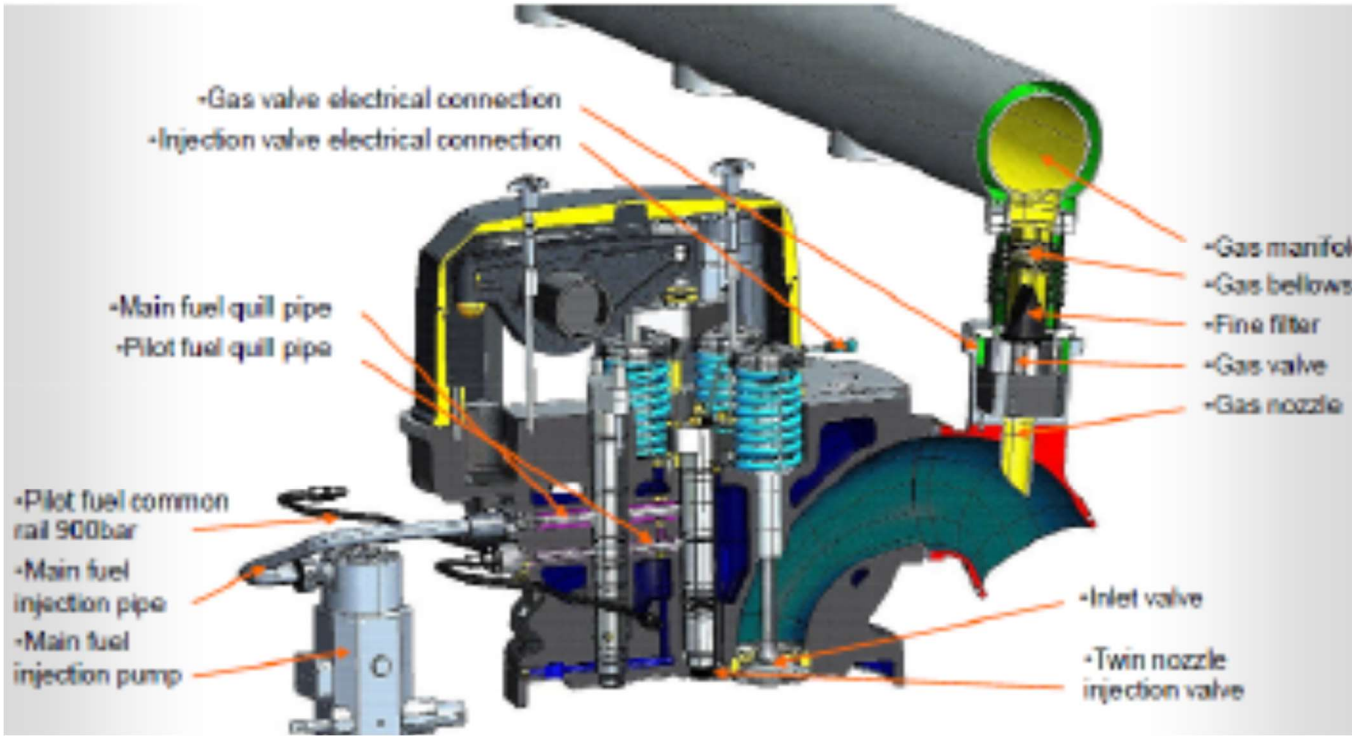

Figure 1-22. The basic elements of the dual-fuel engine gas supply system [28-34]

Compared to single-wall piping, the requirements in the engine room in terms of gas detection system, ventilation, etc. are less stringent in the case of double-wall

piping, making the engine room less complex and more economical to construct [23-37].

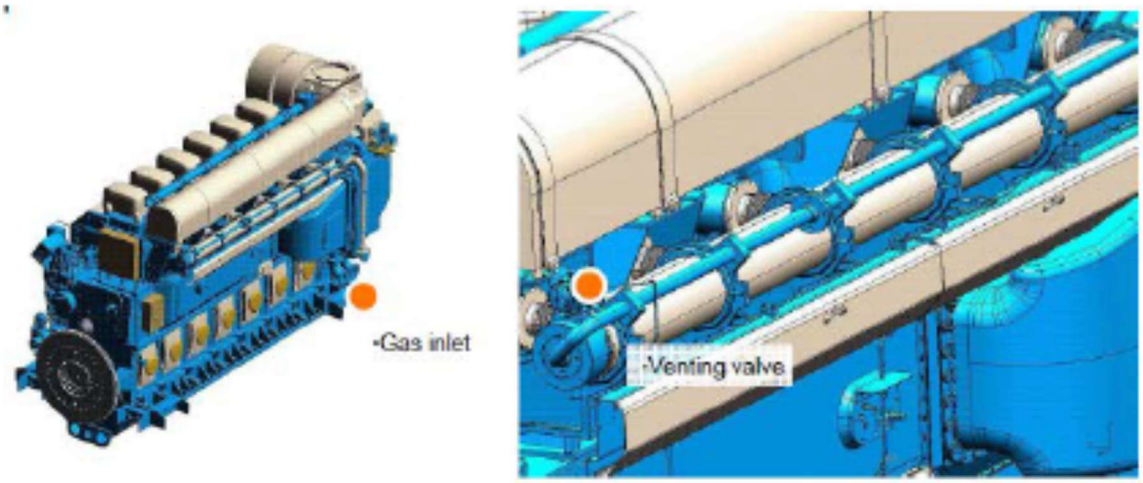

Figure 1-23. The gas inlet and the ventilation valve in the dual fuel engine [28-34]

Four-stroke dual-fuel engines have the following advantages over spark-ignition gas engines [28-34]:

- Simple mechanical application of propulsion.
- Ability to achieve maximum power during dual fuel operation and conventional fuel oil operation.
- Same load application capability as spark ignition engines.
- Dual fuel can change the liquid fuel in the case of instantaneous abnormal high load and no-load requirements.
- The switching point can be programmed according to the application.
- Dual-fuel engines improve safety significantly.

1.7.2 Technical characteristics and performance of 4-S dual-fuel compression-ignition engines

The following are data from the international literature on 4-S dual-fuel (gas-oil) engines. The figures given are for engines from Caterpillar, MAN and Wartsila. In particular, the following table provides data for the Caterpillar M34 4-S dual-fuel, medium-speed engine.

Table 1-9. Characteristics of M34F Caterpillar [28-34]

		Diesel Mode	Gas Mode
Emission		IMO II	IMO III*
Bore	mm	340	340
Stroke	mm	460	460
Speed	rpm	720/750	720/750
Power	kW/cyl. (MN≥80)	500	500
BMEP	bar	19.9/19.1	19.9/19.1
Liquid fuel consumption	g/kWh @100%	188	1.8
Gas fuel consumption	kJ/kWh @100%	–	7,708
Efficiency (development target)	%	- 44.8	> 46.7

The following table lists the basic dimensions of the Cat M34F dual-fuel engine.

Table 1-10. Dimensions of the Cat M34F engine [28-34]

Propulsion Engine Dimensions (mm) and Weights (t)										
Engine	L1	L2	L3	L4	H1	H2	H3	W1	W2	t
6 M 34 DF	5934	788	852	1168	2784	1052	550	2418	962	39.5
8 M 34 DF	7298	1044	852	1472	2969	1052	550	2229	262	49.0
9 M 34 DF	7828	1044	852	1472	2969	1052	550	2229	262	52.0

MAN offers two dual-fuel engine options, the mid-engine 51/60 and the high-speed 35/44. The following table lists the characteristics of the MAN 51/60 DF dual-fuel engine and Figure 1-24 shows the MAN 51/60 DF engine [28-34].

Table 1-11. Key characteristics and performance of the MAN 51/60 DF dual fuel engine [28-34]

Bore: 510 mm, Stroke: 600 mm

Speed	r/min	514	500
mep	bar	19.1	19.1
		kW	kW
12V51/60DF		12,000	11,700
14V51/60DF		14,000	13,650
16V51/60DF		16,000	15,600
18V51/60DF		18,000	17,550

LHV of fuel gas ≥ 28,000 kJ/Nm³
(Nm³ corresponds to one cubic meter of gas at 0 °C and 1.013 bar)

Specific Fuel Oil Consumption (SFOC) and Heat Rate to ISO conditions

MCR	100%	85%
Specific fuel oil consumption[1]	180.0 g/kWh[3] 180.0 g/kWh[4]	179.0 g/kWh[3] 179.0 g/kWh[4]
Heat rate[2]	7,400 kJ/kWh[3] 7,520 kJ/kWh[4]	7,390 kJ/kWh[3] 7,570 kJ/kWh[4]
Specific lube oil consumption 0.4 g/kWh		
Engine type specific reference charge air temperature before cylinder 43 °C		

[1] *Liquid fuel operation*
[2] *Gas operation (including pilot fuel), gas fuel: methane no. ≥ 80*
[3] *Electric propulsion*
[4] *Mechanical propulsion with CPP*
Speed 500 r/min for generator drive only

Dimensions

Cyl. No.		12	14	16	18
L	mm	10,254	11,254	12,254	13,644
L_1	mm	9,088	10,088	11,088	12,088
Dry mass	t	187	213	240	265

Minimum centreline distance for twin engine installation: 4,800 mm

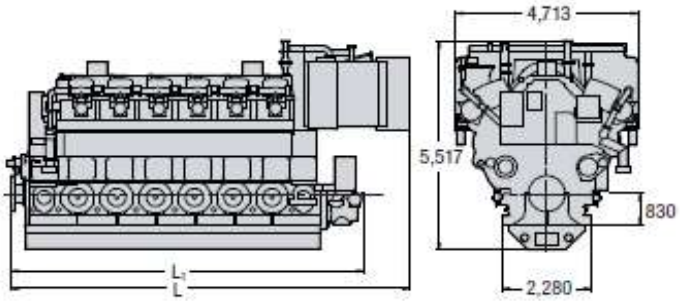

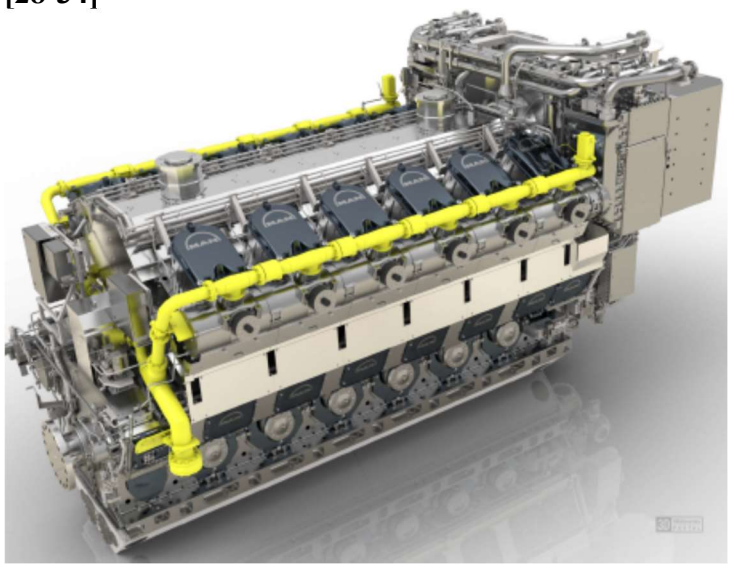

Figure 1-24. The MAN 51/60 DF dual-fuel engine [28-34]

With regard to Wartsila's dual-fuel engine options, the following table shows the basic construction and functional data of the Wartsila 46DF engine. It is worth noting that this engine has several options, from 6 to 16 cylinders with 2 design options of high output (high output - 1145kw/cyl) or high efficiency (high efficiency - 1045kW/cyl).

Table 1-12. Basic construction and operational data of the Wartsila 46DF dual-fuel engine [28-34]

Wärtsilä 46DF		IMO Tier II, EPA T2/T3	
Cylinder bore	460 mm	Fuel specification: Fuel oil	
Piston stroke	580 mm	700 cSt/50°C	7200 sR1/100°F
Cylinder output	1045, 1145 kW/cyl	ISO 8217, category ISO-F-DMX, DMA & DMB	
Speed	600 rpm		
Mean effective pressure	21.7, 23.8 bar	BSEC 7060 kJ/kWh at ISO cond.	
Piston speed	11.6 m/s		

Rated power

Engine type	High output 1145 kW/cyl	High efficiency 1045 kW/cyl
6L46DF	6 870	6 270
7L46DF	8 015	7 315
8L46DF	9 160	8 360
9L46DF	10 305	9 405
12V46DF	13 740	12 540
14V46DF	16 030	14 630
16V46DF	18 320	16 720

Dimensions (mm) and weights (tonnes)

Engine type	A*	A	B	C	D	F	Weight
6L46DF	8 670	8 833	3 255	3 185	3 750	1 430	102
7L46DF	9 350	9 513	3 255	3 185	3 750	1 430	116
8L46DF	10 310	10 830	3 445	3 185	3 750	1 430	130
9L46DF	10 990	11 510	3 445	3 185	3 750	1 430	146
12V46DF	11 120	10 350	3 670	4 555	3 800	1 620	154
14V46DF	12 170	11 400	3 670	4 555	3 800	1 620	223
16V46DF	13 450	12 780	3 860	5 174	3 800	1 620	235

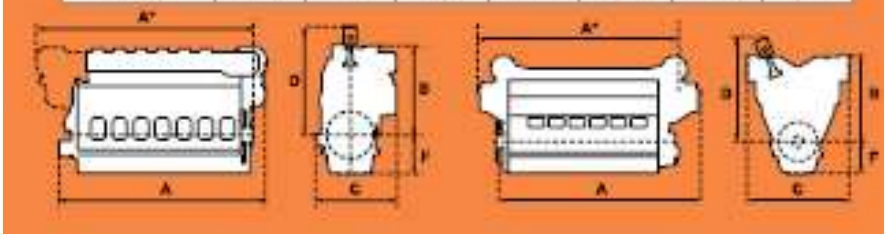

1.7.3 Installation applications of 4-S dual-fuel compression ignition engines

Wärtsilä has signed a contract with the Construcciones Navales del Norte SL (LaNaval) shipyard in Sestao, Spain for the design and supply of the propulsion plant for a new Ro-Ro passenger ferry. There is also an option for a second ship. The vessel is under construction for Spanish company Balearia, the leading operator serving the Balearic Islands. Wärtsilä will also provide inclusive project support services at the

shipyard, including engineering integration and on-site consultancy, as well as the provision of the combined systems [28 - 34].

Figure 1-25. The first passenger ferry with dual-fuel engines in the Mediterranean [28-34]

When entering regular service in 2019, this eco-efficient "superstructure" will be the first Ro-Ro passenger ferry operating in the Mediterranean Sea and among the largest ships in Europe. It is 232 meters long and has a capacity of 331 vehicles and 1700 passengers, 70% of which can be accommodated in cabins. Due to the ship's extensive accommodation facilities and the need to prioritise passenger comfort, strict noise and vibration reduction standards will be applied to Wärtsilä's main and auxiliary engines, propellers and bow thrusters. The environmental footprint of the ship is expected to be significantly reduced due to the use of natural gas. Compared to diesel-fueled ships, Wärtsilä's LNG solution reduces CO_2 emissions by 25%, nitrogen oxides (NOx) by 85%, and sulphur and particulate matter are almost completely eliminated [28-34].

Wärtsilä is responsible for the supply of this contract which includes four 8-cylinder Wärtsilä 50DF dual-fuel main engines, four 9-cylinder Wärtsilä 20DF dual-fuel auxiliary engines, fuel storage and management through the Wärtsilä LNG Pac system, two reducers, two Wärtsilä variable pitch propellers (CPPs) and two Wärtsilä bow thrusters.

1.7.4 Conversion of existing diesel engines for gas operation – TARBIT Project

Converting a diesel engine to run on natural gas requires several steps. As can be seen in the figure below, the cylinder heads, cylinder liners and their corresponding piston springs, the camshaft must be replaced so that it utilizes Miller timing, the dual-

needle nozzle fuel injectors, the upper heads of the distributors, the turbochargers for dual fuel use and the electronic control system for engine operation must be replaced [28-34].

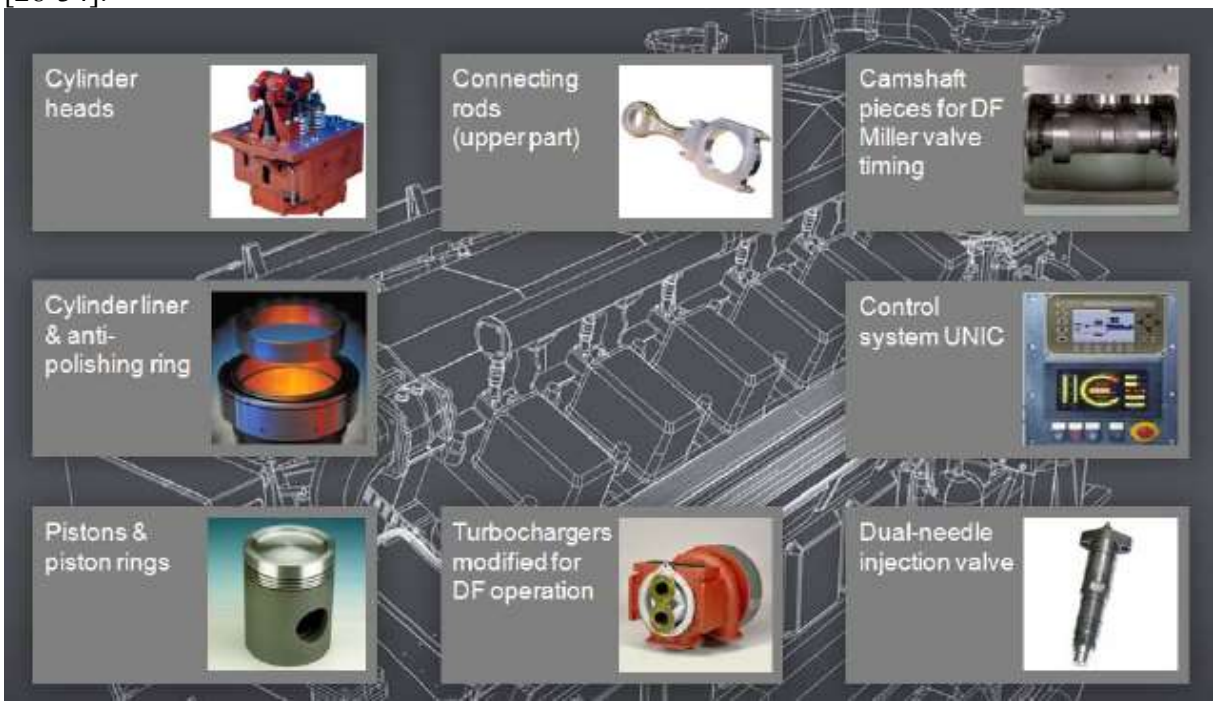

Figure 1-26. The components that need to be replaced to convert an engine to dual fuel [28-34]

The components that need to be added so that a diesel engine can run on natural gas are as follows [28-34]:

- The gas inlet valves
- The exhaust outlet duct
- The gas inlet pipeline

The pilot ignition system includes [28-34]:

- Pilot fuel filter
- Pilot fuel pump
- Fuel inlet pipe

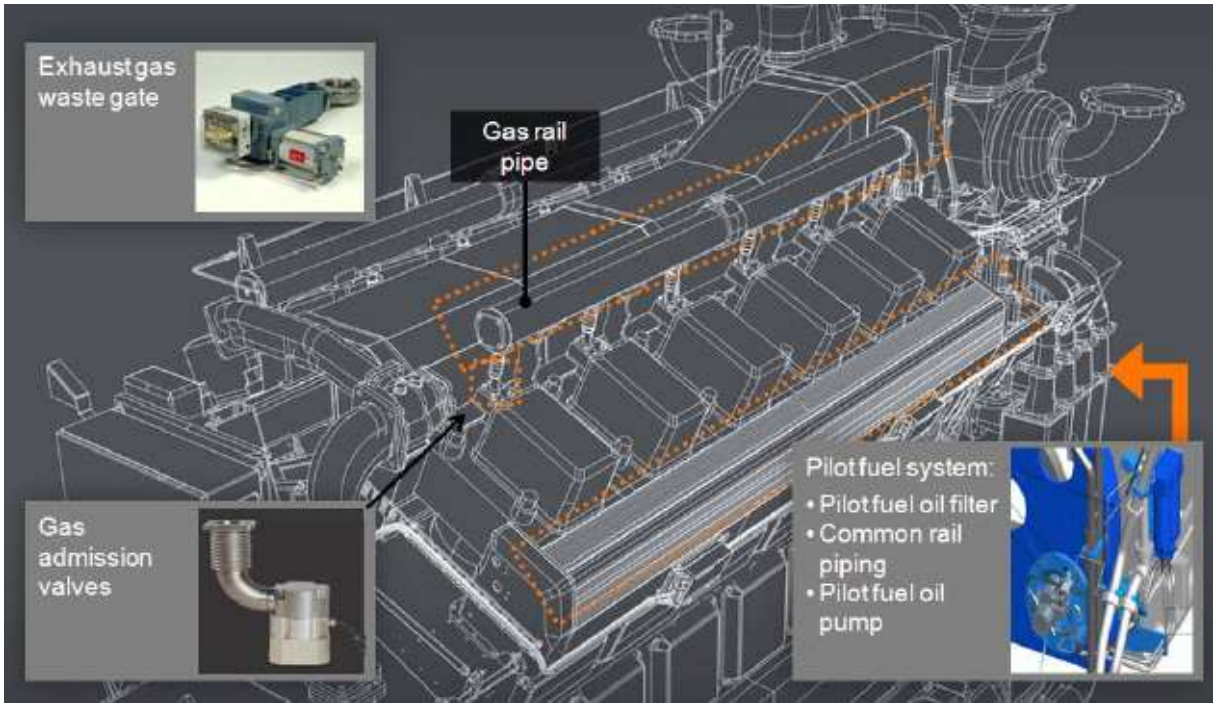

Figure 1-27. The components that need to be added to convert an engine to dual fuel [28-34]

In addition, gas storage tanks must be installed. The following figures show the two different proposals [28-34].

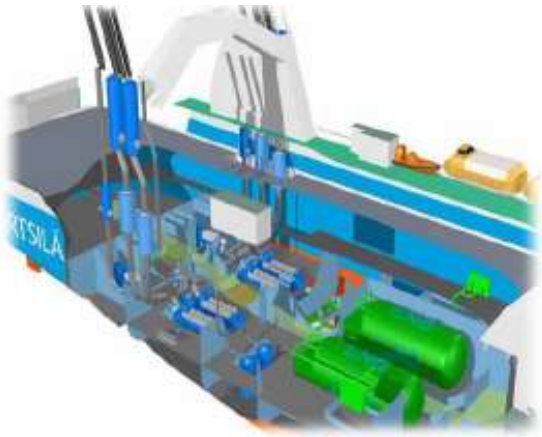

Figure 1-28. Alternative ways of storing natural gas [28-34]

The process of converting the TAPVIT's MT BIT VIKING ship so that its main and auxiliary diesel engines can run on natural gas. The MT BIT VIKING was one of the first ships to be converted to be able to carry and burn natural gas in its engines. The conversion was carried out by Wärtsilä itself [28-37].

Figure 1-29. Conversion of TARBIT MT BIT VIKING for operation of its main and auxiliary engines with natural gas. The figure shows the location of LNG tanks on the deck of the ship [28-34]

The equipment added to the ship to enable it to carry natural gas was the gas storage tanks, the gas transport piping, and auxiliary equipment installed in a separate compartment [28-34].

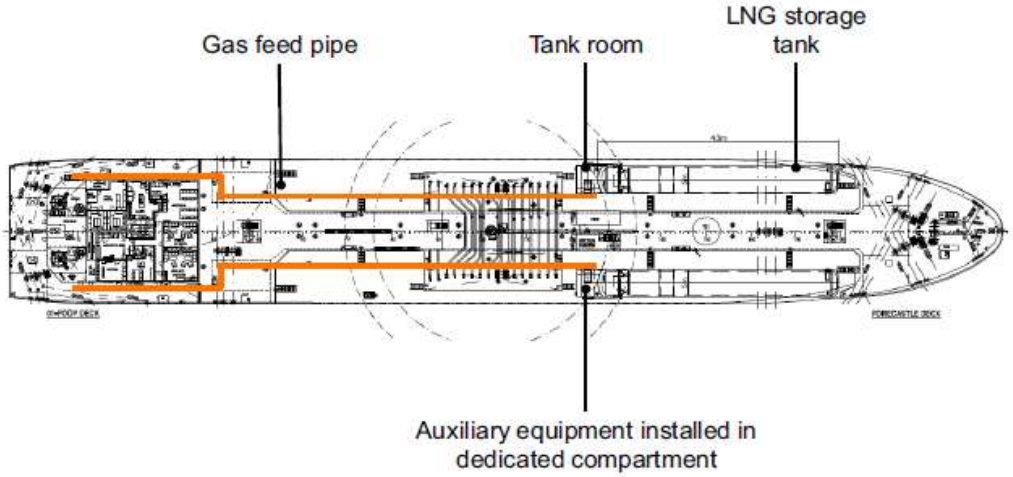

Figure 1-10.Equipment added to the TARBIT to convert it into a gas carrier [28-34]

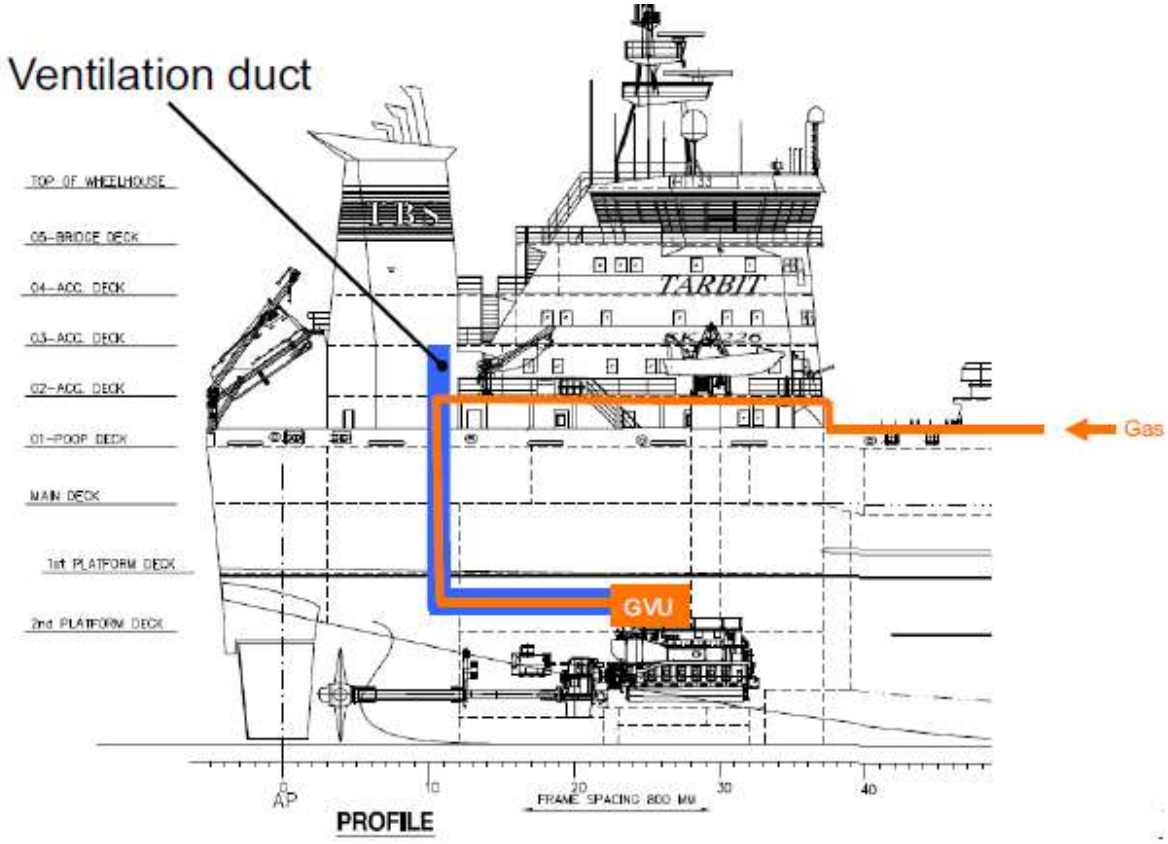

Figure 1-31. Profile of the ship TARBIT. The figure shows in orange the line feeding the main diesel engines with gas from the respective tanks on deck. The location of the gas valve unit (GVU) for the main engines is shown [28-34].

In summary, the following modifications were required to the TARBIT ship to enable its engines to run on gas [28-34]:

- Conversion of main and auxiliary engines.

- Installation of two gas tanks on the deck of the ship with a capacity of 500 m^3 each.
- Gas Valve Unit (GVU) for the main and auxiliary engines with natural gas
- Installation of a torque measuring system (torquemeter) on the engines.
- Engine gas supply piping (double wall)
- Modification of the exhaust system
- Upgrade to fire-fighting equipment
- Gas leak detection system

1.8 Evaluation of different LNG propulsion technologies using the Energy Efficiency Design Index (EEDI)

1.8.1 Introduction

The use of natural gas as a fuel for power generation has become more widespread in the last decade, the reasons for this being mainly because it is abundant, cheaper, and produces fewer emissions than other established fossil fuels. For ease of storage and/or transportation, natural gas (NG) is converted to liquid form (LNG - Liquefied Natural Gas) by cooling the gas to -160°C, taking 600 times less volume than when it is in gaseous state, and can then be transported by sea using specially designed cryogenic vessels - the LNG Carriers (LNGCs) [32]. The use of these LNGCs is an efficient way of transporting natural gas over long distances, where pipelines are not available, to specially designed terminals, from where the LNG is re-gasified and distributed by pipelines [32]. As of July 2014 there are 335 LNGCs in operation [32], with each using three different types of propulsion with the dominant one being steam turbine propulsion (STPS), the others being the dual fuel diesel electric (DFDE) combined diesel-electric propulsion system and traditional slow-speed two-stroke diesel engines with re-liquefaction facilities (SSDR) [32]. As LNG is transported at -160°C and near atmospheric pressure, it inevitably evaporates due to imperfect insulation in the tanks. This resulted in these ships using the vapors in the propulsion system. This is a propulsion system with a long dominance of 40 years on LNG carriers. Steam boilers burn natural gas as easily as fuel oil, whereas other propulsion options

could not [32]. While steam turbines have proven to be extremely reliable at this time, compared to other propulsion alternatives, they are inefficient in terms of fuel consumption due to the inherent properties and limitations of the Rankine Cycle. The fuel consumption in steamships compared to diesel-powered vessels is too high for non-LNG use and therefore steam turbines have been mainly replaced by two-stroke diesel engines [32]. For LNG carriers built 10-30 years ago, there was little or no incentive to develop alternative propulsion facilities, since the condition of the cargo insulation was such that on a full voyage, the gas evaporated was sufficient to provide 100% of the fuel requirements. Even assuming that there were more efficient natural gas firing plants available at the time, it is likely that they could not be used without requiring an alternative to boil off gas (BOG) [32]. However, the development of technology upon insulation, have led to significantly lower rates of LNG being gasified. This has led to insufficient amounts of natural gas to supply the propulsion plant resulting in the need to supplement with either the use of mandatory natural gas vaporization or the use of heavy fuel oil (HFO). This has led to the development of alternative and more efficient propulsion systems that offer economic advantages over conventional steam turbine installation and/or new liquefaction (conversion of gasified gas back into LNG. In addition, during this period the IMO began introducing regulations to govern exhaust pollutants from ships, including NOx and more recently carbon dioxide. This led to a shift in the propulsion plant design of LNGCs from STPS to DFDE and SSDR [32]. From the 1960s to 1990s, STPS was applied to almost all LNG carriers with few exceptions. By the 2000s, the percentage had dropped to 69% and in the current decade to 21%. In this section, the energy efficiency of different LNG carriers is evaluated on two main propulsion issues (a) To review the energy efficiency of different LNGC designs over time and compare them with the current designs having different types of propulsion systems through a detailed study (b) To consider the potential impact of this propulsion change in combination with the regulations on emissions in terms of achieving CO_2 emission reductions [32].

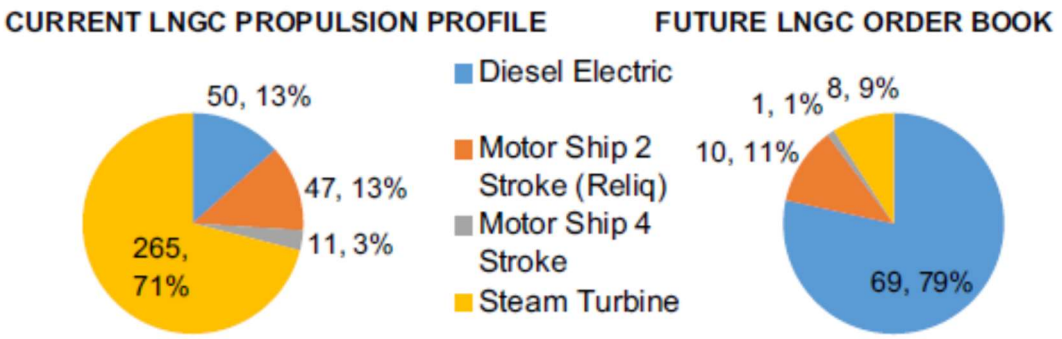

Figure 1-32. The LNG vessel fleet at present and corresponding future projections [32]

1.8.2 Description of alternative natural gas propulsion systems

1.8.2.1 Steam turbines

STPS ships occupy 71% of the current LNG fleet [32], and this majority is mainly due to the easy handling of the BOG, simple operation and internal safety. When the cargo tank pressure is elevated, the steam boilers burn the BOG to produce high pressure steam that drives the turbines which are connected to the propeller. During periods when the engine load is not sufficient to burn all the BOG the remaining gas is directed to the condensers for re-liquefaction. It is this simple philosophy that eliminates the need for a gas combustion unit, which is a requirement for the other two propulsion systems - the SSDR and DFDEs [32].

The diagram of the STPS installation is shown in the following figure and usually consists of two boilers using natural gas/mazut as fuel. The steam produced is also used to supply auxiliary systems including generators and pumps. The propulsion diagram is similar on every steam LNG ship in service and has remained largely unchanged since the first steam LNG ships entered service in 1964 [32].

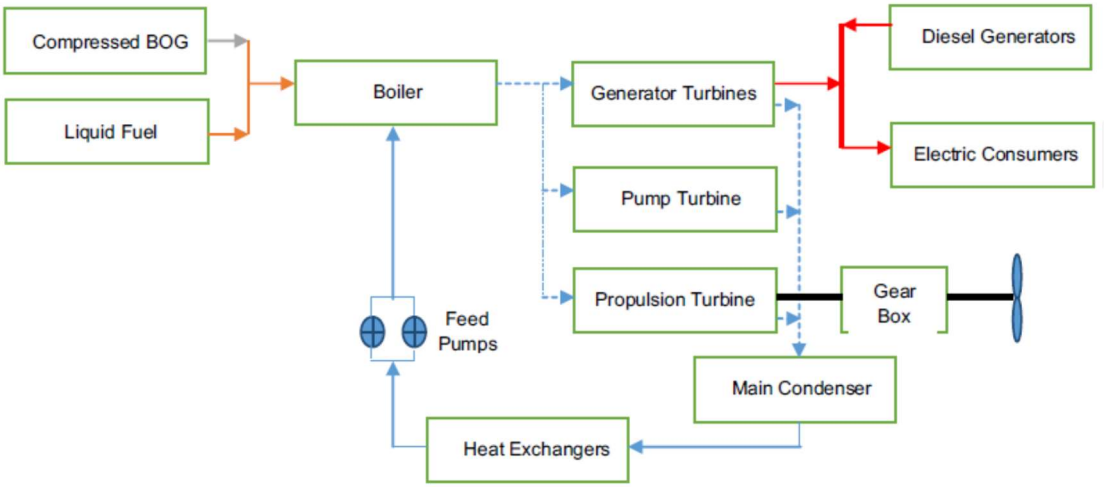

Figure 1-33. Schematic illustration of a natural gas steam turbine prop.system (STPS) [32]

1.8.2.2 Slow-speed diesel engines with boil off gas re-liquefaction facilities

The SSDR is a single propulsion system with a re-liquefaction facility where the BOG is liquefied and returned to the cargo tanks instead of being burned in the engine. The arrangement of the idle diesels in these systems is typically the twin screw configuration with the two diesel engines connected directly by two propellers, as shown in Fig. 1-34. This propulsion unit is also equipped with a Gas Control Unit to select the BOG in cases where the BOG capacity is greater than the capacity of the re-liquefaction facility. The BOG liquefaction facility is based on a closed nitrogen cycle to extract heat from the BOG. This ensures that all hydrocarbons in the gas are condensed so that they are converted back into LNG, while nitrogen and other non-condensables remain as gas bubbles in the LNG. These bubbles, however, are removed by a liquid separator where the LNG is separated and pumped back to the cargo tanks with the nitrogen-rich non-condensables being discharged to the atmosphere or burned in the GCU [32]. For LNG carriers this additional re-liquefaction system would impose an additional electricity load of between 3 and 4 MW, although some current LNGCs with diesel configurations have capacities of between 216,000^{m3} and 260,000^{m3} thus requiring between 4.5 and 5.5 MW of electricity [32].

].

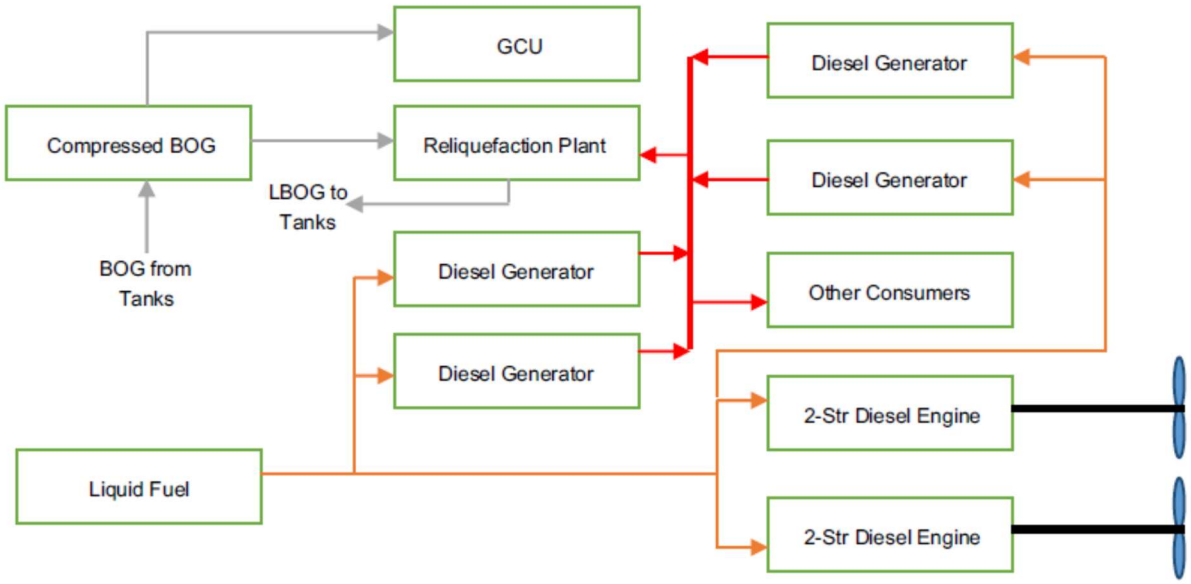

Figure ***1-34. Schematic illustration of a ship propulsion installation with slow-speed diesel engines and boil off gas*** *gas re-liquefaction* ***(SSDR) devices [32]***

1.8.2.3 Dual fuel diesel electric propulsion system - DFDE

The DFDE propulsion system has modified diesel engines designed to burn BOG as well as intermediate fuel oil (IFO) as shown in the following figure [32]. This propulsion facility uses multiple diesel generators, typically four, to meet all the power requirements of the vessel which, in this case, also includes the main system as the diesel engines generate electricity and the electric motors use this electricity to propel the vessel [32]. The engine, however, runs on natural gas with diesel pilot ignition, where the gas is premixed in the inlet ports, or on liquid fuel, such as IFO, but cannot burn both fuels (natural gas and IFO) at the same time [32]. This is a disadvantage compared to the steam turbine propulsion system that can burn various ratios of gas and oil simultaneously [32]. The provision of multiple diesel gensets provides flexibility of operation and high autonomy [32].

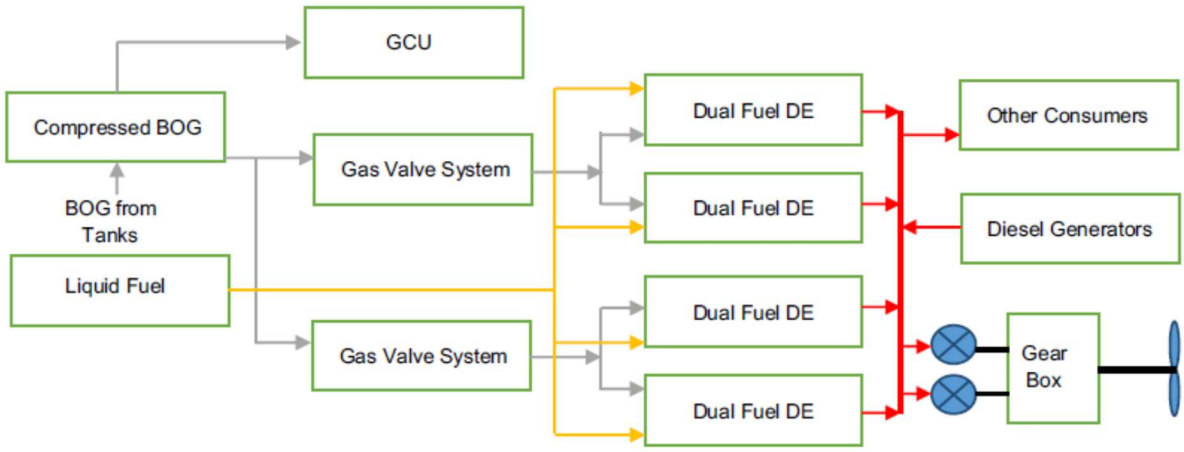

Figure 1-35. Schematic illustration of a ship propulsion installation with a dual fuel diesel electric propulsion system based on dual fuel (DFDE) engines [32]

1.8.3 Methodology for benchmarking natural gas propulsion systems based on the energy efficiency index EEDI

The energy efficiency of a system is the ratio of the energy input to the energy output of the system. In shipping, this is usually translated into the amount of fuel energy required relative to the transport work performed [32]. Energy efficiency has been described as a general term, therefore, there is no single measure of energy efficiency, and instead there is a reliance on different types of indicators to quantify improvements in energy efficiency [32]. While most indicators are based on the simple principle of using less energy to produce the same amount of services provided, there

is a tendency to quantify energy efficiency in relation to environmental benefits, such as the reduction of anthropogenic emissions. [32]

This is the case with the International Maritime Organization (IMO) Energy Efficiency Design Index (EEDI), which is based on a formula for calculating the mass of CO_2 emitted per transport project (metric ton per nautical mile) in a given operational power plant. The actual EEDI is calculated based on formulas and guidelines published by the IMO, and achieving an index value should be below a predetermined initial value that then gradually decreases over a five-year period and it is expected that this will stimulate more efficient projects. This paper uses the EEDI as an analytical tool to analyze the efficiency of the current LNGC fleet. [32]

Although the EEDI only applies to new ships, many studies have attempted to use the EEDI as a tool for analysis on existing ship designs, so as to be able to either predict the impact of this new regulation on propulsion technology or to improve EEDI values for future ship designs. Due to the fact that the majority of LNG carriers use unconventional propulsion systems and were thus excluded from the original EEDI regulations, most studies have focused on a method of calculating EEDI for these unconventional propulsion systems. No study analyzed the EEDI of steam turbine-powered vessels, which made up over 80% of vessels at that time. In 2011, however, there were more detailed studies, covering more types of propulsion, publishing an EEDI calculation method for STPS and DFDE technology. Consequently, these studies were adopted by IMO as the standard on which the current EEDI regulations for LNGCs are based. [32]

An important advantage of the EEDI analysis method is that it is based on established regulations, so its relevance for future LNGC projects needs to be assessed. It is expected that the new LNGC EEDI regulations, adopted in 2014, will come into force from September 2015 for all LNGCs now being received [32]. Another advantage is that as a performance analysis method, it is very detailed and can be specific to LNGCs with different design philosophies and categories such as STPS, DFDE, and SSDR are clearly defined [32]. Future GI propulsion systems are also clearly defined in this method. Also, the efficiency measure using an emission index will have the advantage of reducing man-made emissions [32].

The use of the EEDI analysis method does not take into account emissions other than CO_2. Although the majority of other emissions are covered by other existing regulations, others such as methane emissions are not covered by any regulations, and

therefore there is a possibility that a scheme, while reducing$_{CO2}$ emissions, could result in an increase in other uncontrolled emissions such as methane [32]. Furthermore, using a common EEDI benchmark for three different technologies and their associated efficiencies is likely to cause a large spread within the data as we move from less efficient STPS to more efficient configurations such as diesel propulsion (see following table).

Table 1-13. Comparison of the different propulsion systems used in the energy analysis based on the EEDI index [32]

Prime mover	STPS	DFDE	SSDR
Configuration	Two boilers; HP & LP turbines – 2 cylinder impulse/ reaction turbines	4 Gas/MDO diesel engines (some might be upgraded to burn HFO)	2 Slow speed diesel engines (MAN B&W or Sulzer RT Series)
Fuel used for prime mover	Gas/HFO/MDO	Gas/HFO	HFO
Fuel treatment	HFO preheating, BOG compressing	BOG compressing	HFO purifiers
BOG handling	Burn in boilers, steam dumping	Burning in DF engines, gas combustion unit	2 100% Reliquefaction plants
Transmission	Mechanical drive with reduction gear	Electric drive with 2 slow/high speed propulsion motors	Direct drive
Electric power	2 Steam turbine generators	Available from main generator engines	3 or 4 diesel MDO generator sets
Additional equipment	Boiler exhaust economiser	Exhaust gas auxiliary boiler	Exhaust gas auxiliary boiler
Propulsion unit	FPP; bow and stern thrusters	1 or 2 FPP/CPP with 2 bow thrusters	2 FPP; 2 bow/stern thrusters
Plant efficiencies	Fuel/BOG 100% Boilers 89% St'm cycle 35% Shafting 99% Propulsion eff'cy: 30%	Fuel/BOG 100% DF engines 48% Conversion 98% Motors 98% Gearbox 98% Shafting 99% Propulsion eff'cy: 43%	Fuel 100% Engines 49% Shafting 98% Propulsion eff'cy: 48%
	Fuel BOG 100% Boilers 89% St'm cycle 30% Conversion 96% Electric pwr eff'y: 26%	Fuel/BOG 100% DF engines 48% Alternators 97% Electric pwr eff'y: 47%	Fuel 100% Aux engines 45% Conversion 96% Electric pwr eff'y: 43%

1.8.4 Analysis of the EEDI methodology

The main objectives of the EEDI are to quantify CO_2 emissions from ships and therefore establish baselines for new ships. EEDI regulations were issued for many new ship designs such as oil tankers, cargo ships and container ships from January 2013, while LNG carriers were excluded from these regulations due to initial difficulties in calculating the EEDI values of steam turbine and diesel propulsion which collectively make up over 90% of the current LNG fleet and the corresponding future projections [32]. However, following a comprehensive review, the IMO adopted amendments to MARPOL Annex VI to extend the application of the EEDI for LNG carriers and this was adopted in April 2014 with implementation expected from September 2015 [32] The baseline adopted for LNGCs is shown in the equation below with the phase distribution in the following table [32]].

$$Baseline \text{ value} = 2253.7 \times \text{deadweight}^{-0.474} \quad (1.25)$$

Table 1-14. EEDI limits for LNG carriers [32]

Vessel type	Size	Phase 0	Phase 1 - Sep 2015 - Dec 2019	Phase 2 - 1 Jan. 2020 - 31 Dec. 2024	Phase 3 - 1 Jan. 2025 - thereafter
LNG carrier	>10,000DWT	Not available	10%	20%	30%

1.8.4.1 EEDI analysis of the current LNG fleet

In order to effectively predict the impact of the baseline EEDI limits for LNGCs on the design of future LNG carriers, a statistical analysis of the current fleet of LNGCs was performed. Data of the existing fleet was taken from the Clarkson Global Fleet Register and only ships built in 2000 or later are considered. An estimate for these ships is calculated using the EEDI formula, which takes into account only the main and auxiliary engine ishes, standard fuel consumption (based on MEPC 65 of the International Maritime Organization, 2013), with the tonnage and speed of the ship taken from the Clarkson Global Fleet Register and verified by the registers of the

respective registry [32]. For the different propulsion systems, the estimated EEDI values are summarized in the following table [32].

Table 1-15. EEDI calculation formulas for LNG carriers [32]

	Direct drive diesel	Dual Fuel Diesel Electric	Steam turbine
Margin	Engine: 10% Sea: 20%	Engine: - Sea: 20%	Engine: - Sea: 20%
Design Margin	Margin = $\frac{0.9}{1.2}$ Margin = 75%	Margin = $\frac{1}{1.2}$ Margin = 83%	Margin = $\frac{1}{1.2}$ Margin = 83%
P_{ME}	$P_{ME} = 0.75 \times MCR_{ME}$	$P_{ME} = 0.83 \times \frac{MPP}{\eta_{Electrical}}$	$P_{ME} = 0.83 \times MCR_{ME}$
SFC_{ME} (g/kWh)	190 (HFO)	175 (FBO)	285 (FBO)
P_{AE}	$P_{AE} = (0.025 \times MCR_{ME}) + 250 + (Capacity \times BOR \times COP_{reliq} \times R_{reliq})$	$P_{AE} = (0.025 + 0.02) \times P_{ME} + 250$	$P_{AE} = 0$
EEDI	$3.1144(gCO_2/gHFO) \times \frac{(190 \times P_{ME}) + 215 \times P_{AE}}{Capacity \times V_{ref}}$	$2.75(gCO_2/gBOG) \times \frac{(175 \times P_{ME}) + 175 \times P_{AE}}{Capacity \times V_{ref}}$	$2.75(gCO_2/gBOG) \times \frac{285 \times P_{ME}}{Capacity \times V_{ref}}$

1.8.4.2 Including methane leakage in the calculation of the index EEDI

With diesel-electric propulsion, despite having the best EEDI values of all propulsion types, it suffers from a major drawback: methane slip [32]. This term refers to the escape of the exhaust gas released into the atmosphere by the internal combustion engine. Methane is a very potent gas that contributes significantly to global warming, so that this has a negative impact that outweighs the benefits to the EEDI value from reduced CO_2 emissions [32]. The result is worrying because methane has a 20 to 25 times worse effect on global warming than carbon dioxide if we calculate the effects over a 100-year cycle, while over a 20-year period the effect is 72 times worse [32]. This means that the release of even very small volumes of natural gas will offset the entire gain in CO_2 emission reductions from increased engine efficiency [32]. Therefore, when calculating the effect of CO_2 emissions, based on the EEDI calculation relationships, methane emissions should be taken into account as CO_2 equivalent emissions [32].

The issue of methane leakage is more pronounced in four-stroke engines used in diesel-electric propulsion (DFDEs) than in gas and diesel injection engines, primarily because in four-stroke DFDEs, unburned methane is trapped in combustion chamber clearances such as piston springs and valve seats. In these gaps, the mixture has an air-fuel ratio such that the gas cannot be completely burned during combustion and is thus released with the exhaust gases during the exhaust path [32]. On the other hand, gas injection engines operate with direct gas injection as in conventional diesel engines, ensuring that the gas is present during the compression stroke or during the sweep period, thus reducing methane emissions to levels almost comparable to conventional liquid fuels [32]. Considerable research has been carried out to reduce methane emissions, focusing on the use of a combustion chamber and on improving combustion

technology (optimizing injection timing, increasing injection pressure and increasing intake air temperature) [32]. In the case where it is not possible to reduce methane leakage within the combustion chamber, the use of an oxidation catalyst to capture methane in the engine exhaust has been considered [32]. However, for most DFDE technology engines, methane leakage has been reduced to 3-4 g/kWh compared to 8-15 g/kWh for existing DFDEs [32]. For the Wartsila 50DF engine installed in the majority of DFDE engines the methane escape is about 8 g/kWh [32]. Since the average specific fuel consumption (SFC) of these engines is about 175 g/kWh, the following calculations are used to convert methane to CO_2 equivalent emissions [32]:

Methane emissions = 8 g/kWh

SFC = 175 g/kWh

Equivalent methane: SFCme = 8/175 = 4.57%

Assuming that 1 tonne of fuel gas containing methane is burned in the DFDE engines then 2.75 tonnes of CO_2 is produced assuming 4.57% methane leakage. Therefore 1 ton of fuel gas containing methane produces 2.624 tons of CO_2 and 0.0457 tons of CH_4 [32]. Considering that over a 100 year life cycle the effect of methane is 21 times greater than that of carbon dioxide we conclude that the total equivalent CO_2 emissions are:

Total CO_{2equiv} = 2.624 + (0.0457 x 21) = 3.5837 tCO_{2equiv}

Considering that over a 20-year life cycle the effect of methane escaping into the atmosphere is 72 times greater than that of carbon dioxide, it follows that:

Total CO_{2equiv} = 2.624 + (0.0457 x 72) = 5.9144 tCO_{2equiv}

Thus, the CO_2 equivalent emissions taking into account the escape of 1 tonne of methane into the atmosphere are 3.5837 tonnes of CO_2 equivalent with a 100-year life cycle analysis and 5.9144 tonnes of CO_2 equivalent with a 20-year life cycle reference [32].

1.8.5 Results and comments

1.8.5.1 Results of the EEDI analysis

Table 1-15 summarizes the results from the EEDI analysis for the different types of natural gas propulsion considered here. The base equation is a fair representation of the fleet with approximately 23% of the fleet around or just below the baseline during the Phase 0 period, as shown in Figure 1-36. If Phase 1 is applied, almost all steam turbine vessels are outside the predicted EEDI limits [32]. 76% of the propulsion systems with direct drive diesel engines are above the initial limit. LNG carriers with diesel propulsion systems are all below the initial limit (Figures 1-36 to 1-39). If Phase 2 is implemented all steam turbine and direct drive diesel propulsion systems will be above the original EEDI curve while 97% of diesel propulsion systems are still below the baseline EEDI limits [32]. Two main conclusions can be drawn from the EEDI-based analysis of the current LNG carrier fleet:

1. In terms of energy efficiency in g CO_2//tNM of the current fleet compared to the current EEDI baseline, diesel-electric propulsion offers the most efficient propulsion option with steam turbines offering the least efficient solution. The solution of direct connection of diesel engines to propellers is in between the two previous solutions in terms of efficiency [32].
2. The current limits from IMO are a fair representation of the current fleet with approximately 23% of the current fleet analyzed being around or below the baseline. However, this figure is a summary of the different propulsion systems used by LNG carriers and due to the large dispersion around the EEDI baseline curve the most efficient diesel propulsion solution falls well below the initial threshold [32]. Considering that 72% of future orders for LNG carriers will be with a diesel propulsion system, the 30% improvement of the EEDI index as suggested by IMO from 2025 onwards will have no effect on diesel propulsion systems since they already meet these future thresholds [32]. This has the effect of not motivating technology improvements for future LNG carrier designs [32].

Table 1-16. Compliance of different LNG carrier propulsion types with the EEDI energy index [32]

Type of propulsion (number of vessels)	**Compliance with Phase 0**	**Phase 1, Compliance Sep 2015 - Dec 2019**	**Phase 2, Compliance 21 Jan 2020 - 31 Dec 2024**	**Phase 3, Compliance 1 Jan 2025 - onwards**

Diesel-electric propulsion (32)	32 (100%)	32 (100%)	31 (97%)	18 (56%)
Direct engine - propeller connection (21)	8 (38%)	5 (24%)	0 (0%)	0 (0%)
Steam Turbine (159)	7 (6%)	1 (0.6%)	0 (0%)	0 (0%)
Total (212)	47 (23%)	38 (18%)	31 (15%)	18 (8%)

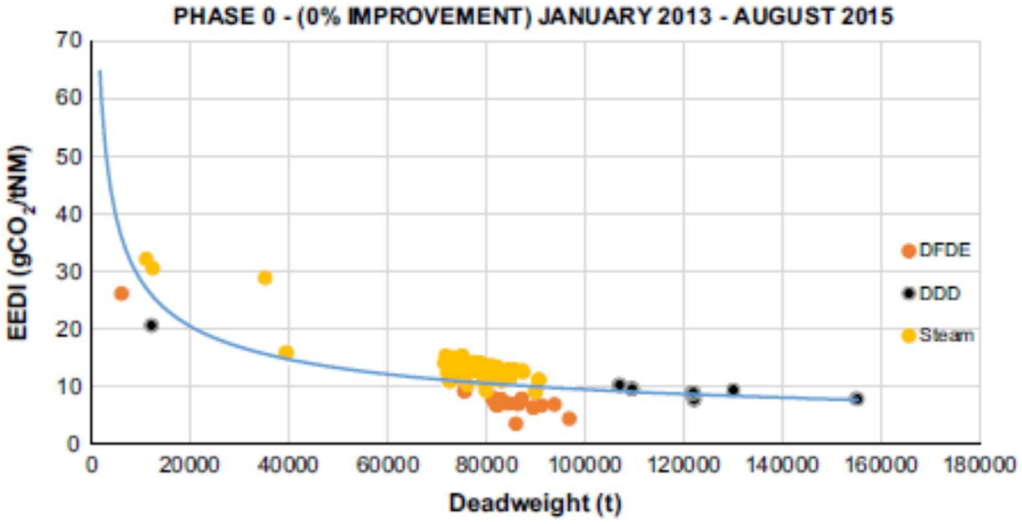

Figure 1-36. Phase 0 (0% improvement) January 2013 - August 2015 [32]

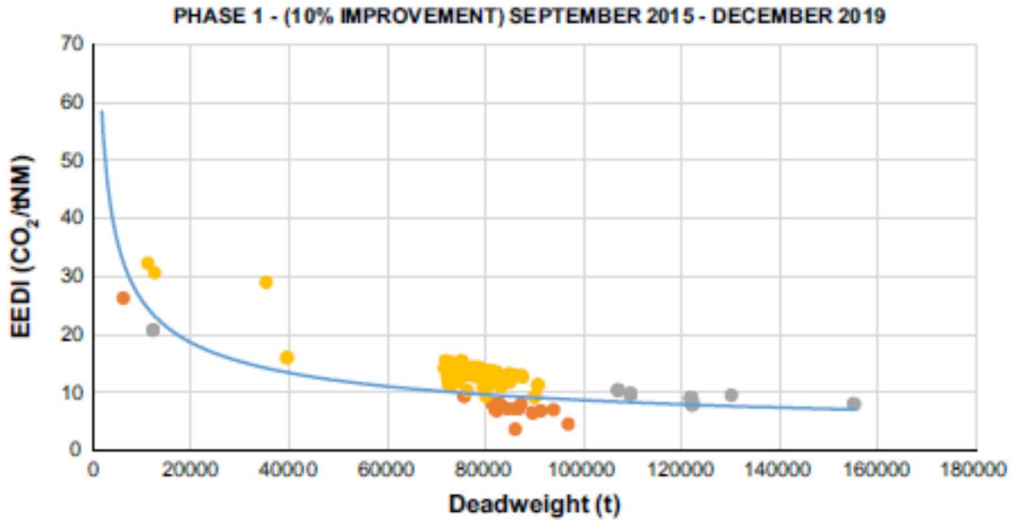

Figure 1-37. Phase 1 (10% improvement) September 2015 - December 2019 [32]

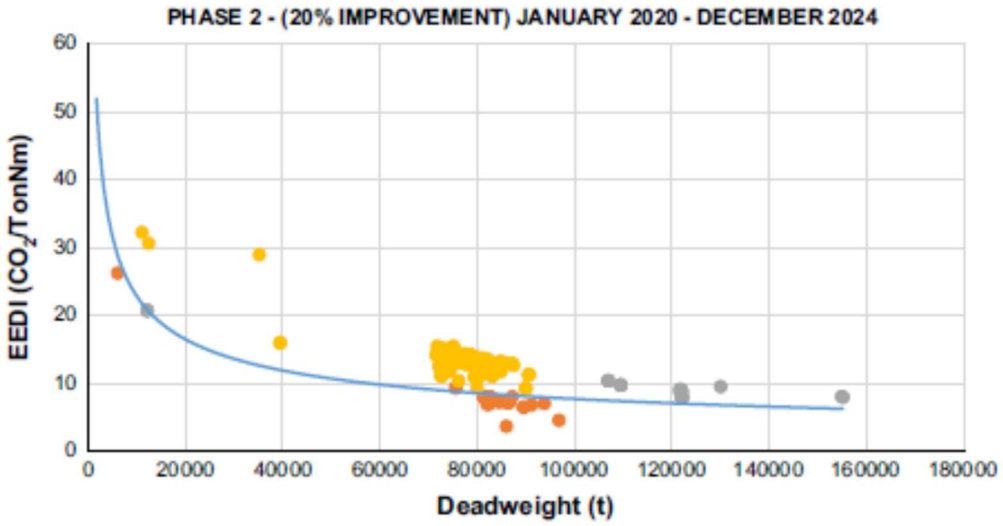

Figure 1-38. Phase 2 (20% improvement) January 2020 - December 2024 [32]

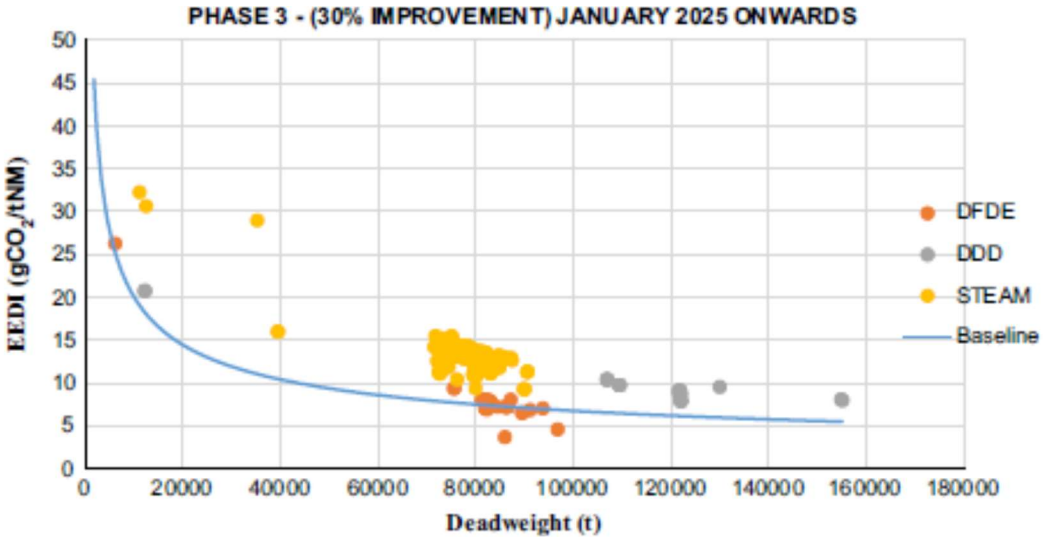

Figure 1-39. Phase 3 (30% improvement) January 2025 and beyond [32]

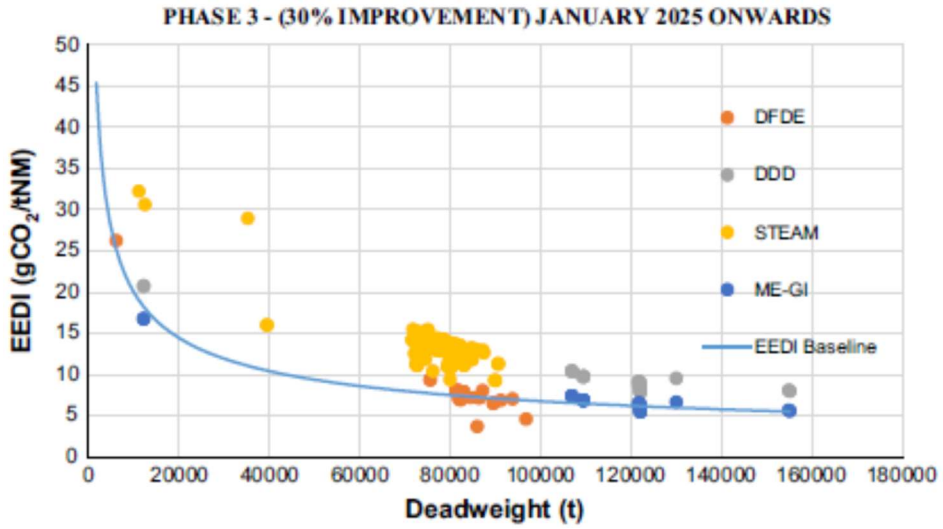

Figure 1-40. Phase 3 (30% improvement) from 2025 onwards with gas injection engines [32]

1.8.5.2 EEDI results of gas injection engines

Figure 1-41 shows the results of the EEDI analysis of ships with gas injection engines. The upcoming gas injection engines that will be in 60% of future orders with direct drive diesel engines of LNG carriers offer a 30% improvement in EEDI values compared to current Direct Drive Diesels (DDD) propeller direct drive solutions and this is due to the reduction in specific fuel consumption, reduction in carbon factor and elimination of the need for a re-liquefaction facility [32]. Such improvements in DDD technology puts it on par with DFDEs to comply with the EEDI regulation from 2025 onwards [32]

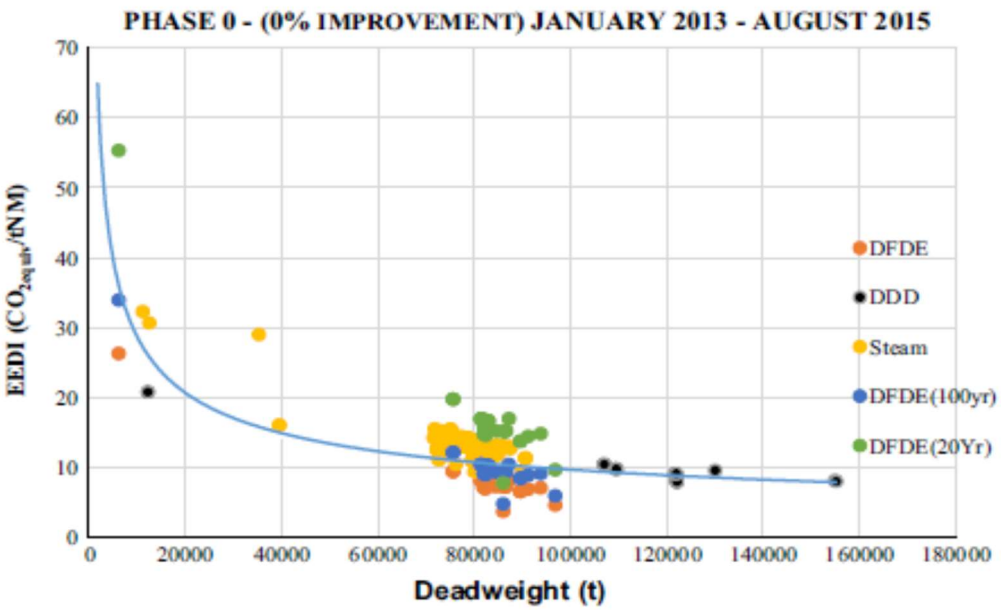

Figure 1-41. Phase 0 (with 0% improvement of the baseline EEDI curve), representing the CO_2 emission index to indicate the 20 and 100 year increase [32

]

1.8.5.3 Considering methane leakage

When methane is analyzed as part of the EEDI analysis the aforementioned efficiency of diesel propulsion systems is reduced [32]. Taking a time horizon of 100 years, the CO_2 equivalent emissions increase by 30%, with the corresponding index value falling around or just below the baseline, while with a time horizon of 20 years the carbon factor increases by 115%, with the corresponding EEDI (modified) value being well above the baseline. This carbon factor is much higher than that of steam turbine propulsion systems, which have the lowest efficiency [32].

1.8.5.4 The effects of methane leakage

It is obvious that the impact of methane leakage on the global environment needs to be considered in more detail, especially in light of the fact that methane emissions are potentially higher on LNG ships with diesel-electric propulsion systems [32]. Some researchers [32] have attempted to downplay the methane emission impacts of diesel propulsion by stating that the combination of methane and CO_2 emissions are actually lower as total equivalent CO_2 emissions than fuel oil propulsion system options [32]. The results of the EEDI analysis presented here clearly refute these claims, as the analysis showed that methane emissions are much higher than other LNG ship propulsion options when considering the impacts over a 20-year life cycle [32]. The lifetime of methane is also shorter than 20 years, so how the environmental impacts of methane emissions compare to CO_2 emissions, which remain in the atmosphere for a much longer period of time than methane emissions need further investigation [32].

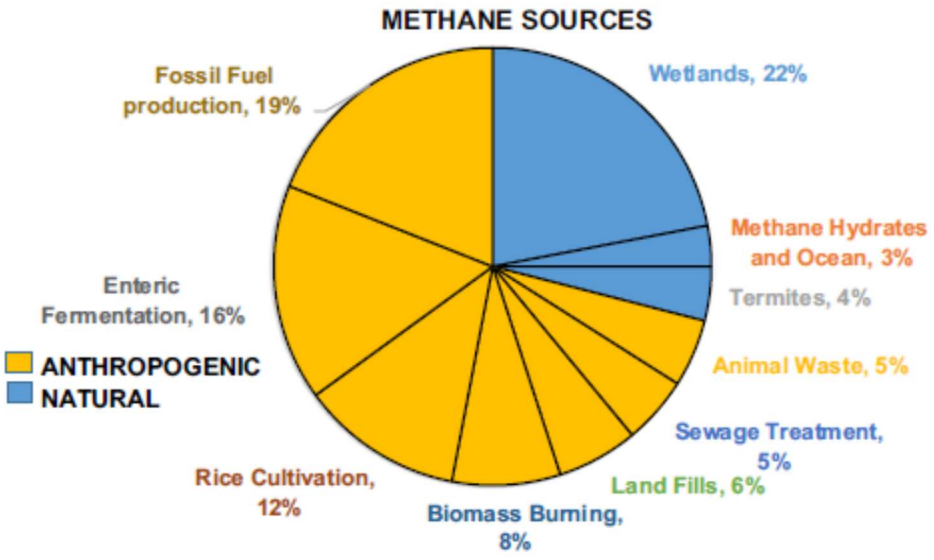

Figure 1-42. Sources of methane emissions [32]

Methane emissions are released into the atmosphere through a variety of sources, classified as natural as well as anthropogenic sources related to human activity. The natural sources of methane are wetlands, termites and oceans which account for 29% of emissions, while anthropogenic sources including fossil fuels, agriculture, landfills and biomass burning make up the other 71% of methane emissions [32] (see Fig. Figure 1-42 which shows the full distribution of methane emission sources). Methane is removed from the atmosphere by a number of chemical and biological processes including tropospheric oxidation, stratospheric oxidation and uptake by soils [32]. These processes convert methane into less environmentally harmful products.

Most methane occurs in the troposphere where tropospheric oxidation removes 87% of the total amount of methane absorbed from the atmosphere [32]. Above the troposphere is the stratosphere where 7% of methane uptake occurs through stratospheric oxidation while the remaining 6% is captured by soil uptake during the soil-atmosphere interface phase, where bacteria present in the soil oxidize methane by excluding it from the atmosphere [32].

Because methane removal processes are stable, increases in methane emissions continuously increase methane atmospheric pollution [32]. It is estimated from the atmospheric concentration of methane that it has increased by a factor of 2.6 since the pre-industrial era [32], which is significantly higher than CO_2 emissions which are estimated to have increased by only 40%, as shown in Table 1-17. These increases in greenhouse gas concentrations increase the amount of energy remaining in the atmosphere, and this extra energy called "radiative forcing" is estimated to be 2.9 W/m^2 [32] Of this, 1.88 W/m^2 is attributed to CO_2, making it the most important cause of global warming, while 0.49 W/m^2 is attributed to methane [32]. It is evident that methane contributes 17% of the total radiative forcing, proportionally much higher than expected according to the atmospheric concentration of gases, since only 1,190 ppb contributes 17% of the total radiative forcing compared to 115,400 ppb of CO_2 which contributes 64% of the total radiative forcing, thus highlighting the high activity of methane emissions [32].

Table 1-16. Atmospheric concentration of greenhouse gases [32]

	CO_2	**CH_4**	**N_2O**
Pre-industrial concentration (reference year 1750), ppb	280,000	700	270
Concentration in 2013 (ppb)	422,000	1934	336
Relative change in concentration 2013 to 1750	1.4	2.6	1.21
Radiation potential (W/m^2)	1.88	0.49	0.17
Lifespan in the atmosphere (years)	5 - 200	12	114

Table 1-17. Lifespan of greenhouse gases in the atmosphere and relative Global Warming Potential (GWP) for 20-year, 100-year and 500-year lifespans [32]

Greenhouse gas	Lifespan (years)	GWP 20 years	GWP 100 years	GWP 500 years
CO_2	5 – 200	1	1	1
CH_4	12	72	25	7,6
N_2O	114	289	298	153
HFCs	0.3 – 260	40 – 12,000	12 – 14,800	4 – 12,200
PFCs	2600 – 50,000	3900 – 8000	5700 – 11,900	8900 – 18,000
SF_6	3200	16,300	22,800	32,6000

1.8.6 Conclusions of the theoretical evaluation of different types of LNG carrier propulsion based on the EEDI

In order to investigate the impact of LNG transport on the EEDI, the energy and environmental performance of three different propulsion systems that can be used on LNG carriers was examined, mainly in terms of CO_2 and CH_4 emissions. In particular, the use of a steam turbine propulsion system, the use of a 2-S marine diesel engine with gas injection directly connected to the ship's propeller (Diesel Direct Drive - DDD) and the use of a Dual Fuel electric propulsion (DFDE) system were examined. This study resulted in the following four main conclusions:

- From the point of view of specific CO_2 emissions (in grams per normal ship tonnage), the diesel-electric propulsion system (DFDE) shows the lowest specific CO_2 emissions among the three different propulsion systems tested for LNG carriers. In contrast, the steam turbine propulsion system had the highest specific CO_2 emissions while the direct engine-propeller coupling system had specific CO_2 emissions among the two mentioned above [32].
- The current IMO limits for the EEDI are more or less met by about 23% of the current LNG carrier fleet. On this percentage of existing LNG carriers various propulsion systems are used. It is worth noting that the EEDI values corresponding to LNG carriers' diesel propulsion systems are much lower than the existing EEDI baseline. Considering that 72% of future orders (reference year 2015) for LNG carriers will have a dual-fuel diesel propulsion system, a 30% improvement of the current EEDI values from 2025 onwards, as suggested by the IMO, does not require additional measures to improve the energy efficiency of current dual-fuel diesel propulsion systems as they already meet these limits [32].

- 2-Stroke Gas-injected auto-ignition engines, which constitute 60% of the LNG carriers ordered for the near future and which will be used in direct-drive propulsion (DDD) systems, are expected to offer about 30% improvement in the EIDI compared to current DDD systems due to the reduction in specific fuel consumption, the reduction in CO_2 emissions and the elimination of the need to install a Boil Off Gas (BOG) unit [32]. Such improvements in DDD technology brings them on a par, in terms of EEDI achieved, with diesel-electric propulsion systems with dual-fuel engines. Both propulsion systems (DDD and DFDEs) are fully compliant with EEDI requirements from 2025 onwards [32].
- When methane leakage is taken into account in the EEDI 'picture' as CO_2 equivalent emissions, the energy efficiency of dual-fuel diesel propulsion systems is reduced. Taking a time horizon of 100 years, total CO_2 emissions increase by 30% with the corresponding EEDI value falling around or just below the current baseline of the EEDI values. In contrast, over a 20-year time horizon, total CO_2 emissions increase by 115% with the corresponding estimated EEDI value being well above the current baseline, outperforming even the current steam turbine propulsion system with the lowest efficiency [32].

1.9 Conclusions from the literature review

The following main conclusions on the advantages and disadvantages of using natural gas in marine diesel engines were drawn from a thorough study of the literature:

- Today and for many years to come there is a large availability of natural gas for use in various applications due to the recent discovery of large underground reserves in various parts of the world. This is an advantage of natural gas as it ensures its uninterrupted use in marine engines for many years to come.
- Natural gas is significantly less expensive than heavy and light oil derivatives currently used in marine engines. This competitive cost advantage of natural gas over other marine fuels is expected to remain until at least 2035.
- The combustion of natural gas in 2-S and 4-S marine SI engines leads to significantly lower NOx and CO_2 emissions than conventional diesel engines. It also leads to elimination of SOx emissions, minimization of particulate matter (PM emissions) and leaves no solid residues as fuel oil combustion does. In contrast to the above, the combustion of natural gas in compression ignition

engines leads to a significant increase in unburned hydrocarbons and a worsening of the phenomenon of gross methane leakage compared to conventional operation. In particular on the issue of methane, if this is taken into account by the IMO in the formulation of energy efficiency indicators and measures to record and reduce CO_2 emissions from ships, it is expected to significantly change the relevant IMO legislation in the field of CO_2 emissions.

- Several classification societies have developed specific rules for the construction of LNG and LPG carriers in recent years, resulting in a "road map" for the construction of such ships.
- Nowadays a very large number of dual fuel marine engines of different sizes and operational performance are available on the commercial market from various major engine manufacturers. However, the use of natural gas as a marine fuel in shipping requires structural modifications to existing marine engines and additions to the fuel supply systems of a ship's main and auxiliary engines. Additional modifications to the ship's networks are also required for safety reasons regarding the handling of natural gas on board ships.
- Over the last decades, shipyards, shipowners, engine manufacturers and classification societies have accumulated considerable experience in the construction and management of LNG and, to a lesser extent, CNG carriers, which guarantees the seamless management of new and existing offshore gas transport constructions. However, what must be taken into account in any case is the higher cost of building newbuild LNG carriers compared to conventional tankers.
- Finally, a disadvantage of using natural gas in shipping is the limited onshore infrastructure for supplying ships with natural gas: In particular, to make it attractive to transport LNG and use it as a fuel for the majority of ships, an international network of LNG onshore transhipment terminals would have to be built.

2 Operational and Environmental Assessment of 4-S Dual Fuel Engines

2.1 Introduction

In this chapter the operational and environmental assessment of dual-fuel compression ignition engines is carried out, with emphasis on those used in marine applications. This evaluation is divided into two parts: in the first part, the effect of natural gas combustion in compression ignition engines will be studied based mainly on experimental results from extensive and thorough studies by the engine developer AVL [37,38]. These experimental results concern measurements carried out on dual-fuel auto-ignition engines with pilot injection of oil up to 5% of the respective required quantity at a given load and on dual-fuel auto-ignition engines with pilot injection of oil in the pre-chamber at 1% of the respective required quantity at a given load. In the second part of this chapter, experimental results for the operating parameters and air and particulate pollutant emissions of a marine diesel engine that also operates as a dual-fuel engine will be examined. In this study, the results for the operational behavior and emissions of the diesel engine for conventional diesel operation are compared with corresponding results obtained for dual fuel (diesel/gas) operation of the same engine [39].

2.2 Experimental investigation of AVL for natural gas combustion in compression ignition engines with or without pre-chamber

2.2.1 Description of the experimental test engine and experimental test cycles

This detailed investigation of AVL [38] was carried out on the FM250 single-cylinder turbocharged auto-ignition engine. The experimental setup of this engine is shown in Figure 2-1. The AVL [37] FM250 compression ignition engine [37] has a cylinder diameter of 250 mm and a piston stroke of 320 mm. This engine can be operated either

burning only oil or burning almost only gas with pilot injection of a small quantity of oil or finally as a dual fuel compression ignition engine. The maximum rotational speed of this engine is 1050 RPM and the maximum average piston speed is 10,7 m/s. The maximum value of the average effective pressure of this AVL engine is 30 bar. The maximum limit set by AVL in the design of the specific engine in terms of maximum combustion pressure [38] is equal to 250 bar. AVL's FM250 engine has a variable geometry combustion chamber, which allows the engine to be operated with different compression ratios [38]. The fuel oil injection system used in the AVL FM250 engine is a high-pressure common rail fuel injection system which develops a maximum injection pressure equal to 2500 bar. As far as the gas supply system of this test engine is concerned, this can be done either by central mixing or by injecting the gas into the engine intake [38].

Figure 2-1. Photo of the experimental installation of the AVL FM250 single-cylinder compression-ignition engine [38]

As part of an extensive experimental investigation to examine the effect of natural gas on marine SI engines, AVL carried out experimental tests on the FM250 engine considering that:

- This engine operates on the basis of the E3 experimental test cycle whereby the engine operates as a dual fuel main propulsion engine of a dual fuel ship, which is "loaded" by the brake based on the propeller load demand curve (propeller curve).

- This engine is operated on the basis of the E2 test cycle whereby the engine is operated as a main gas engine propulsion engine at constant speed with the engine's propulsion chamber supplied with natural gas.
- This engine shall operate on the basis of the D2 test cycle whereby the engine shall operate as an auxiliary gas engine for the production of electric power at constant speed with the supply of natural gas to the engine propulsion chamber.

Figure 2-2 schematically illustrates the variation of motor load versus speed for the experimental cycles E3, E2 and D2 [38].

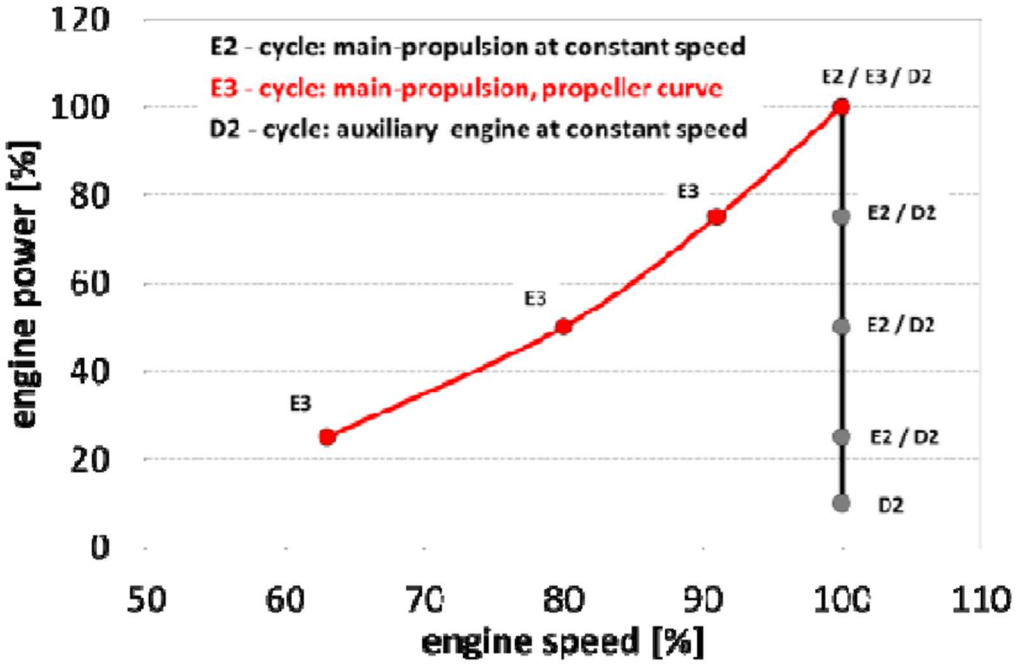

Figure 2-2. Schematic illustration of the variation of motor load versus speed for the experimental cycles E3, E2 and D2 [38]

2.2.2 Experimental results of AVL FM250 engine – E3 dual fuel main propulsion engine test cycle

Figure 2-3 shows experimental results of AVL's FM250 gas engine, which display the variation of the average effective pressure, effective efficiency, maximum combustion pressure, pilot oil injection rate, and the time duration in degrees of crank angle of the combustion duration of 50% of the total fuel quantity as a function of engine rotation speed [38]. The previously mentioned results refer to experimental tests carried out based on the E3 test cycle on AVL's FM250 engine, which was operated as a dual fuel main propulsion engine with a compression ratio equal to 12:1, with a maximum rotational speed of 750 RPM, with a piston volume Vh = 16 dm^3, with a pilot

injection pressure of 1000 bar and an intake temperature of 45ºC. For the above measurement cases the FM 250 engine had a single-stage supercharging system and the methane number of the gas was equal to 90.

As can be seen from the examination of the experimental results in Figure 2-3, the highest actual efficiency (about 42.5%) of the AVL dual-fuel FM 250 dual-fuel engine is achieved at the maximum rotational speed and maximum power of this engine with a pilot oil injection amount of 1% [38]. Further as observed from Figure 2-3 when the rotational speed of the engine is reduced then:

- The pilot injection lead time and the corresponding burn time of 50% of the fuel quantity (MFB50%) should be reduced to keep the covariance (COV) of the mean indicated pressure (IMEP) less than 2%.
- The pilot fuel oil quantity should be increased to achieve efficient combustion initiation (Constant NOx emissions).

Furthermore, observation of the experimental results in Figure 2-3 shows that the maximum combustion pressure did not exceed 200 bar at maximum power, which is particularly encouraging because it means that never during the tests did the engine exceed the 250 bar maximum combustion pressure limit and therefore there was never an issue of engine durability.

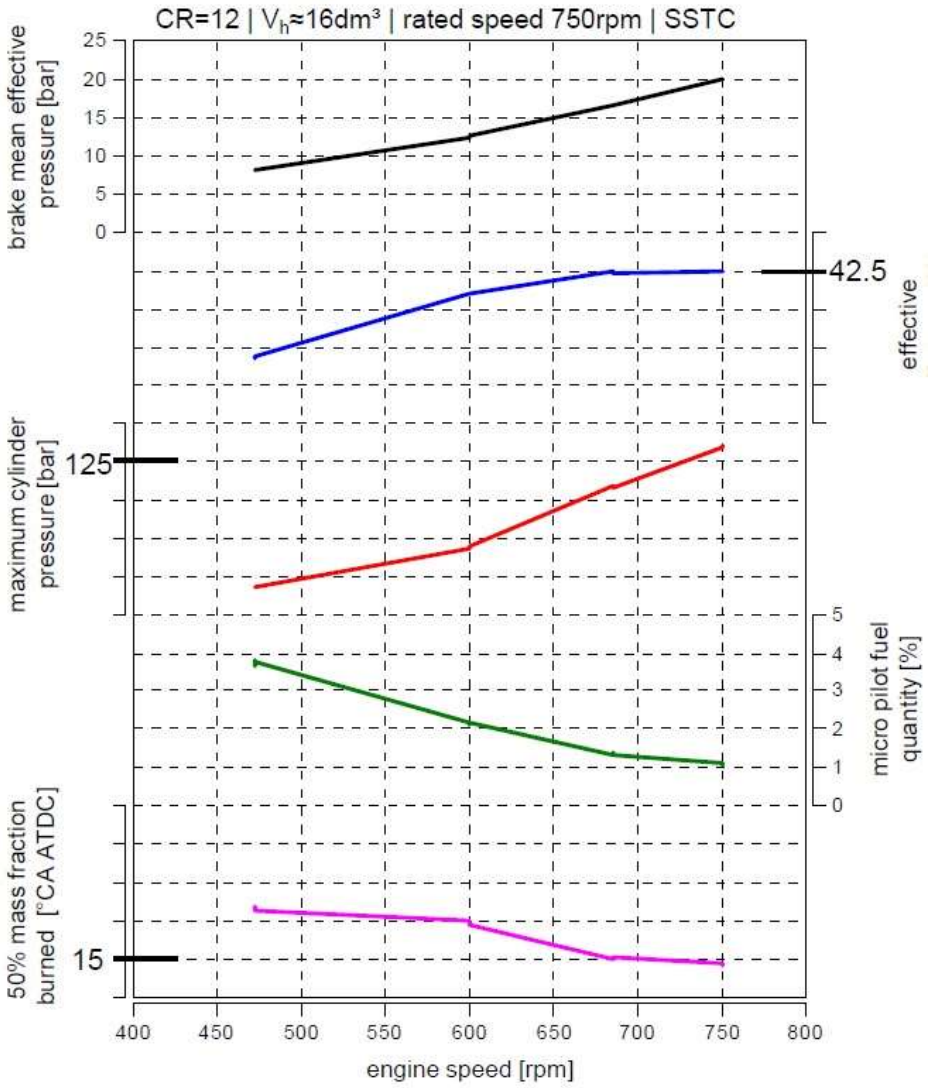

Figure 2-3. Experimental results of AVL's FM250 gas engine for the variation of the average effective pressure, effective efficiency, maximum combustion pressure, pilot oil injection micro-quantity and the time duration in degrees of crank angle of 50% of the total fuel quantity as a function of engine rotation speed [38]. The experimental results have been obtained for test cycle E3 of AVL's FM 250 single cylinder compression ignition engine [38].

Figure 2-4 shows experimental results of the AVL FM250 gas engine, which show the variation of fuel air equivalence ratio, specific NOx emissions (in g/kWh), specific THC emissions (in g/kWh), specific CO emissions (in g/kWh) and soot emissions (in FSN) as a function of engine speed [38]. The aforementioned results refer to experimental tests carried out based on the E3 test cycle on the AVL FM250 engine, which was operated as a dual fuel main propulsion engine with a compression ratio equal to 12:1, with a maximum rotational speed of 750 RPM, with a piston volume Vh = 16 dm^3, with a pilot injection pressure of 1000 bar and an intake temperature of 45ºC.

For the above measurement cases, the FM 250 engine had a single-stage supercharging system and the methane number of the gas was equal to 90 [38].

As can be seen by examining the experimental results in Figure 2-4, the air/fuel equivalence ratio remains approximately the same with varying speed and load. This indicates that the FM 250 engine during the E3 cycle tests had a constant air/fuel combustion ratio within the combustion chamber. Furthermore, according to Figure 2-4, at all four test points of the E3 cycle an extremely low NOx emission level equal to about 2 g/kWh can be achieved [38]. What is worth noting is the high THC and CO emission values at all test points, which are higher than in conventional operation [38]. Finally, it is particularly encouraging that soot is not a significant issue during operation of the dual fuel FM 250 engine at all tested speeds since its absolute value was approximately equal to zero (smokeless operation).

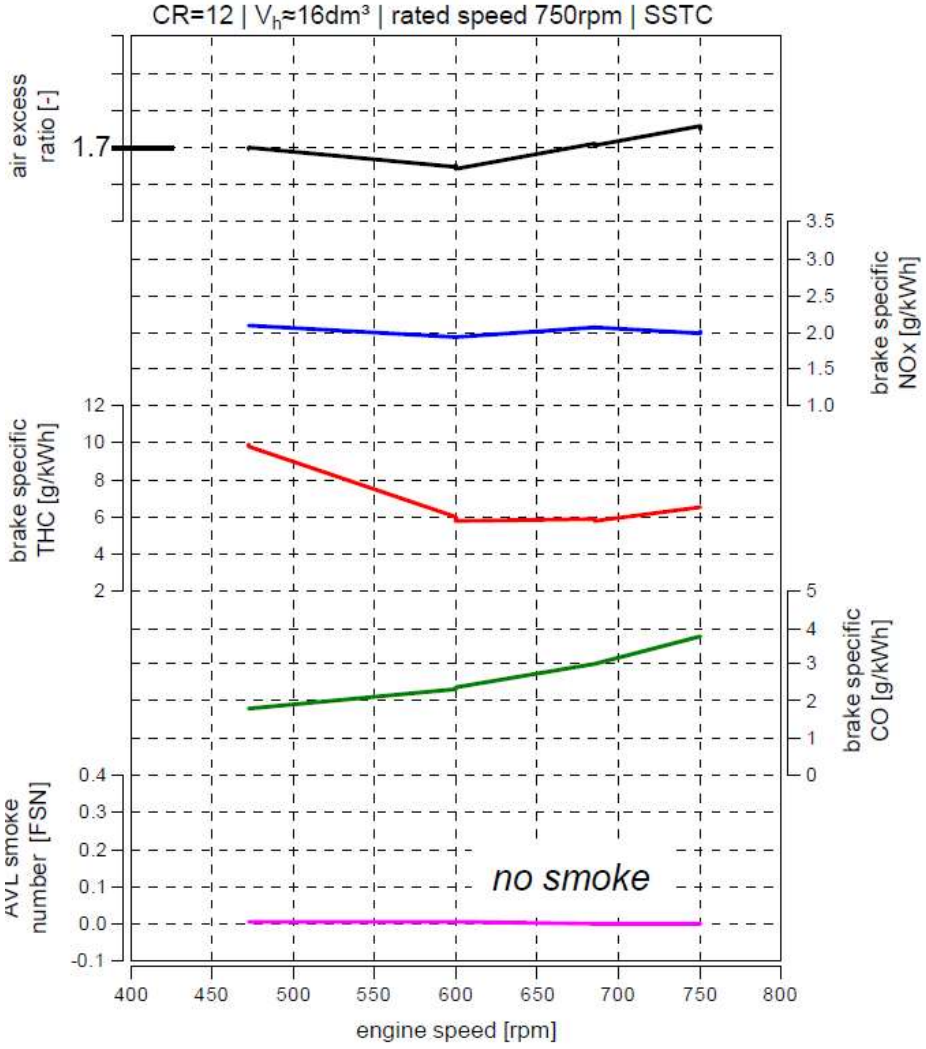

Figure 2-4. Experimental results of AVL's FM250 gas engine for the variation of fuel air equivalence ratio, specific NOx emissions (in g/kWh), specific THC emissions (in g/kWh), specific CO emissions (in g/kWh) and soot emissions (in FSN) as a function of engine speed

[38]. The experimental results have been obtained for test cycle E3 of AVL's FM 250 single cylinder compression ignition engine [38].

2.2.3 Experimental results of AVL FM250 engine - Test cycles of main and auxiliary gas engine with E2/D2 pre-chamber

Figure 2-5 shows experimental results of AVL's FM250 gas engine, which display the variation of the average effective pressure, effective efficiency, maximum combustion pressure, pilot oil spray micro-quantity in the antechamber and the time duration in degrees of crank angle of the 50% total fuel quantity combustion duration as a function of engine load [38]. The aforementioned results refer to experimental tests carried out based on the E2/D2 test cycles on the AVL FM250 engine, which was operated as a dual fuel main propulsion engine in the E2 cycle and as an auxiliary engine in the D2 cycle with a compression ratio equal to 12:1, with a maximum rotational speed of 1000 RPM, with a piston volume V_h = 16 dm^3 and with an intake temperature of 50ºC. For the above measurement cases, the FM 250 engine had a two-stage supercharging system and the methane number of the gas was equal to 90 [38].

As shown by examining the experimental results in Figure 2-5, the actual efficiency increases significantly with increasing load [38]. The maximum efficiency in the case of these tests occurs at the maximum load and is approximately equal to 46%. The maximum combustion pressure remained high at all loads and even for loads above 95% it exceeded the 200 bar limit [38]. Therefore, running the same engine with pilot oil injection in the pre-chamber leads to higher values of maximum combustion pressure compared to running it as a dual fuel engine during the E3 test cycle. As shown by the straight line variation of the burn time of 50% of the fuel quantity with load, the engine operation was stable at all loads with a covariance of the mean indicated pressure (IMEP) of less than 1%. As evidenced by Figure 2-5, a 1% pilot oil injection micro-quantity in the engine pre-chamber is sufficient for strong ignition, which leads to rapid flame spread in the main combustion chamber [38].

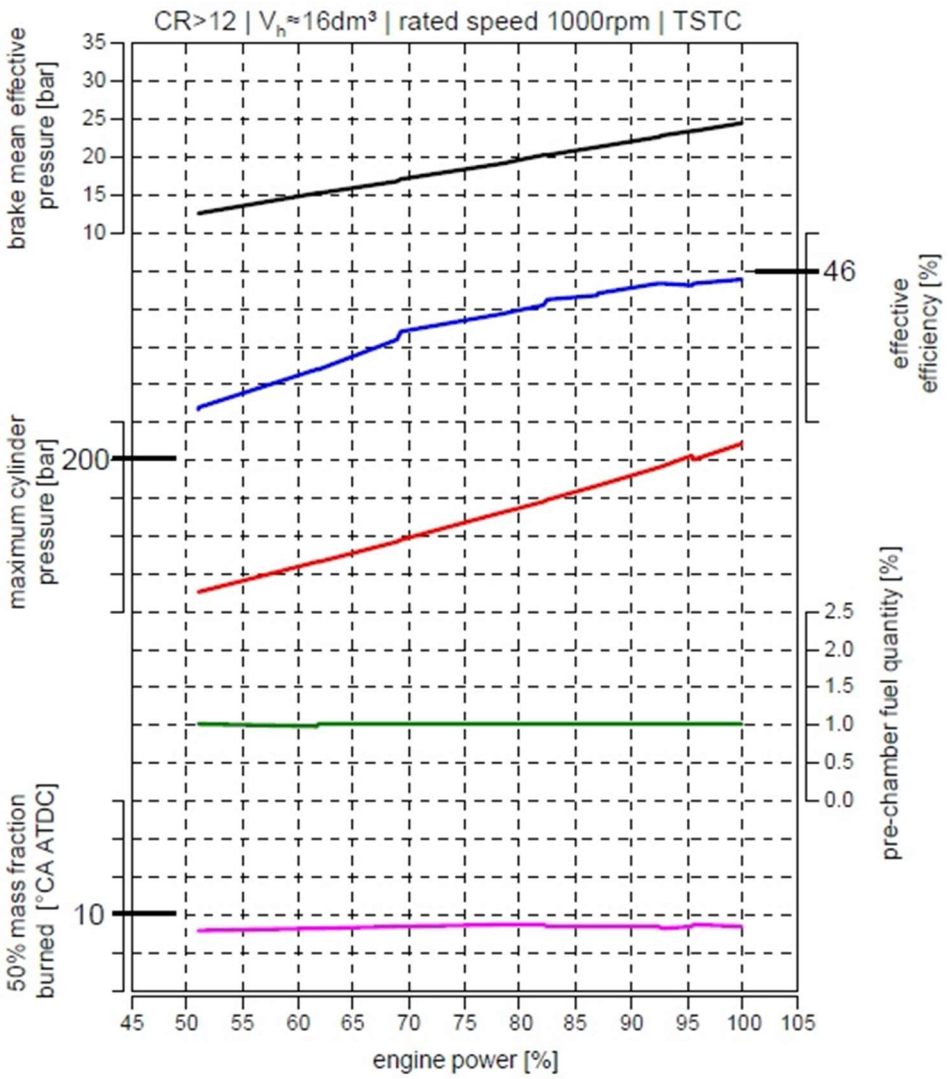

Figure 2-5. Experimental results of AVL's FM250 gas engine for the variation of the average effective pressure, effective efficiency, maximum combustion pressure, pilot oil injection amount in the antechamber and the time duration in degrees of crank angle of 50% of the total fuel quantity as a function of engine load [38]. The experimental results have been obtained for the E2/D2 test cycles of AVL's FM 250 single cylinder compression ignition engine [38].

Figure 2-6 shows experimental results of the AVL FM250 gas engine, which show the variation of fuel air equivalence ratio, specific NOx emissions (in g/kWh), specific THC emissions (in g/kWh), specific CO emissions (in g/kWh) and soot emissions (in FSN) as a function of engine load [38]. The aforementioned results refer to experimental tests carried out based on the E2/D2 test cycles on AVL's FM250 engine, which was operated as a dual-fuel main propulsion engine in the E2 cycle and as an auxiliary engine in the D2 cycle with a compression ratio equal to 12:1, with a maximum rotational speed of 1000 RPM, with a piston volume V_h = 16 dm^3 and an

intake temperature of 50ºC. For the above measurement cases, the FM 250 engine had a two-stage supercharging system and the methane number of the gas was equal to 90 [38].

As shown by examining the experimental results in Figure 2-5, the air/fuel equivalence ratio should increase with increasing load starting from 1.9 and going up to 2.0 at the maximum load tested [38]. When increasing the air/fuel ratio with increasing engine load, NOx emissions were kept constant. Particularly important, during the operation of the compression ignition engine with pilot injection of oil in the pre-chamber and ignition of natural gas in the pre-chamber, it was observed that this engine complied at all loads tested with the strictest nowadays NOx emission limits prescribed by the IMO (Tier III). It is also very important that the emissions of UHC and carbon monoxide (CO) are lower than those of the dual fuel operation of the engine under consideration [38]. Finally, in all cases of operation of the FM 250 gas engine with pre-chamber, smokeless operation or in other words, zero soot emissions are observed [38].

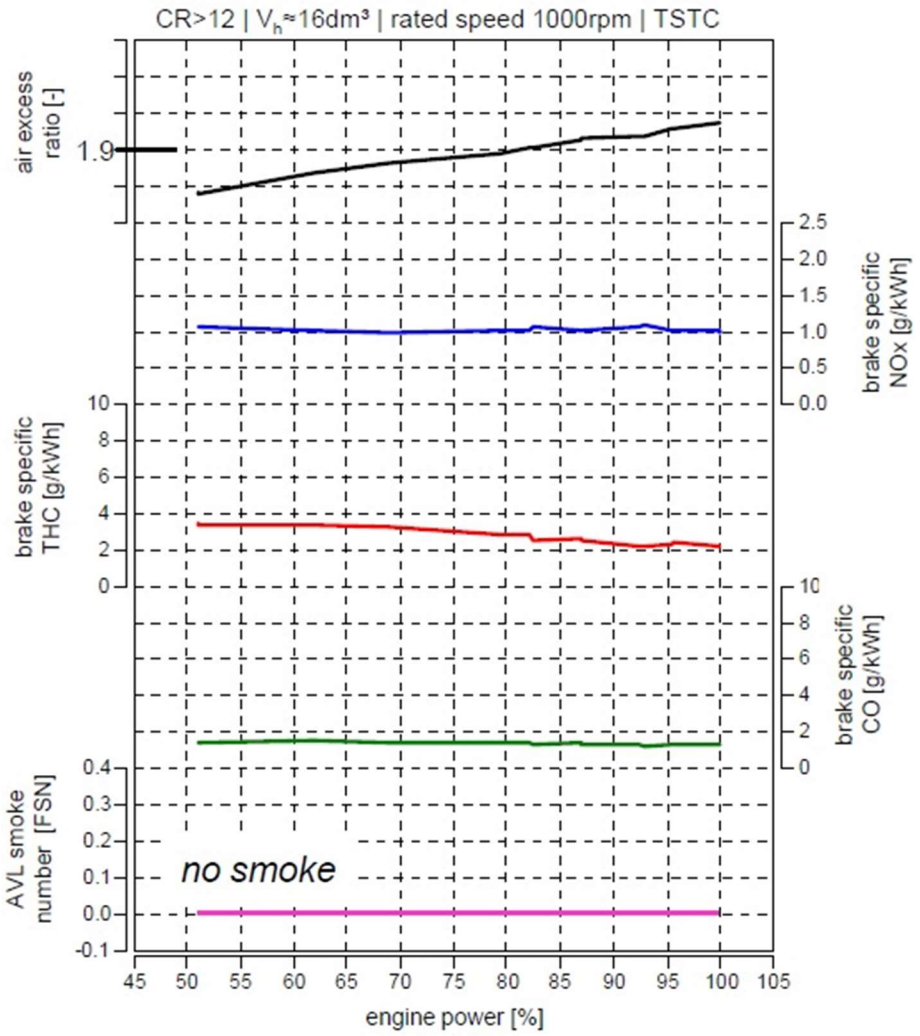

Figure 2-6. Experimental results of AVL's FM250 gas engine for the variation of fuel air equivalence ratio, specific NOx emissions (in g/kWh), specific THC emissions (in g/kWh), specific CO emissions (in g/kWh) and soot emissions (in FSN) as a function of engine load [38]. The experimental results have been obtained for the E2/D2 test cycles of AVL's FM 250 single cylinder compression ignition engine [38].

In the following (Figure 2-7) experimental results are presented from a related investigation carried out on the AVL FM250 engine, which aimed to improve the performance of the AVL FM250 engine when operating as a dual-fuel engine by applying a Miller cycle through variable intake valve timing. Specifically, Figure 2-7 shows the indicated efficiency of the FM250 engine as a function of intake valve closure angle when operating as an open chamber gas engine with single-stage supercharging. In this case the indicated efficiency is 45% but the operating point is close to the limit where we have the worst combustion stability and little occurrence of shock combustion phenomena [38]. Furthermore, Figure 2-7 shows a second operating

point (blue circle) which refers to the operation of AVL's FM250 engine as a dual fuel engine with single-stage supercharging and pilot injection of 1% oil. This operating point corresponds to an angle of closure of the intake valves equal to the crank angle when the piston is in the BDC and corresponds to an indicated efficiency of approximately 40.5% [38]. The objective is to find a technical solution that will lead to an increase in the indicated efficiency and power of the FM250 dual fuel engine without problems of shock occurrence and without combustion stability problems [38].

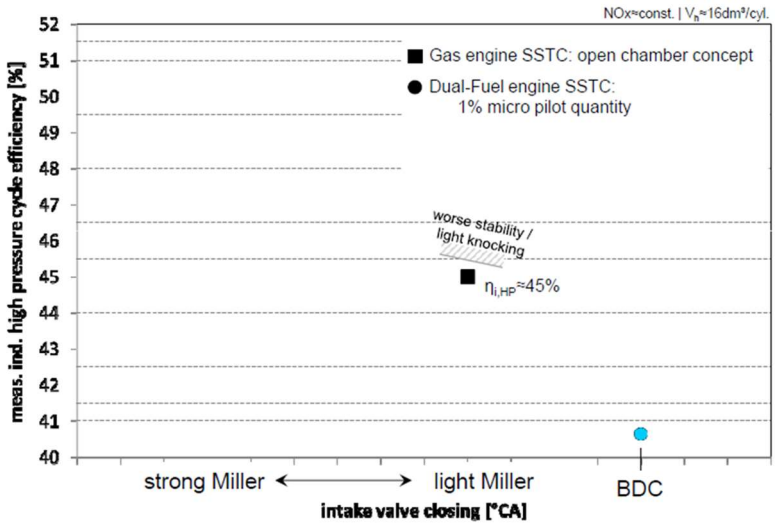

Figure 2-7. Indicated efficiency as a function of intake valve closing angle for an open-chamber gas engine with single-stage turbocharging and a dual-fuel engine with single-stage turbocharging (Two different combustion chamber designs of AVL's FM250 engine) [38]. Experimental results have been obtained for stable NOx emissions in AVL's FM250 gas engine [38].

From the experimental results of Figure 2-8 we observe that the increase in average effective pressure, i.e. the increase in power for the same engine displacement, for an Intake Valve Closing (IVC) angle equal to the Bottom Dead Centre (BDC) angle leads to an increase in the indicated efficiency (from 40. 5% to 43%) but the operating point is dangerously close to the knocking threshold due to an increase in pressure values within the combustion chamber [38]. Therefore, it is concluded that it is necessary to vary the timing of the intake valves (application of Miller cycle) to simultaneously increase the power and efficiency of the engine [38].

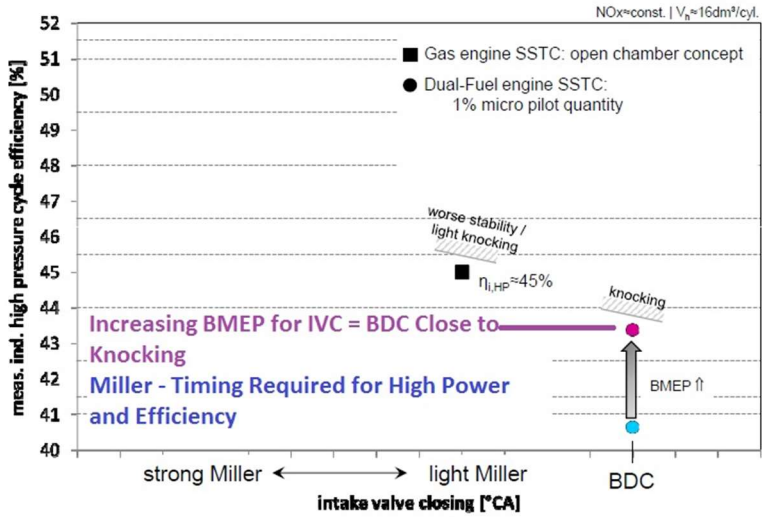

Figure 2-8. Indicated efficiency as a function of intake valve closing angle for an open-chamber gas engine with single-stage turbocharging and a dual-fuel engine with single-stage turbocharging (Two different combustion chamber designs of AVL's FM250 engine) [38]. Experimental results have been obtained for constant NOx emissions in AVL's FM250 gas engine [38].

Figure 2-9 illustrates the improvement of the indicated efficiency from 43% to 45% by applying a "strong" Miller cycle, i.e. by closing the intake valves earlier before the BDC while keeping the average effective pressure and compression ratio of the engine at constant levels [38].

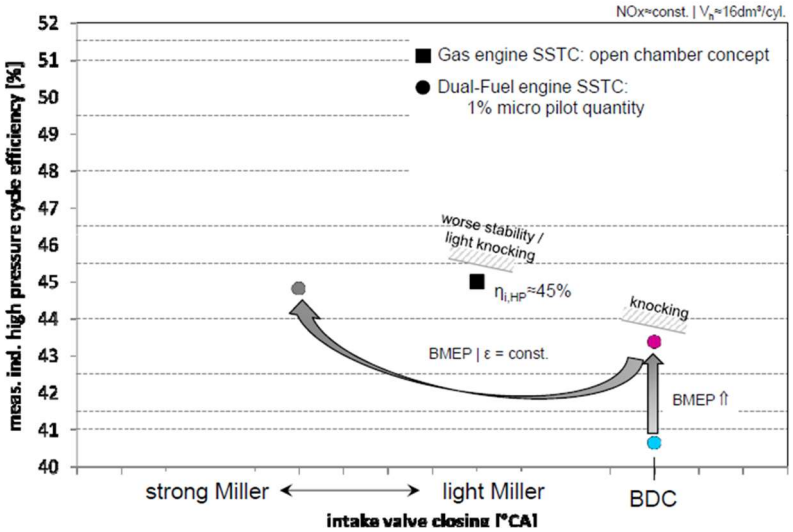

Figure 2-9. Improvement of the indicated efficiency of the AVL FM250 dual-fuel engine by applying a "strong" Miller cycle while keeping the average effective pressure and compression ratio constant [38].

Next, to further increase the indicated efficiency from the last point reached in Figure 2-9 we increase the average effective pressure by increasing the power and then increase the compression ratio "e" (see Figure 2-10). As shown in Figure 2-10 by increasing the bmep and the compression ratio "e" we can increase the indicated efficiency of the AVL FM250 dual fuel engine from 45% to about 47% [38]. However, in this case as shown in Figure 2-10 the operating point is very close to the threshold for shock combustion occurrence [38].

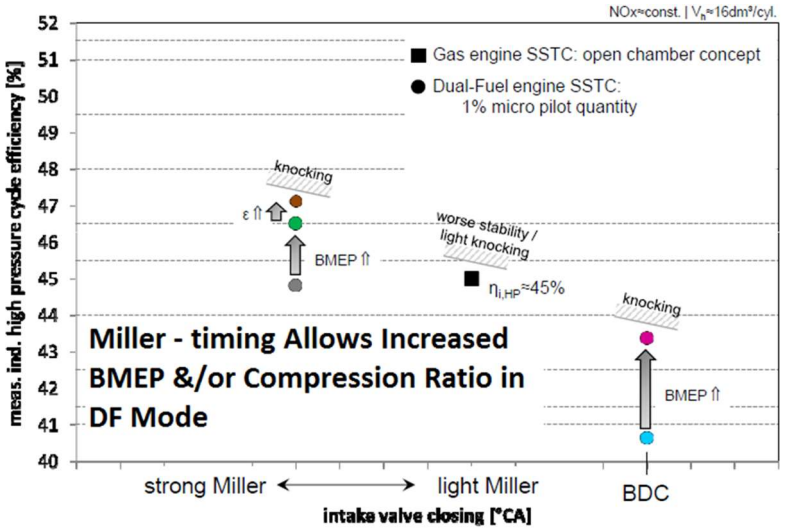

Figure 2-10. Further improvement over Figure 2-9 of the indicated efficiency of the AVL FM250 dual fuel engine by increasing the power per unit engine displacement (increasing the average effective pressure bmep) and by increasing the compression ratio "e" [38].

2.3 AVL research results for NOx emissions from medium-speed dual-fuel and medium-speed gas engines

Figure 2-11 shows experimental results of extensive experimental investigations by AVL [38] for the specific NOx emissions in g/kWh emitted from: (a) diesel/dual-fuel engines used as main propulsion engines, (b) auxiliary spark-ignition gas engines, (c) dual-fuel engines used as main propulsion engines, and (d) diesel engines used as both main and auxiliary engines [38]. The particularly encouraging observation that can be derived from Figure 2-11 is that dual fuel engines (green diamonds) used on board ships as main propulsion engines fully comply with the currently stricter NOx emission limits from marine engines in environmentally controlled areas (Tier III) without the need for any other measure inside or outside the engine [38].

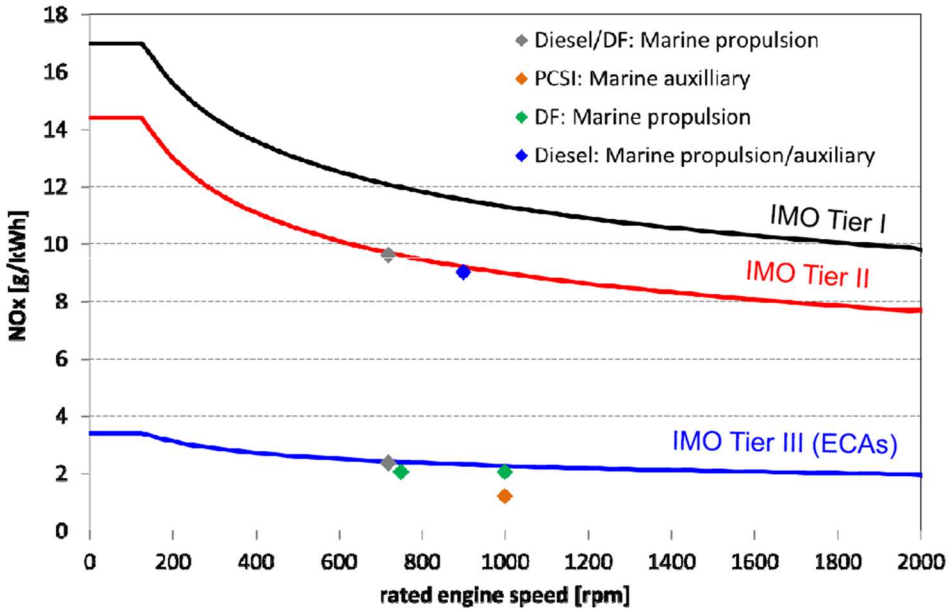

Figure 2-11. Experimental results of AVL specific NOx emissions for (a) Diesel/D dual fuel engines used as main propulsion engines, (b) Auxiliary spark ignition gas engines, (c) Dual fuel engines used as main propulsion engines, and (d) Diesel engines used as both main and auxiliary engines [38].

2.4 Experimental investigation of the effect of a new control system on the operational and environmental behavior of a dual-fuel (LNG Diesel) marine auto-ignition engine

2.4.1 Introduction

In this paragraph, results from an extensive experimental investigation carried out on a dual-fuel LNG marine engine will be presented and commented on [39]. In particular, a dual-fuel engine operation control system was developed using the design method based on the development and application of a computer model (Model-based Design - MBD) [39]. Specifically, without changing the original design of the marine SI engine, an LNG feed system and an electronic control system for engine operation were added to the engine [39]. Subsequently, measurements were carried out on the fuel consumption and pollutant emissions of the marine engine during its initial operation as a compression ignition/diesel engine and after its conversion to a dual fuel (LNG/diesel) compression ignition engine [39]. From the above-mentioned procedure, results were extracted for operating costs, Brake Specific Fuel Consumption (BSFC), gross hydrocarbon (HC) emissions, nitrogen oxides (NOx) emissions, carbon monoxide (CO) emissions and particulate matter (PM) emissions. These experimental results will be discussed in detail in the following paragraphs.

2.4.2 Dual fuel marine engine control system design

2.4.2.1 Description of the control system

Figure 2-12 schematically illustrates the layout of the dual-fuel marine SI engine operation control system, which consists of a dual-fuel supply system, a safety system and an ECU communication system. Each subsystem of the control system and its respective function is described in detail in the following paragraphs.

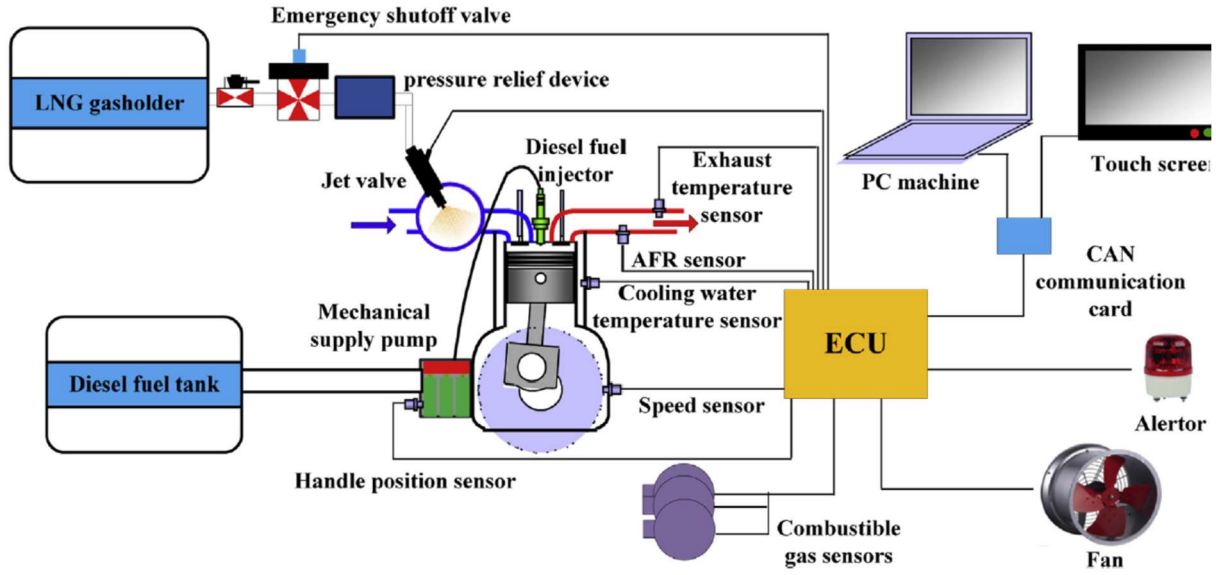

Figure 2-12. Gas and diesel fueling system of a marine diesel and gas engine [39]

2.4.2.2 Dual fuel supply system

The dual-fuel supply system consists of the engine fuel oil supply system and the LNG supply system [39]. The diesel engine fueling system consists of the conventional T8138ZLCz diesel engine without major modifications [39]. The LNG fueling system consists of the LNG storage tank, the vaporizer, the pressure relief device, which maintains the inlet pressure at the gas injection valve equal to 0.3 MPa [39]. Furthermore, the engine gas supply system contains gas pipes and two injection valves. Still on the T8138ZLCz engine are mounted sensors for measuring rotational speed, position control, coolant temperature and exhaust gas temperature. These sensors are used to control the amount of injected gas [39]. The operating parameters recorded by the above-mentioned sensors are transmitted to the Electronic Control Unit (ECU), which controls the gas injection valve according to specific control algorithms.

To avoid overheating of the injection valve, two injection valves are operated alternately [39].

2.4.2.3 Safety system

The safety system of the T8138ZLCz dual-fuel marine engine consists of an early warning system (alarm), an indicator light, ventilation fans and gas fuel logging sensors, which are mounted in different locations [39]. When these sensors detect that the fuel gas concentration reaches a certain level, the control system will generate early warning (alarm) signals, the ventilation fans will open and the LNG supply to the engine can be cut off [39].

2.4.2.4 Communication system

This system is responsible for establishing communication between an industrial touch screen, a PC and the central control unit of the T8138LZCz dual-fuel marine engine [39]. The communication of the three above-mentioned subsystems is done through a CAN protocol. The industrial touch screen can monitor and intervene in the operation of the dual fuel marine engine [39]. There are at least two engines for power generation on ships. Considering that at least two main dual fuel engines are required in a ship, it is necessary to build communication between the ECUs of the two main engines [39].

2.4.2.5 Control system operation principle

Initially, the T8138ZLCz marine spark ignition engine starts running on fuel oil to warm up. The operation of this engine with natural gas is activated in case the engine speed and coolant temperature reach their preset values and then, the gas injection valve in the engine is opened [39]. The amount of injected gas is gradually increased determined by the control algorithms resulting in an increase in engine speed. In order for the dual fuel engine to operate stably, the amount of injected oil is reduced by the engine speed control system until a minimum threshold is reached beyond which the injected pilot amount of oil fails to ignite the gas and air mixture [39]. In this case there is a fluctuation in engine speed i.e. the engine cannot maintain a constant speed and an ignition failure indication signal is generated [39]. Therefore, the amount of injected gas can be modified by the speed control algorithm to make the engine run at stable

conditions. Under steady-state operating conditions, the Air-Fuel Ratio (AFR) decreases with an increase in the injected amount of gas as recorded by the AFR sensor [39]. If the injected amount of gas is too large, the combustion quality is degraded and the cylinder wall temperature increases [39]. When this operating condition occurs and is detected by the exhaust gas temperature sensor, the injected amount of gas is reduced by the AFR air/fuel ratio control algorithm until the exhaust gas temperature returns to its allowable limits [39].

2.4.2.6 The engine control unit (ECU) software development process

Figure 2-13 shows through a flowchart the structure and operation of the software developed in a scientific project [39] to control the operation of a dual-fuel marine engine. Initially, the variables and parameters of the T8138ZLCz dual fuel engine control system are stored in MAT files of MATLAB [39]. Then, the different functions of the control system are generated using SIMULINK and STATEFLOW [39]. The OSEK platform, which specializes in vehicle engine operation control systems, is applied to the central control unit (ECU) of the T8138ZLCz engine and the RTW tool is used to automatically generate an embedded C programming language code. Then the C language code of the OSEK application can be reproduced by the RTW tool [39]. To ensure that the C language code is reliable, it is necessary to verify that the C language code developed in C. Then POLYSPACE is often used to verify whether the C language code developed in C satisfies the international criteria [39]. T8138ZLCz dual fuel engine can be found in the publication [39].

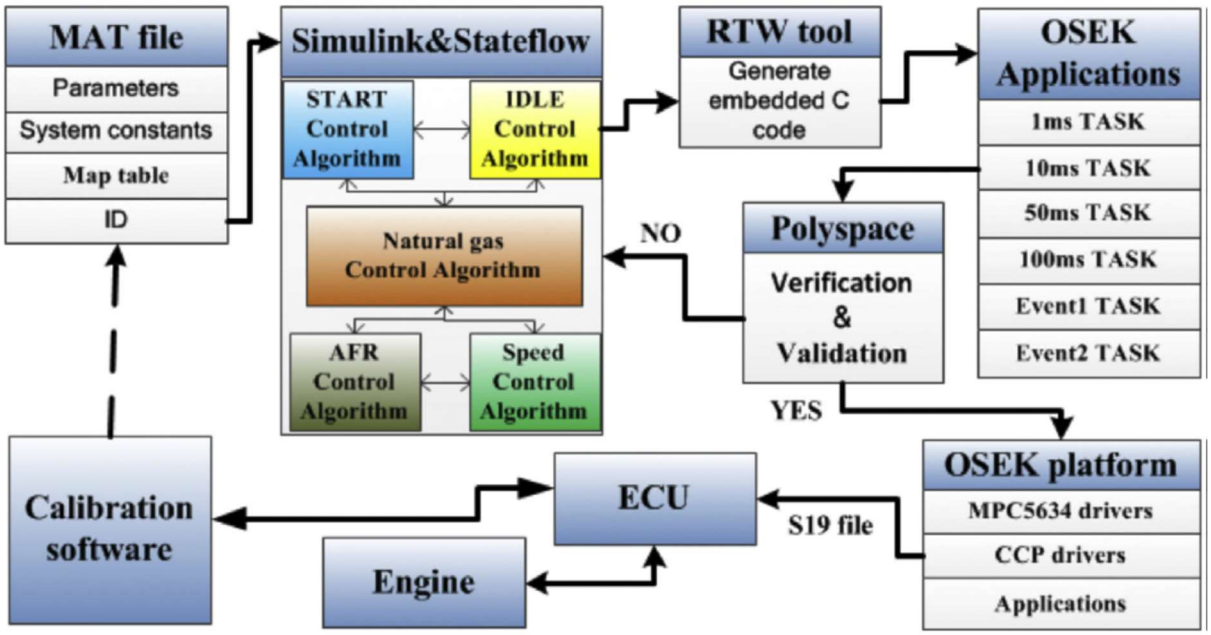

Figure 2-13. Flowchart of the process of controlling the operation of a dual-fuel marine engine by means of appropriately developed software [39]

2.4.3 Dual-fuel marine engine control strategy

The optimum performance of the dual-fuel engine under different operating conditions is conducted through the ECU. To achieve the maximum portion of natural gas under different conditions, different control strategies are expected to be established. When the engine is operated under the start or idling condition, it is difficult to ignite the mixture gas in dual-fuel mode. Thus, the pure diesel mode will be used. Considering that marine engines mostly operate under middle- and high-load conditions, the dual – fuel mode should be adopted to reduce fuel consumption, combustion noise, emissions and cost.

2.4.3.1 Strategy for the control of a marine spark-ignition engine when operating on diesel fuel oil only

The handle is used to improve the performance of the diesel engine by controlling the engine speed. Thus, the quantity of the injected diesel fuel is regulated by the speed governor according to the engine working conditions, which are the start and idling conditions.

2.4.3.2 Control strategy for a marine compression ignition engine when operating as a dual fuel engine

Signals of target speed are transmitted to ECU by monitoring the handle position. The corresponding basic natural gas supply quantity is looked up in the well-designed injection MAP table. Meanwhile, exhaust temperature correction, body temperature correction and AFR correction will be added in basic natural gas injection quantity. Then, the jet valve opens for the corresponding duration.

2.4.3.3 Control strategy for the gas percentage

To achieve the maximum portion of natural gas, the system must reduce the consumption of diesel fuel as much as possible. When the injected diesel fuel fails to ignite the mixed gas, misfire occurs in the cylinder, and then, large fluctuations of engine speed will appear. By calculating the speed error variation rate d, as shown in Equations 2.1 – 2.3, misfire is identified.

Fig. 2-14 demonstrates that d varies with the speed fluctuations under speeds of 900 rpm, 1000 rpm, 1100 rpm and 1200 rpm. The results show that d is equal to 1 under normal conditions and that the minimum value of d is 1.83 under different speed fluctuations. Therefore, a speed control algorithm is used to modify the portion of natural gas. Under full load conditions, the AFR closed-loop control algorithm is used to achieve the maximum portion of natural gas.

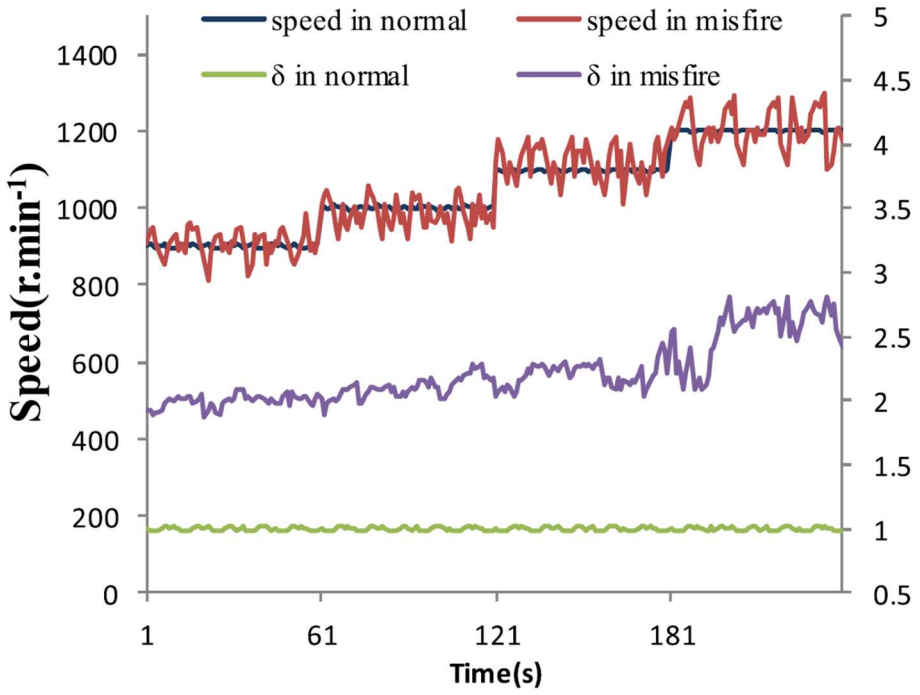

Figure 2-14. Variation of dual-fuel marine engine rotation speed with d values [39]

$$\bar{x} = \frac{\sum_{i=1}^{8} x_i}{8} \tag{2.1}$$

$$J_n = K_1 \frac{\sum_{i=1}^{8} |x_i - \bar{x}|^2}{8} \tag{2.2}$$

$$\delta = \frac{J_n}{J_{n-1}} \tag{2.3}$$

where xi is the value of speed at the different sample times (r min1); here, i is 1e8 and x is the average speed (r min1). K1 is constant, Jn is the n sample time of speed mean square error, Jn1 is
the n1 sample time of the speed mean square error, and d is the speed error variation rate.

2.4.4 Total quantity of natural gas injected

The natural gas total injection quantity equation is given by:

$$Gas_m = Gas_b \times M_n \times (1 + M_{et} + M_{wt} + M_l) \quad (2.4)$$

where Gasm is the total quantity (ms), Gasb is the basic quantity (ms), Mn is the volume correction coefficient, Met is the exhaust temperature correction coefficient, Mwt is the body temperature correction coefficient, and Ml is the engine load change correction coefficient, which is closely related to the governor handle position and exhaust temperature.

2.4.5 Description of an experimental installation of dual-fuel marine engine

The experiment aimed to investigate the fuel economy and emissions of the marine dual fuel engine. The engine that was used was the T8138ZLCz marine diesel engine produced by Nan Tong Diesel Engine. The detailed specifications of this engine are listed in Table 2-1.

Table 2-1. Key construction and operational characteristics of the T8138ZLCz dual-fuel marine compression-ignition engine [39]

Number of cylinders	8
Cylinder diameter and piston stroke	138 mm and 163 mm
Compression ratio	15.5:1
Cubism	19.5 L
Exhaust gas temperature	< 470ºC
Maximum power/Speed of rotation	323.4 kW/1545 rpm
Maximum continuous power/Rotation speed	294 kW/1500 rpm
Combustion chamber	Direct injection
Intake system	Turbocharging with intermediate air cooling
Cooling system	Water-cooled engine

The LNG supply system and control system were installed in the engine. The engine was coupled to an AVL AC-dynamometer rated at 2500 Nm with a maximum speed of

7500 r min1. The MSC-960 fuel consumption meter and LCB-50M flow meter were used to measure the consumptions of diesel fuel and natural gas, respectively. The Horiba Mexa-7100D exhaust gas analyzer was used to measure emissions, and PM was measured by an AVL 439 smoke opacity meter. The engine running parameters were monitored by a PC and touch screen, and the control operations were carried out by the touch screen. Meanwhile, the PC can be used to calibrate the engine running the MAP tables. The experimental setup is shown in Fig. 2-15.

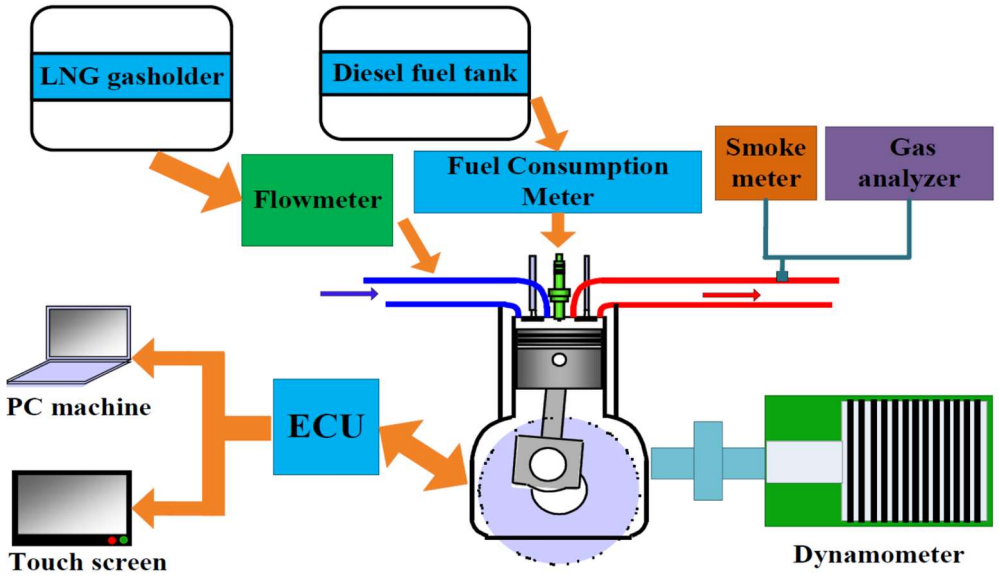

Figure 2-15. Schematic illustration of the experimental installation of a dual-fuel auto-ignition marine engine with advanced operation control system [39]

2.4.6 Procedure for carrying out experimental measurements

Ship navigation is supplied by the propeller, and the marine propeller is driven by propulsion systems. In this experiment, a high-speed diesel engine propulsion system is used in the experimental ship. A diesel engine works under marine propulsion characteristics, which are shown in Equation (2.5).

$$P_e = c_1 \times n^3 \tag{2.5}$$

where Pe is the effective power (kW), C1 is the calibrated coefficient, and n is the speed (r min1).

Economic calculation refers to the Chinese market price, 8.24 RMB/kg for diesel fuel and 7 RMB/kg for natural gas. The total price formulas are given by:

$$P_D = D_1 \times 8.24 \tag{2.6}$$

$$P_M = D_2 \times 8.24 + G \times 7 \tag{2.7}$$

Where PD is the cost in pure diesel mode (RMB h1); PM is the cost in dual-fuel mode (RMB h1); D1 is the diesel fuel consumption rate in the pure diesel mode (kg/h); D2 is the diesel fuel consumption rate in the dual fuel mode (kg/h); and G is the natural gas consumption rate in dual fuel mode (kg/h).

2.4.7 Results of experimental investigation of a dual fuel marine engine and related comments

To comprehensively evaluate the performance of the marine diesel engine, the fuel economy and emissions were tested separately under the conditions of the propulsion characteristics and load characteristics. The load characteristics were carried out at a speed of 1200 rpm under loads of 25%, 50%, 75%, 90% and 100%.

2.4.7.1 Specific fuel consumption and operating costs

Figure 2-16(α) shows the BSFC of the pure diesel mode and dual-fuel mode with engine speed. The BSFC of the dual-fuel mode is higher than that of the pure diesel mode under the low-speed range. The main reason for this result is that natural gas is difficult to ignite under low loads. However, when the speed is greater than 700 r min1, the BSFC of the dual-fuel mode is lower than that of the pure diesel mode. The maximum decrease is 14.7% at 1300 r min1, which means that the dual-fuel mode is more economical than the pure diesel mode in the high-speed range. In general, marine engines often run at speeds from 1000 r min1 to 1300 r min1; as a result, the dual-fuel mode is very economical for use in marine engines. When the engine speed exceeds 1300 r min1, the BSFC of the dual-fuel mode increases further because the portion of natural gas decreases.

Figure 2-16(β) shows that the BSFC varies with the load. The graph shows that the BSFC of dual fuel is less than that of pure diesel. Under low loads, the in-cylinder temperature was too low to oxidize natural gas, and more natural gas was consumed. The in-cylinder temperature increased as the load increased, and natural gas burned much more completely. Under high and full loads, the BSFC of dual

fuel increases sharply because the portion of natural gas decreases. The maximum decrease of BSFC is 13.4% at a load of 75%.

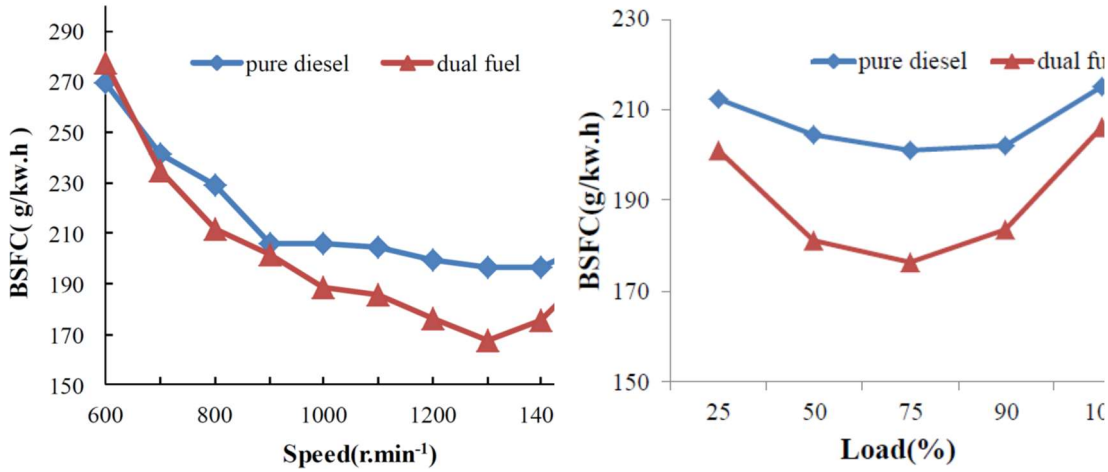

Figure 2-16. Experimental results for the variation of specific fuel consumption (a) with rpm and (b) with load for the T8138ZLCz marine engine. In both figures (a) and (b) the blue curve corresponds to running the T8138ZLCz engine on diesel only and the red curve corresponds to running the same engine as a dual fuel (LNG/oil) engine [39]

The running cost is an essential factor in the development process of dual-fuel marine engines. As shown in Fig. 2-17(a), the cost of dual-fuel mode is overall lower than that of pure diesel mode, with a maximum decrease of 28.7% at 1300 r min1. As previously mentioned, the marine engine is generally operated between 1000 r min1 and 1300 r min1. Therefore, the average cost decrease of the dual fuel mode is 26% less than that of the pure diesel mode. Considering long-distance and long-time transportation in ships, the dual-fuel mode is more economically attractive.

Fig. 2-17(b) shows the cost with load. The loads from 60% to 80% have a significantly large difference between pure diesel and dual fuel. The maximum decrease is 121 RMB h1 at a load of 75%. This decrease occurs due to the high portion of natural gas in the above load range. When the load is greater than 80%, the difference becomes small because the portion of natural gas decreases.

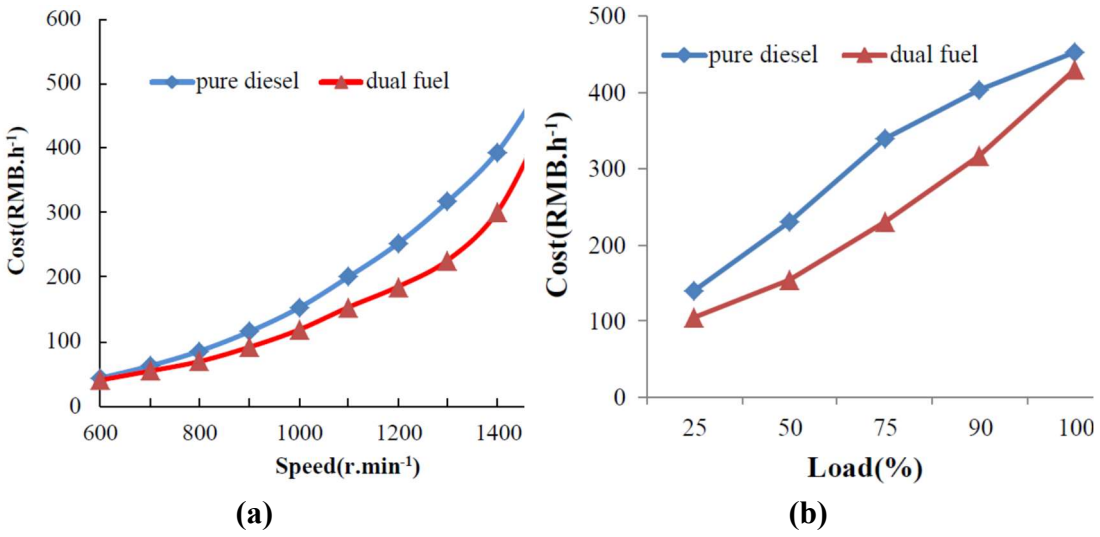

Figure 2-17. Results for the variation of operating cost in Chinese RMB (renminbi or yuan) currency per hr (a) with rpm and (b) with load of the T8138ZLCz marine engine. In both figures (a) and (b) the blue curve corresponds to running the T8138ZLCz engine on diesel only and the red curve corresponds to running the same engine as a dual fuel (LNG/oil) engine [39]

2.4.7.2 Pollutant emissions (CO, HC, NOx και PM)

Fig. 2-18 (a) shows the CO emissions of pure diesel and dual fuel. When the speed is less than 1000 r min1, the CO emissions decrease as the engine speed increases. However, when the speed is greater than 1000 rpm, the CO emissions increase as the engine speed increases. This result occurs because incomplete combustion occurs under the conditions of low load due to a lack of oxidants or low temperature. When the engine is operated under high and full loads, the mixture gas becomes much richer as the load increases, and incomplete combustion occurs heavily. Both changes result in the substantial formation of CO. Note that the CO emission of the dual-fuel mode is higher than that of the pure diesel fuel mode because natural gas injected into an air inlet pipe occupies a proportion of the air volume, which makes the actual AFR smaller than AFR of pure diesel mode [40] and thus liable to cause incomplete combustion.

Fig. 2-18 (b) shows the CO emissions with load. The CO emission of dual fuel was greater than that of pure diesel because the mixture gas of dual fuel is richer than that of pure diesel, and the mixture gas burns incompletely. When the load was greater than 75%, the CO emissions increased sharply because under high and full loads, incomplete combustion occurs heavily.

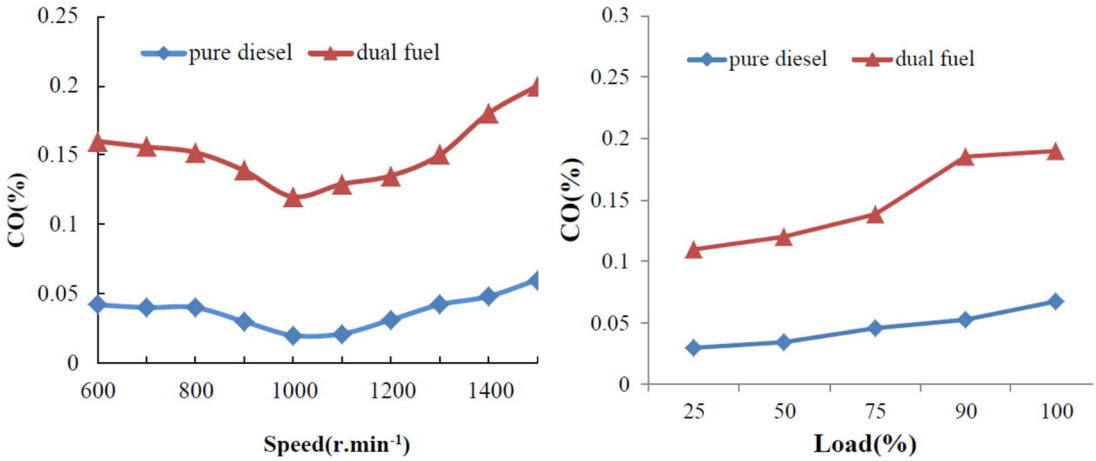

Figure 2-18. Experimental results for the variation of CO emissions (a) with rpm and (b) with load for the T8138ZLCz marine engine. In both figures (a) and (b), the blue curve corresponds to running the T8138ZLCz engine on diesel only and the red curve corresponds to running the same engine as a dual fuel (LNG/oil) engine [39]

Fig. 2-19 (a) shows the HC emissions of two modes. The HC emissions of the pure diesel mode maintained a very low value (approximate 22 ppm) within the whole speed range. However, the HC emissions of the dual fuel mode were relatively high. When the engine speed was less than 1000 r min1, the HC emissions increased as the natural gas injection quantity increased because the combustion temperature in the dual-fuel mode was lower than that of the pure diesel fuel mode, resulting in incomplete combustion. However, given that the intake and exhaust valves overlap, the natural gas that is injected into air inlet pipe is partially discharged through the exhaust valve [41]. When the speed is greater than 1200 rpm, the HC emissions gradually decrease because the combustion temperature increases as the engine load increases, and the mixture gas burns completely. Meanwhile, because the portion of natural gas decreases, the natural gas that is discharged through the exhaust valve also decreases.

Fig. 2-19 (b) shows the HC emissions with load. Under loads from 25% to 75%, there are two reasons for a high level of HC emissions. One reason is that under low loads, the in-cylinder temperature is relatively low, which can easily cause incomplete combustion. The other reason is that some natural gas might be scavenged outside the cylinder during the overlap opening period of intake and exhaust valves. When the load was greater than 75%, the HC emissions of dual fuel decreased sharply because the portion of natural gas decreases significantly.

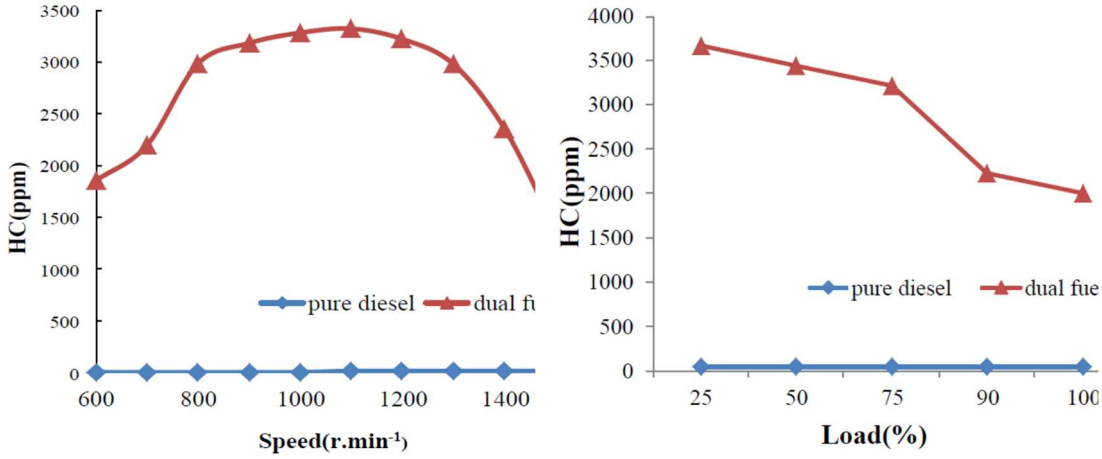

Figure 2-19. Experimental results for the variation of HC emissions (a) with rpm and (b) with load for the T8138ZLCz marine engine. In both figures (a) and (b), the blue curve corresponds to running the T8138ZLCz engine on diesel only and the red curve corresponds to running the same engine as a dual fuel (LNG/oil) engine [39]

Fig. 2-20 (a) shows the NOx emissions varying with speed. In pure diesel mode, NOx emissions gradually increase within speeds from 600 rpm to 800 rpm and then increase sharply and peak at 1038 ppm and 1200 rpm, eventually decreasing. The in-cylinder temperature increases as the speed increases. A high temperature might allow NOx to be easily generated. In the high-speed region (1200 r min1 to 1500 rpm), the mixture gas is rich, resulting in low oxygen concentration, making it difficult to generate NOx. However, the NOx emission of the dual-fuel mode is lower than that of the pure diesel fuel mode in the whole speed range, especially at 600 rpm, with a maximum reduction percentage of 68.3%. In the speed range between 1000 rpm and 1300 rpm, the average reduction percent of NOx emissions is 48.2%, which shows the great potential of the dual-fuel engine to reduce NOx emissions because the theoretical AFR values of natural gas and diesel fuel are 17.2 and 14.3, respectively. Greater air amounts are required for complete combustion in dual-fuel mode. Lower air amounts react with N2. In addition, the in-cylinder combustion temperature of dual fuel is lower than that of pure diesel.

Fig. 2-20 (b) shows NOx emissions with load. NOx emissions are sensitive to the combustion temperature and oxygen content. The NOx emission of dual fuel is overall less than that of pure diesel. The maximum decrease is 55.2% at a load of 75%. The in-cylinder combustion temperature of natural gas is lower than that of diesel fuel. Under high and full loads, the NOx emission of dual fuel increases sharply because the portion

of natural gas decreases, and the in-cylinder combustion temperature increases significantly under high and full loads

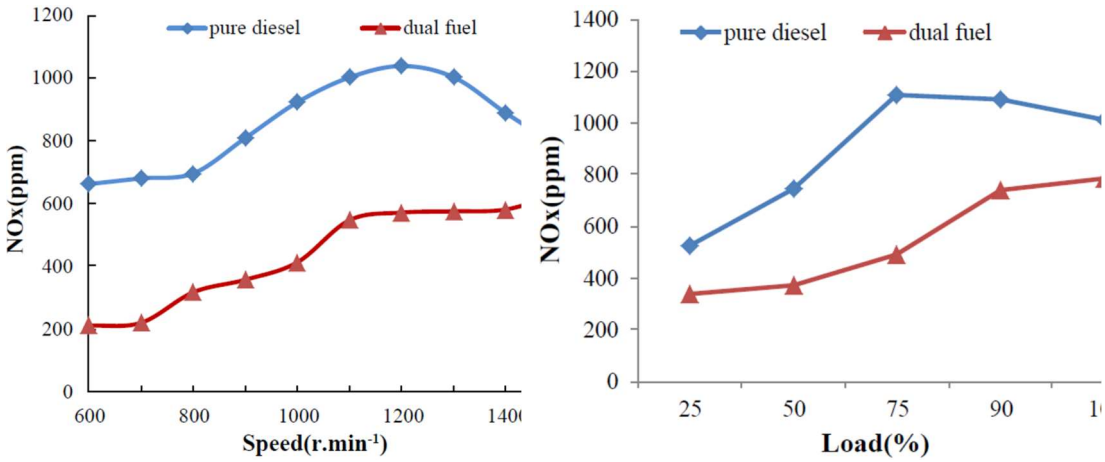

Figure 2-20. Experimental results for the variation of NOx emissions (a) with rpm and (b) with load for the T8138ZLCz marine engine. In both figures (a) and (b), the blue curve corresponds to running the T8138ZLCz engine on diesel only and the red curve corresponds to running the same engine as a dual fuel (LNG/oil) engine [39]

Optical absorption coefficient (K) is often used to evaluate PM emissions because it is tightly correlated with PM weight. Fig. 2-20 (a) shows K with speed. In the speed range from 600 rpm to 1300 rpm, PM emissions of pure diesel mode increase slightly. When the speed is greater than 1300 rpm, PM emissions increase greatly, with a maximum value of 0.26 m-1 at 1500 rpm. The reason for this result is that the mixture gas is too rich to burn completely within high-speed regions. Note that the PM emissions of the dual-fuel mode are lower than those of the pure diesel fuel mode in the whole speed range, with a maximum reduction percentage of 78% at 1200 rpm and an average drop percentage of 69.3% in the speed range between 1000 rpm and 1300 rpm. The PM emissions of the dual-fuel mode increase significantly when the engine speed is greater than 1300 rpm because of the sharp decrease in the portion of natural gas within the high-speed range. In addition, the main component of natural gas is methane; thus, the amount of HC structure is less than that of diesel fuel, making it more difficult for natural gas to produce PM.

Fig. 2-21 (b) shows the PM emissions with load. The PM emission of dual fuel is less than that of pure diesel. Considering that natural gas is directly injected into intake air, the mixture gas of dual fuel is more homogeneous, allowing the mixture gas to burn

more completely. However, when the load is greater than 75%, PM emissions of dual fuel increase sharply because the portion of natural gas decreases under high and full loads, causing more diesel fuel to burn.

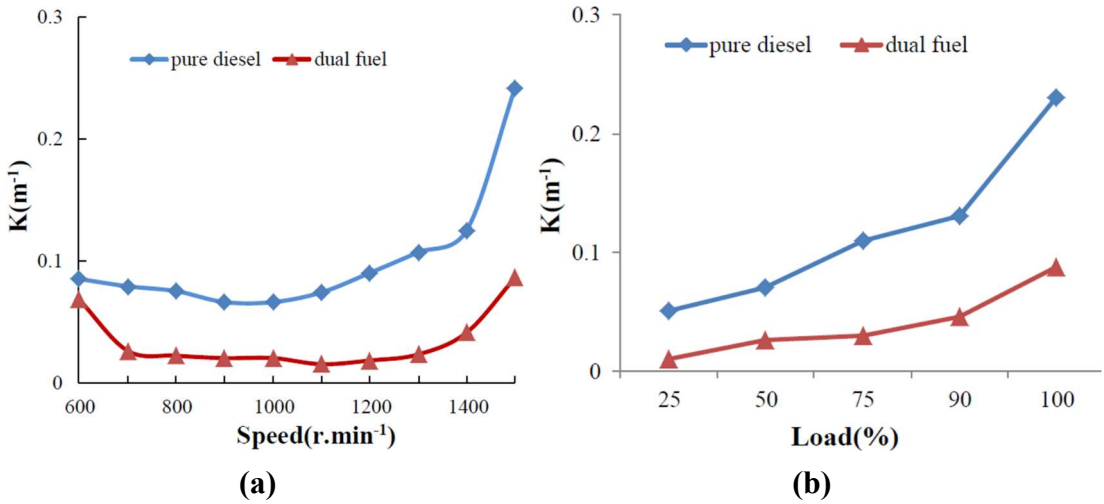

Figure 2-21. Experimental results for the variation of PM emissions (a) with rpm and (b) with load for the T8138ZLCz marine engine. In both figures (a) and (b), the blue curve corresponds to running the T8138ZLCz engine on diesel only and the red curve corresponds to running the same engine as a dual fuel (LNG/oil) engine [39]

2.4.8 Conclusions on the operational and environmental performance of the T8138ZLCz dual-fuel marine compression ignition engine

1. Marine diesel engines are required to be refitted slightly to generate LNG-diesel dual fuel engines, where the LNG supply system and control system are equipped independently in the original machine. The pure diesel fuel mode and dual fuel mode can be switched intelligently.

2. In the speed range between 1000 rpm and 1300 rpm, the average value of the portion of natural gas in the dual fuel mode is 82.2%, with a maximum value of 85.9% at 1200 rpm. The running cost of the dual-fuel mode is less than that of the pure diesel mode, and the maximum saving percentage reaches 28.7% at 1300 rpm. Hence, for long term and long-distance waterway transportation, the LNG diesel dual-fuel engine has great promise.

3. NOx and PM emissions are significantly decreased in the dual-fuel mode, with a maximum drop percentage of 68.3% at 600 rpm and 78.3% at 1500 rpm, respectively. However, the HC and CO emissions of the dual-fuel mode are higher than those of pure diesel mode.

4. Under a speed of 1200 rpm and a load of 75%, the fuel economy and emissions of dual fuel are the lowest.

2.5 General conclusions on the operational and environmental performance of dual-fuel compression ignition marine engines

A detailed examination of the experimental investigations carried out by AVL on dual-fuel and gas engines with pilot oil injection and pre-chamber led to the following conclusions:

- During operation with gas and pilot injection in the pre-chamber the highest engine efficiency is observed, which at maximum load reaches about 46%. The maximum efficiency when operating the same engine as a dual fuel engine reached 42.5%.
- The addition of a pre-chamber to a gas engine ensures stable ignition and stable operation without substantial fluctuations in the average indicated pressure.
- 4-S dual-fuel engines and gas engines with pilot-injected diesel pre-chamber can directly and without further intervention meet the existing stricter NOx emission limits in areas where these pollutants are controlled (Tier III).
- The problem of the deterioration of hydrocarbons (THC) and CO due to gas combustion is less in gas engines with a pre-chamber and pilot fuel injection than in dual-fuel engines.
- Both dual-fuel engines and gas engines with pre-chamber and pilot fuel injection have zero soot emissions at all loads and all speeds (smokeless operation).

3 Techno-economic study of marine diesel engines retrofit to dual fuel engines

3.1 Introduction

In this chapter, we will present a techno-economic study – evaluation, of the conversion of the main and auxiliary diesel engines of the ferry 'ANO HORA II' to run on natural gas.

The continuously increasing environmental demands induced the maritime sector to establish new international restrictions on the marine fuel sulphur content and the NOx emissions both in Emission Control Areas zones and in global waters (IMO Tier II and III) as well as on the CO_2 emissions (IMO EEDI).

The objective of the study is to compare the potential solutions able to meet the requirements of the IMO regulations regarding SO_X in the ECA in 2015 and globally in 2020. In 2015, the requirements within ECA call for a reduction of sulphur content in the fuel to 0.1% or alternatively the equivalent level measured in the exhaust gas. Similarly in 2020, the global requirements will be a reduction of sulphur content in the fuel to 0.5% or alternatively the equivalent level measured in the exhaust gas (Christian Klimt-Møllenbach, 2012). [43].

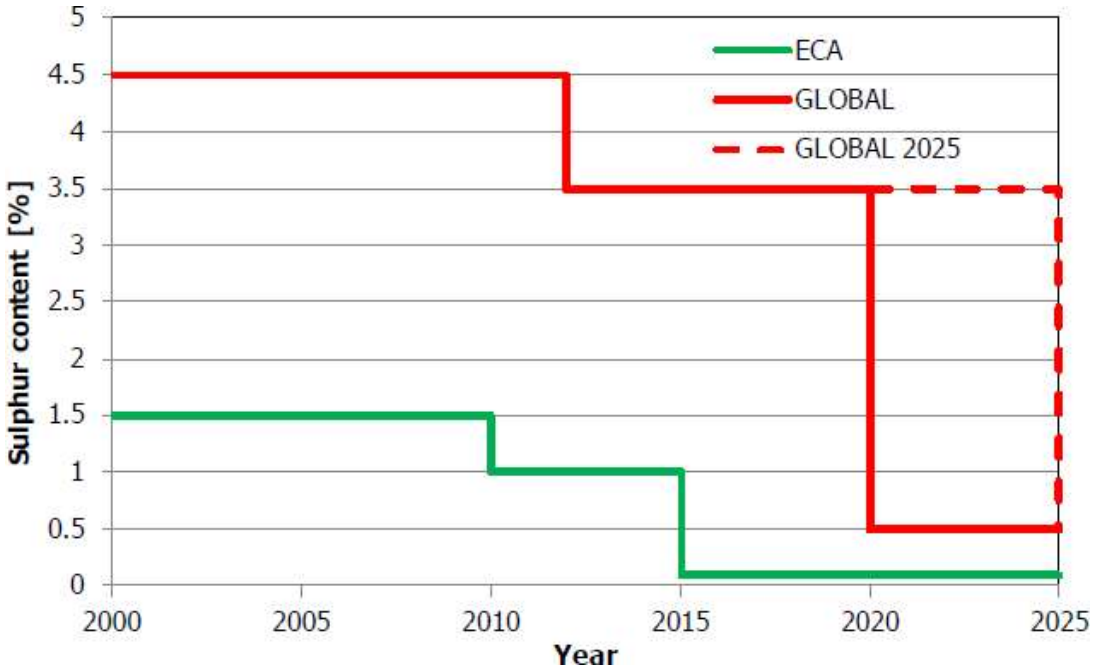

Figure 3-1. IMO regulation of SOx levels

More areas within the Mediterranean Sea will possibly become a future Emission Control Area (ECA) as shown in Figure 3-2. These areas include some of the most heavily congested sea regions of operation in Greece like the Piraeus and Argosaronikos region, northern Ionian Sea and northern Aegean Sea. In addition to the decided designations of ECAs some additional areas are also discussed as indicated by the map below.

Figure 3-2. Decided existing and possible future ECAs. [43]

The use of liquefied natural gas (LNG) as fuel for propulsion of commercial ships can lead to both the significant reduction of the ship engines exhaust gas emissions (CO_2, NOx, SOx, PM), and the lower operational cost due to the substantial lower price of LNG (compared to the Diesel fuels).

The deliverable deals with the economical evaluation of the conversion to LNG fuel mode of a typical open type ferry, used for short distance routes in the Greek territory. The use of low-sulphur fuel/distillate (MGO) will function as reference case as to the feasibility of the other investigated solution. Based on the investment cost (CAPEX) and operating expenses (OPEX) of the retrofit option versus the added operational cost of the base case, the net present value (NPV) and payback period are determined. The alternative solutions will be evaluated by means of various scenarios considering various values for the LNG-Diesel fuel difference and for the interest rates, in order to analyze the feasibility of an LNG fueled ship.

3.2 Economical evaluation of the conversion of an existing passenger ship for operation with Marine Gas Oil (MGO) and Liquefied Natural Gas (LNG)

3.2.1 Case study vessel

The vessel of the case study is the Ro-Ro passenger ship ANO HORA II of Figure 3-3.

It is double side vessel with two engine rooms in the lower deck, one at the aft and one at the fore. It also consists of the main deck for the vehicles, the platform deck with one ramp on each side, the accommodation deck and the upper deck. The operational profile of the vessel is shown in Table 3-4.

Figure 3-13: The case study vessel ANO HORA II (RO-RO passenger ship)

Table 3-4. ANO HORA II operational profile

	Operational profile			
	Engines (diesel)	**Engine load (%)**	**Route duration**	**Duration/day**
Route Igoumenitsa – Kerkyra	2 CAT 3512B + Auxiliary	85% main engines + 50% auxiliary	90 min	450 min
Route Kerkyra – Igoumenitsa	2 CAT 3512B + Auxiliary	85% main engines + 50% auxiliary	90 min	450 min
Port	Auxiliary	85%		540 min

During the journey, to and from the island, the ship uses each time 2 of the 4 its engines at 85% of load, corresponding to the direction of the journey. It, also, uses one of the two auxiliary engines, but its load doesn't exceed the 50% of load. During on port the vessel uses one of its two auxiliary engines at 85% of load. [44]
The route is standard through the year and it is 90 minutes long. It has to be noted that the vessel during port time in between voyages shuts off its engines leaving on only the generators. Also, the vessel does not operate 7 days a week but has at least one day off depending on traffic. When the vessel stays off operation completely shuts off and connects via cable to the shore to cover its electricity demands. The vessel covers the

distance 5 times in an operational day. It is assumed one day off for each week and 10 additional for possible weather distractions or extra day offs. The outcome is 303 days of operation annually.

The present study evaluates the economical feasibility of retrofit conversion into one of the following two operational modes in order to meet the future IMO regulations:

- Operation of main and auxiliary engines with Low Sulphur fuel (Marine Gas Oil – MGO) – Base case
- Operation of main and auxiliary engines with Liquefied Natural Gas (LNG).

3.2.2 Base case: Shift to low sulphur fuel (MGO)

The base case is defined as reference in case of operation in ECA, the vessel will shift to low-sulphur fuel in order to comply with the prevailing emission requirements. Low-sulphur fuel referred to in this study comprises fuel with not more than 0.1% sulphur in the case of ECA operation. In addition, it comprises fuel that will satisfy the global sulphur cap of 0.5% as of 2020 (or 2025). For simplicity reasons, all of these low-sulphur fuels are referred to as 'MGO' (marine grade oil, i.e. distillates).

No major modifications are required in order to run on low-sulphur fuel. According to the characteristics of Ano Hora II the annual MGO consumption is shown in Table 3-5.

Annual Consumption	**Sea-goingconditions**			
	Igoumenitsa-Corfu		**Corfu-Igoumenitsa**	
	Auxiliary	**Main**	**Auxiliary**	**Main**

Engine power (rated)	kW		2102.5		2102.5
Engineload	%		0.85		0.85
Enginepower	kW		1787		1787
Duration (1 day)	min		450		450
Energy	kWh		13403		13403
Heatrate	kJ/kWh		8625.4		8625.4
Fuel consumption	MJ		115610		115610
Fuel mass daily	kg		2707		2707
Fuel volume daily	m^3		2.71		2.71
Duration (1 year)	days		303		303
Annual Consumption	m^3		820.37		820.37
Sum	m^3				**1640.74**

Table 3-5. Annual MGO consumption

(Energy = Engine power x duration (h), Fuel consumption = Energy x Heat rate / 1000, Fuel mass = Fuel consumption / LHV, Fuel volume = Fuel mass / Density, LHV = 42.700MJ/kg, Density = 850kg/m3)

3.2.3 Conversion into LNG propulsion

The only available space to install the LNG tanks that satisfy the safety requirements is on the vessel open deck. The main engines will consume LNG during the sea-going to and from the island. The auxiliary engines will continue to consume diesel and will not be modified. The proposed LNG fuel system consists of the following main units:

- Two LNG storage tanks, comprising of IMO type C pressure vessels with two shells of stainless steel A304L and vacuum insulation.
- Piping system for the LNG and the evaporated natural gas feeding the ship dual fuel engines.

- Evaporator unit and heating system that converts LNG to natural gas at appropriate, so that it can be used by the engines.
- Gas valve units that control and ensures the required gas pressure level.
- The connection to the converted dual fuel engines.

The LNG tank volume is 2x32m^3 and it is capable of 5.5 days autonomy plus a 10% of tank capacity. Therefore, the design of a specially constructed metallic platform next to the after castle of the ship, was proposed.

The proposed solution including the LNG tanks and platform is shown in Figure 3-6.

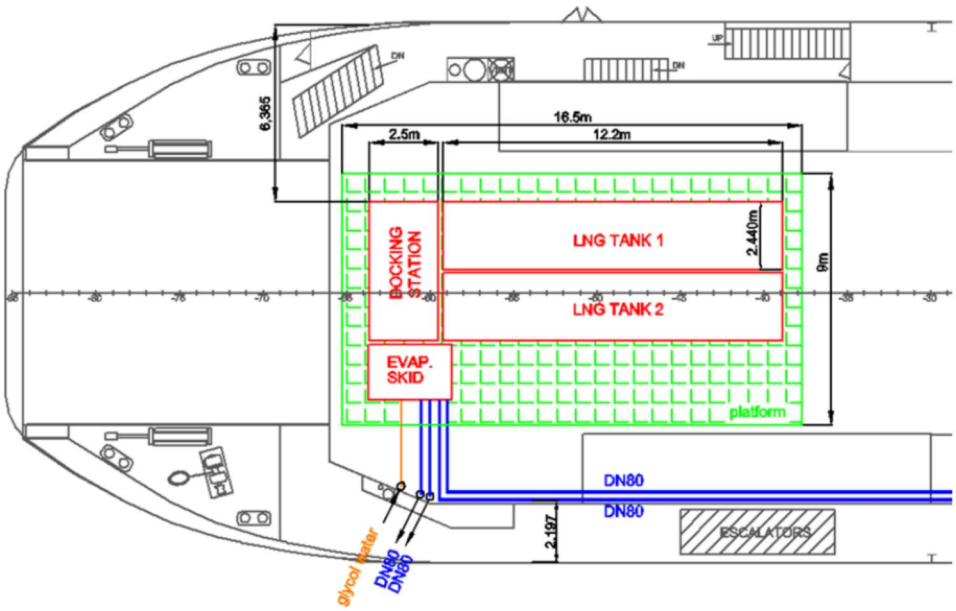

Figure 3-6. Proposed LNG tanks installation on a metallic plat-form at the vessel aft.

Figure 3-7 shows the parts which will be changed in the conversion of the engine and Figure 3-8 shows the components that will be added to the engine.

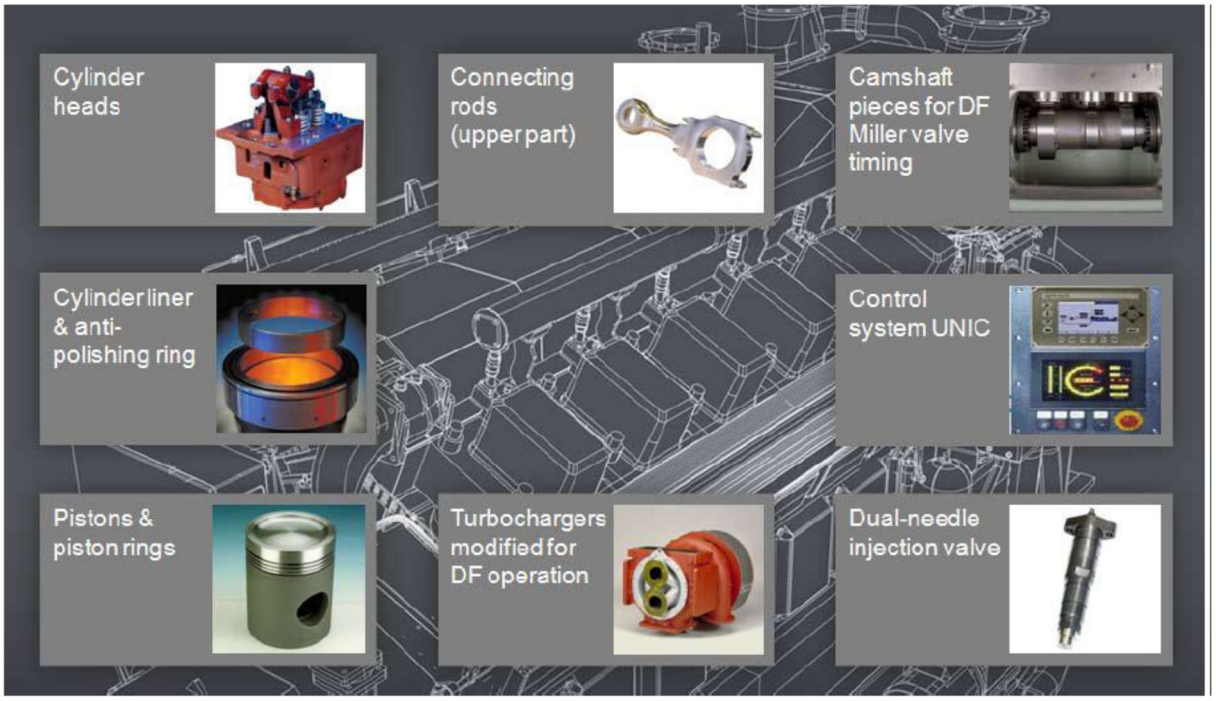

Figure 3-7. Conversion of the engine to operate with LNG – Parts which will be exchanged [3]

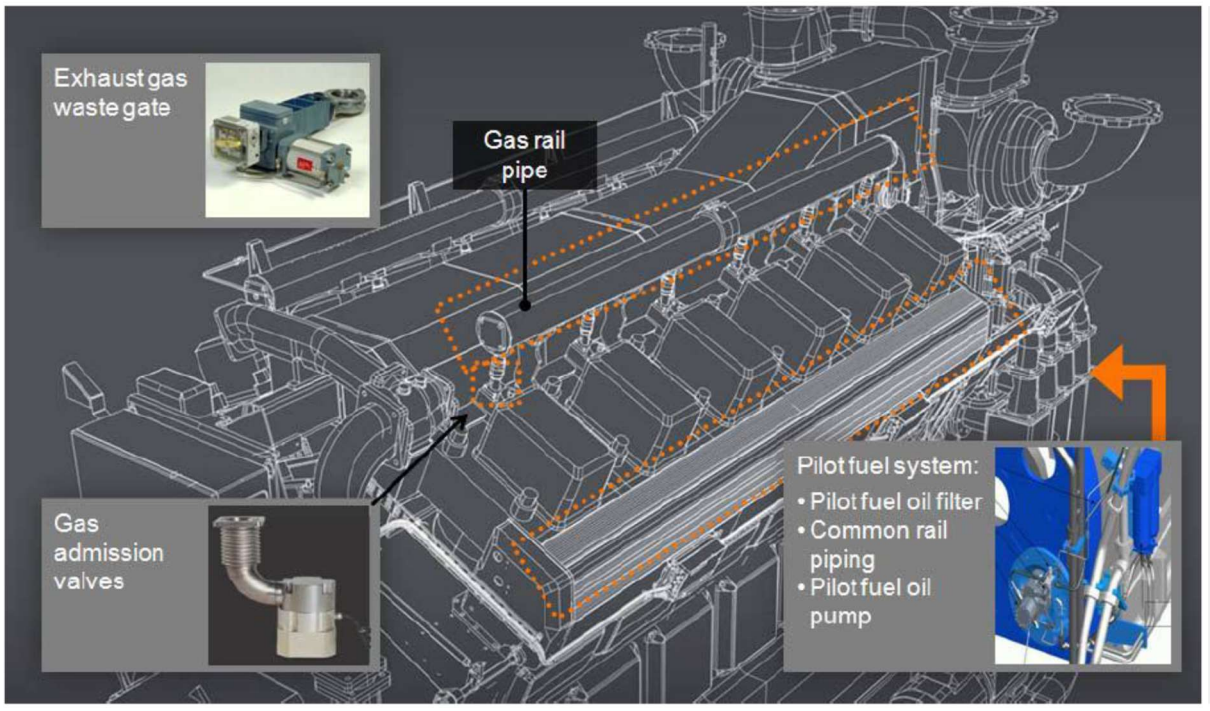

Figure 3-8. Conversion of the engine to operate with LNG - Components added on the Engine

3.2.4 LNG consumption

According to the characteristics of Ano Hora II the annual LNG consumption is shown in Table 3-9.

Table 3-9. Annual LNG consumption

Annual Consumption		Sea-goingconditions			
		Igoumenitsa-Corfu		Corfu-Igoumenitsa	
		Auxiliary	Main	Auxiliary	Main
Engine power (rated)	kW		2102.5		2102.5
Engineload	%		0.85		0.85
Enginepower	kW		1787		1787
Duration (1 day)	min		450		450
Energy	kWh		13403		13403
Heatrate	kJ/kWh		8936		8936
Fuel consumption	MJ		119766		119766
Fuel mass daily	kg		2463		2463
Fuel volume daily	m^3		2.46		2.46
Duration (1 year)	days		303		303
Annual Consumption	m^3		746.20		746.20
Sum	m^3				**1492.40**

(Energy = Engine power x duration (h), Fuel consumption = Energy x Heat rate / 1000, Fuel mass = Fuel consumption / LHV, Fuel volume = Fuel mass / Density, LHV = 48.632MJ/kg, Density = 466kg/m3)

The ship's auxiliary engines will operate on low sulphur MGO in both operational modes (MGO and LNG), but their consumption will not be calculated in the present study as no additional cost occurs.

3.2.5 Financial Analysis

In this section the retrofit alternative of LNG to the base case scenario is considered from a financial perspective. Based on the respective investment costs (CAPEX) and operating expenses (OPEX) of the retrofit option versus the added operational cost of the base case associated with the shift to MGO as required by the regulations, the net present value (NPV) and payback period are determined for opting

the LNG solution instead of the base case. If the NPV and payback are positive and less than 20 years respectively for a chosen alternative, then that solution could be financially more attractive than the base case under the selected circumstances.
It is assumed that from year to year the only profit the ship produces are those of the fuel price difference.

To calculate the NPV and payback time, a discount rate of 8% is assumed, and the savings period is 20 years (2016 – 2035). The calculations start from the next year considering that the current year is when the investment will be made and the vessel should be in dry docking for the retrofit.

3.2.6 Investment Cost of LNG alternative

The following table, Table 3-10, shows the investment cost of the LNG conversion.

Table 3-10. Investment cost (CAPEX) LNG Conversion

LNG Conversion	**Unit Cost**	**Total Cost**
LNG machinery and equipment, main engine conversion	360.39 €/kW	1,515,461 €
Steel (300t)	164.56 €/kW	691,991 €
Design & classification costs		450,000 €
Total		**2,657,452 €**

The cost is estimated by market research. Based on the resulting CAPEX and OPEX values, the NPV and payback period have been calculated for different scenarios.

3.2.7 Fuel Cost scenarios

The current prices of MGO and LNG are shown in Figure 3-11 and 3-12 respectively.

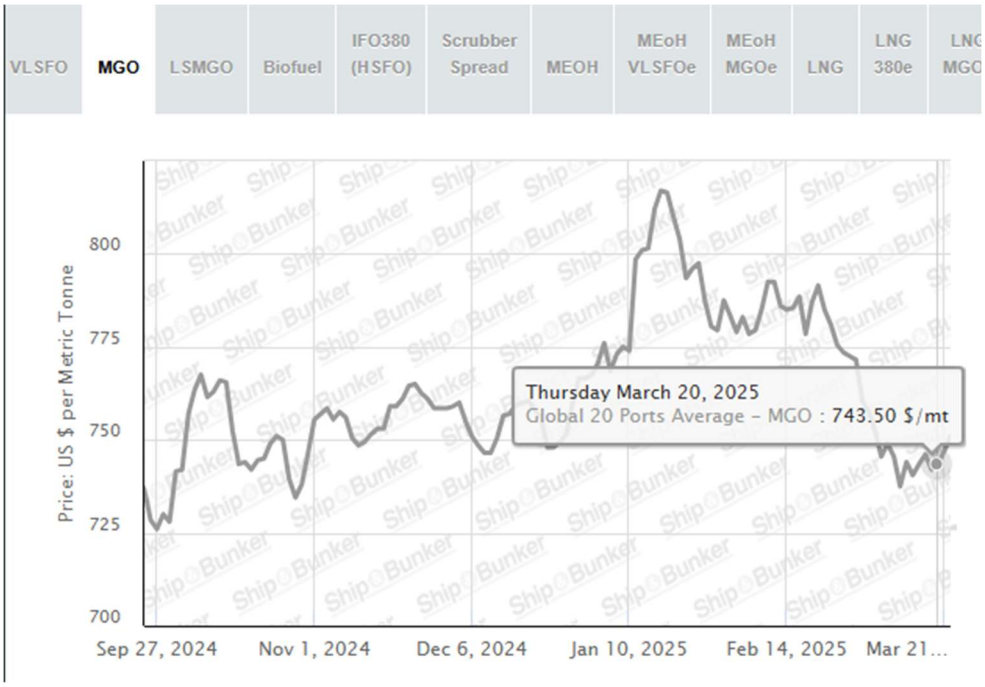

Figure 3-11. MGO prices during current year [45]

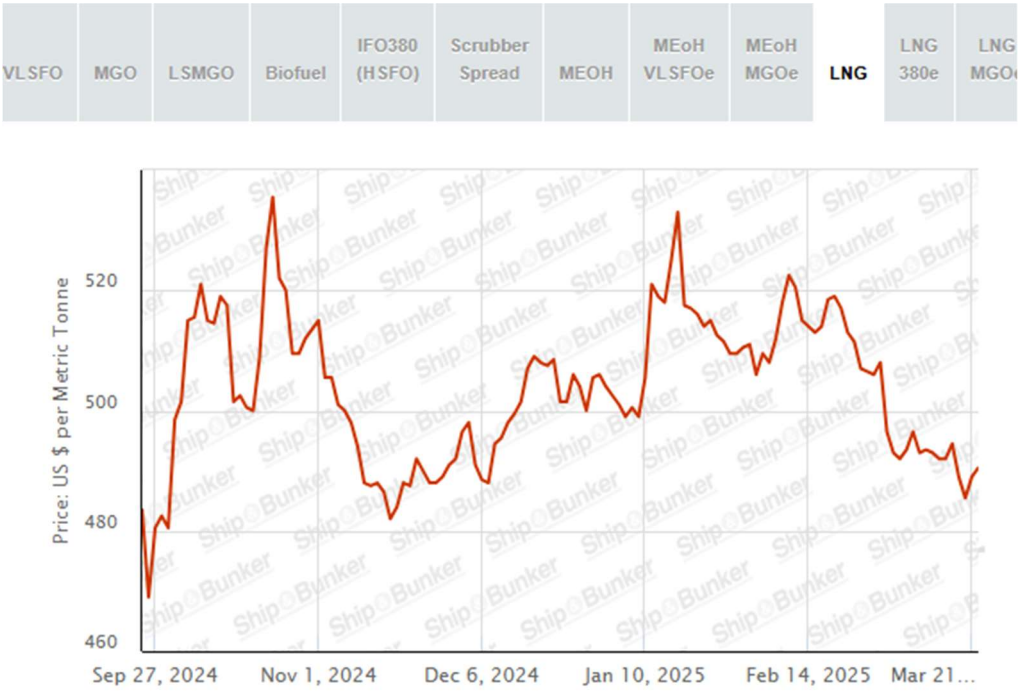

Figure 3-12. LNG prices during current year [4]

Different cost scenarios are considered for MGO and LNG.

Table 3-13. Fuel Cost Scenarios

MGO price	400 $/tn	600 $/tn	800 $/tn	1000 $/tn
	360 €/tn	540 €/tn	720 €/tn	900 €/tn
LNG price	6 $/mmBTU	9 $/mmBTU	12 $/mmBTU	15 $/mmBTU
	248.91€/tn	373.36€/tn	497.82€/tn	622.27 €/tn

(1$ = 0.9 €, 1mmbtu = 1055060 kJ, LHVLNG = 48632 kJ/kg)

In the financial analyses, it is assumed that whatever the selected price levels for the different fuels, they remain constant throughout the period 2016 - 2035. The cost of LNG will depend heavily on where it would be purchased as there is no global LNG market/pricing yet, and also whether it is fixed relative to oil or gas price, hence in view of the significant market uncertainties above values should be considered only as indicative.

The table below (Table 3-14) shows the profit produced from year to year for the current prices of MGO **= 600 $/tn** and **LNG = 9 $/mmBTU**.

Table 3-14. Cash Flow

Years	Present Value of Cash Flow (€)	Accumulative PV (€)
0	-2,657,452	-2,657,452
1	304,440	-2,353,012
2	281,889	-2,071,124
3	261,008	-1,810,116
4	241,674	-1,568,442
5	223,772	-1,344,670
6	207,196	-1,137,473
7	191,849	-945,625
8	177,638	-767,987
9	164,479	-603,508
10	152,296	-451,212
11	141,014	-310,198
12	130,569	-179,629
13	120,897	-58,732
14	111,942	53,210
15	103,650	156,860
16	95,972	252,832

17	88,863	341,695
18	82,281	423,976
19	76,186	500,161
20	70,542	570,704
NPV	**570,704**	
IRR	**10.77%**	
Payback time	**13.5 years**	

Table 3-15 shows the results for each fuel cost scenario. (In cases that the IRR is not calculated, this happens because the annual accumulative present value grows negatively from year to year).

Table 3-15: NPV, IRR and PB for all the fuel cost scenarios

MGO (€/tn)	**LNG(€/tn)**	**NPV(€)**	**IRR (%)**	**PB (years)**
1st scenario				
360	248.91	-505,348	5.33%	>20
	373.36	-2,328,924	-10.61%	>20
	497.82	-4,152,500	-	-
	622.27	-5,976,076	-	-
2nd scenario				
540	248.91	2,394,279	18.74%	7
	373.36	570,704	10.77%	13.5
	497.82	-1,252,872	0.71%	>20
	622.27	-3,076,448	-	-
3rd scenario				
720	248.91	5,293,907	30.32%	4
	373.36	3,470,331	23.12%	5.4
	497.82	1,646,755	15.59%	8.7
	622.27	-176,820	7.09%	>20
4thscenario				
900	248.91	8,193,535	41.55%	2.8
	373.36	6,369,959	34.51%	3.4
	497.82	4,546,383	27.39%	4.4
	622.27	2,722,807	20.09%	6.4

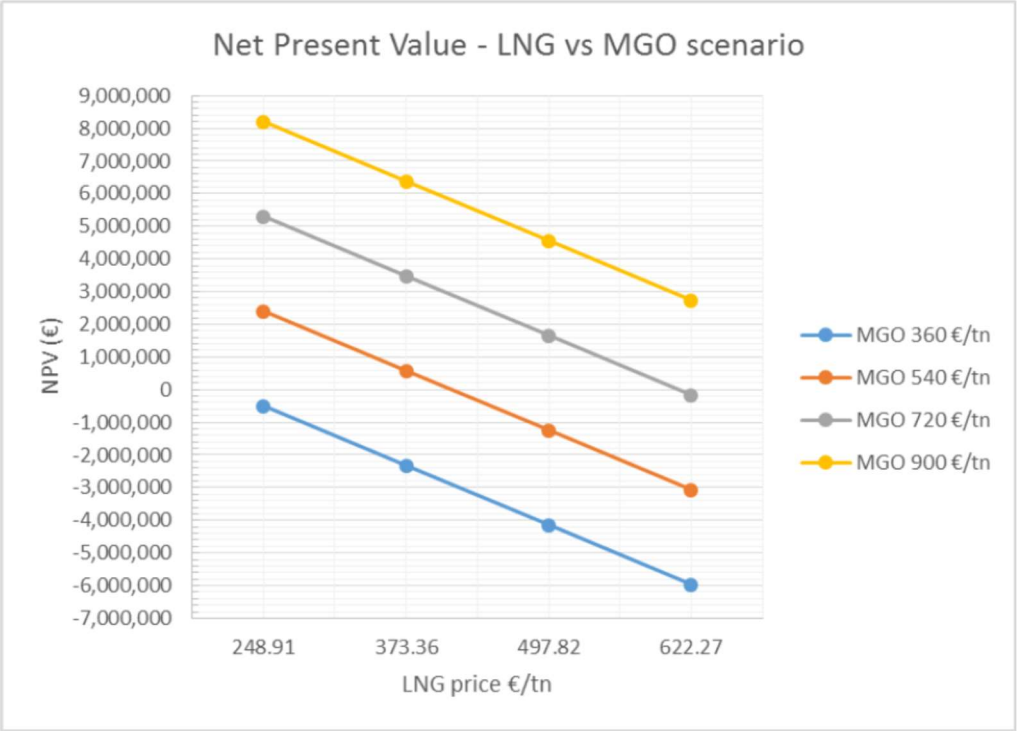

Figure 3-16. NPV for LNG alternative

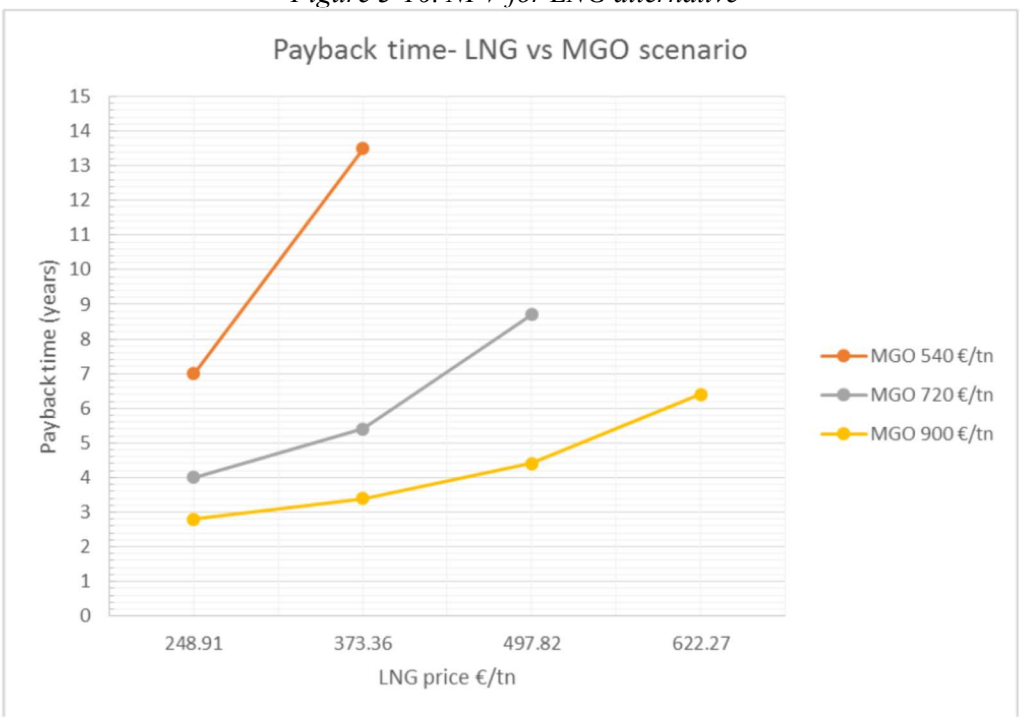

Figure 3-17. Payback period for LNG alternative (in cases that the payback time is more than 20 years it is not shown in the Figure)

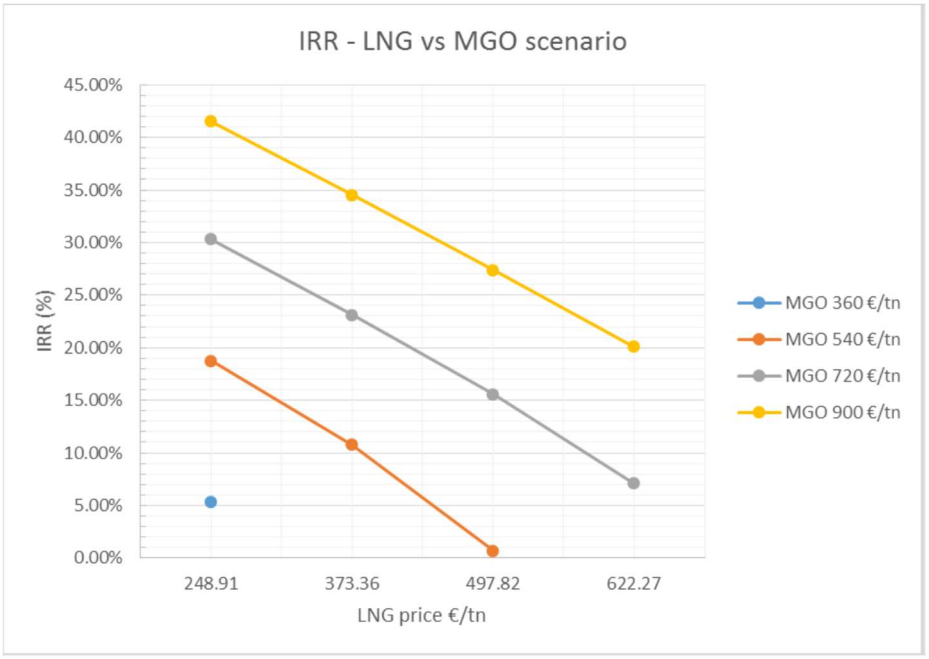

Figure 3-18. IRR (%) for LNG alternative (in case that the IRR is negative it is not shown in the Figure)

Concerning the option of converting to LNG as a fuel, there are a number of factors that will influence the decision to select this option. From a technical and operational perspective, the installation is feasible, as it is analyzed in previous deliverables.

From a financial perspective, the main driver for selecting the LNG alternative will be the cost of LNG and its correlation with the cost of MGO. The payback time is highly sensitive to the LNG price as it is illustrated in Figure 5.4. Under the assumed condition that the price of MGO is constant at 540 €/tn throughout the 20 years, it is observed that the alternative of LNG is acceptable only at low LNG prices (as the current prices). In case of significantly low MGO cost, the LNG alternative is rejected the NPV is negative (at -505,348€) as it is shown in Figure 3-16 and the payback time is more than 20 years. For high MGO price levels the alternative of LNG fuel is profitable with payback time below the 10 years and positive net present values. Figure 3-18 confirms the above observations as the LNG alternative is moneymaking only for IRR higher than 8%.

3.3 Sensitivity Analysis

A **discount rate of 10%** is assumed in order to test the feasibility of an LNG fueled ship. NPV and payback period are calculated for the same fuel cost scenarios as before (Table 3.19).

Table 3-19. NPV, IRR and PB for discount rate 10%.

MGO (€/tn)	LNG(€/tn)	NPV(€)	PB (years)
1st scenario			
360	248.91	-791,308	>20
	373.36	-2,372,577	>20
	497.82	-3,953,846	-
	622.27	-5,535,115	-
2nd scenario			
540	248.91	1,723,032	7.7
	373.36	141,763	17
	497.82	-1,439,505	>20
	622.27	-3,020,774	-
3rd scenario			
720	248.91	4,237,372	4.2
	373.36	2,656,104	5.8
	497.82	1,074,835	9.7
	622.27	-506,434	>20
4th scenario			
900	248.91	6,751,713	2.8
	373.36	5,170,444	3.5
	497.82	3,589,175	4.7
	622.27	2,007,907	7

As it is shown from the above table (Table 3-19) the acceptable fuel cost scenarios (MGO price – LNG price) are the same as with discount rate of 8%. Only in cases of significantly low MGO prices the LNG alternative is not profitable any more.

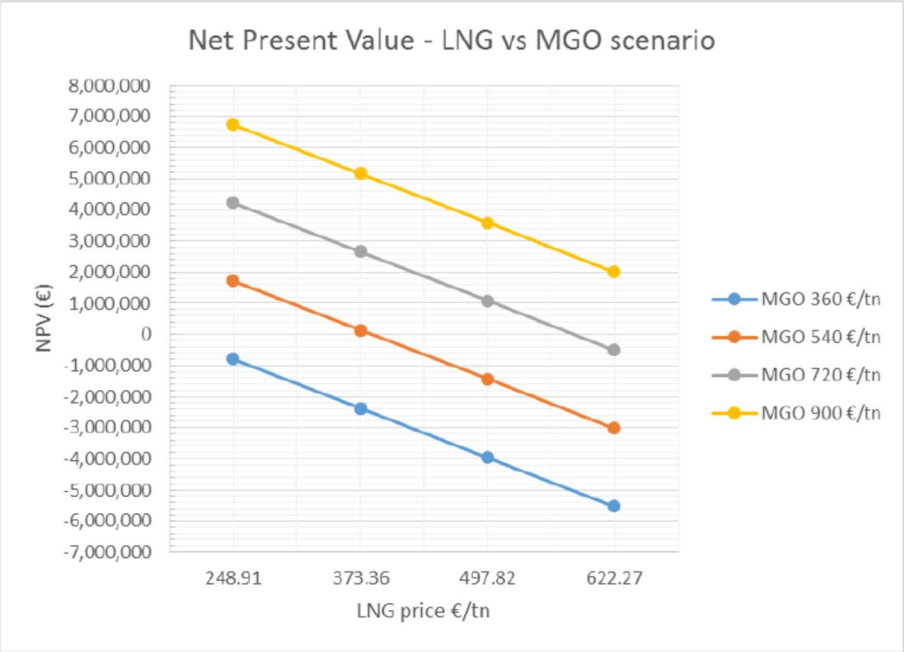

Figure 3-20. NPV for discount rate 10%

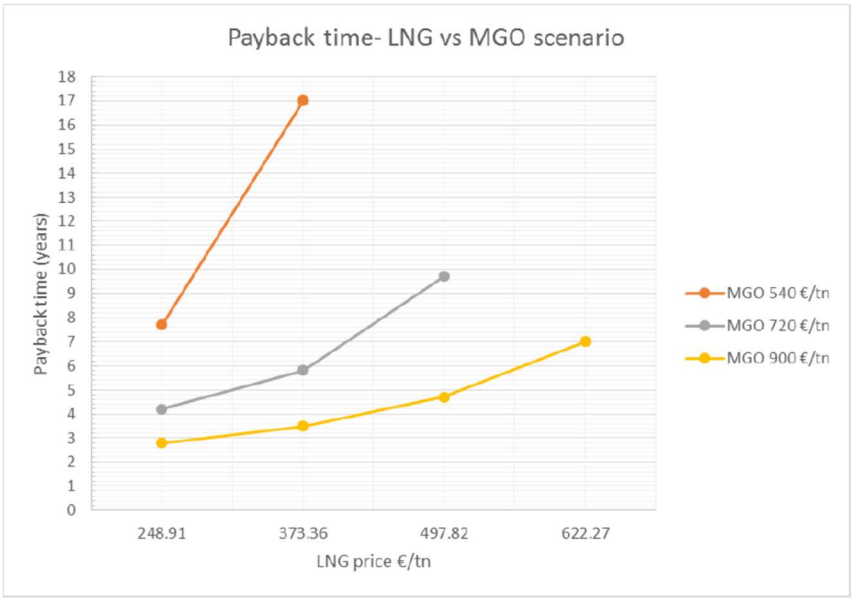

Figure 3-21. Payback period for discount rate 10% (in cases that the payback time is more than 20 years it is not shown in the Figure)

Only the fuel cost scenarios that NPV is positive, the payback period is less than 20 years and the IRR is higher than 8% or 10%, respectively, are acceptable and profitable. As it is shown from Table 3-19, for usual MGO prices, 540€/tn and 720€/tn, the LNG conversion is profitable for a range of prices between 248.91 and 497.82€/tn.

Figure 3-22 and Figure 3-23 show the comparison of the above results for discount rate 8% and 10%.

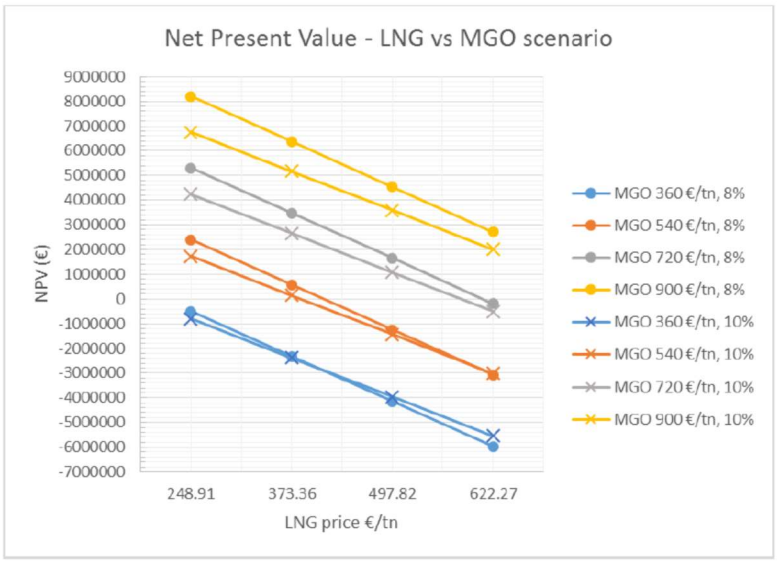

Figure 3-22. NPV for 8% and 10% discount rate

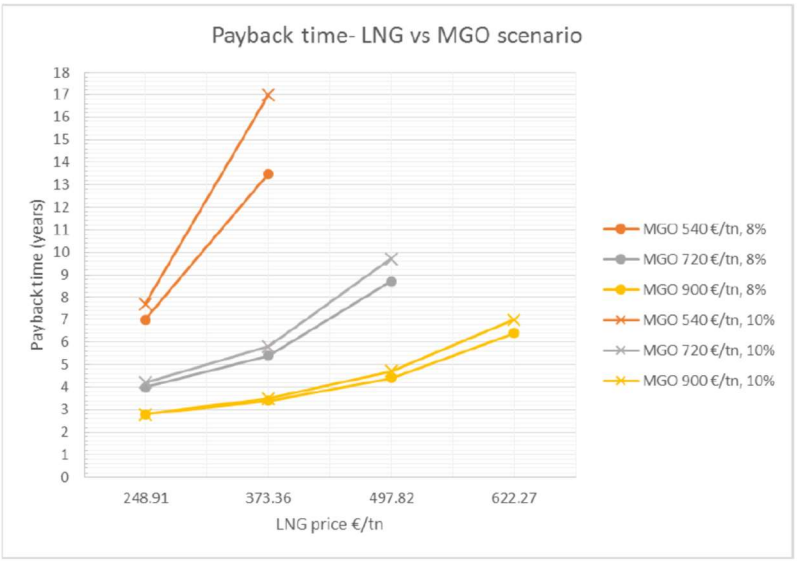

Figure 3-23. Payback period for 8% and 10% discount rate (in cases that the payback time is more than 20 years it is not shown in the Figure)

The differences observed from Figures 3-22 and 3-23 are the lower values of the NPVs and the need of a few more years of payback period, for discount rate 10%.

The LNG solution is about 2.7 million euro expensive in comparison with the MGO solution that doesn't need any change on the ship. However, it is a solution that under feasible circumstances could achieve profit of 10-15%.

3.4 Acknowledgements

Many thanks to Dr. Nikolaos Themelis, Head of the Research and Development Department of the Hellenic Register of Shipping for sending extremely useful research results on the economic evaluation of the conversion of the main and auxiliary diesel engines of a ferry to run on natural gas.

4 References

[1] K. D. Rakopoulos, Principles of Reciprocating Internal Combustion Engines (Introduction – Operation – Thermodynamics). Fountas Publications.

[2] J. B. Heywood, Internal Combustion Engine Fundamentals. New York, NY, USA: McGraw-Hill, 1988.

[3] Th. K. Zannis, "Thermodynamic analysis and experimental investigation of the effect of liquid fuels on diesel engines," Ph.D. dissertation, School of Mechanical Engineering, Nat. Tech. Univ. of Athens, Athens, Greece, 2006.

[4] A. C. Lloyd and T. A. Cackette, "Diesel engines: Environmental impact and control," J. Air Waste Manage. Assoc., vol. 51, pp. 809–847, 2001.

[5] U.-D. Grebe and R. Imarisio, "Gasoline or diesel engine: The race is on!," in Proc. FISITA World Automotive Congr., Barcelona, Spain, 2004, paper F2004V097.

[6] A. Schaeffer, "Diesel technology and the American economy," presented at the National Press Club, Washington, DC, USA, Nov. 30, 2000. Diesel Technology Forum, Herndon, VA, USA, 2000. [Online]. Available: http://www.dieselforum.org/enews/allen_remarks.html

[7] S. I. Raptotasios, "Study of the combined use of exhaust gas recirculation and intake air oxygen enrichment in a direct injection Diesel engine," Diploma thesis, School of Mechanical Engineering, Nat. Tech. Univ. of Athens, Athens, Greece, 2009.

[8] K. D. Rakopoulos and D. Th. Chountalas, Combustion – Pollution of Reciprocating I.C. Engines, Lecture notes, Nat. Tech. Univ. of Athens, Athens, Greece.

[9] Th. K. Zannis, Lecture Notes for the Course "Marine Diesel Engines", 4th Year Mechanical Engineering Track, Hellenic Naval Academy, Greece.

[10] R. Papagiannakis, "Study of the behavior of diesel engines using liquid and gaseous fuels," Diploma thesis, School of Mechanical Engineering, Nat. Tech. Univ. of Athens, Athens, Greece, 2002.

[11] J. E. Dec, "A conceptual model of DI diesel combustion based on laser-sheet imaging," SAE Trans., J. Engines, vol. 106, pp. 1319–1348, 1997, SAE Paper 970873.

[12] DieselNet, "Online information resource on clean diesel engines and diesel emissions," [Online]. Available: http://www.dieselnet.com

[13] Chevron Products Company, Diesel Fuels, Technical Review. [Online]. Available: http://www.chevron.com/products/prodserv/fuels/bulletin/diesel/

[14] Fuels with Particular Reference to the Diesel Engine, in Air Pollution Control in Transport Engine. London, U.K.: Inst. Mech. Eng., 1971, pp. 185–197.

[15] F. Tao, "Numerical modelling of soot and NOx formation in non-stationary diesel flames with complex chemistry," Ph.D. dissertation, Dept. Thermal and Fluid Dynamics, Chalmers Univ. of Technol., Göteborg, Sweden.

[16] R. A. Dobbin and H. Subramaniasivam, "Soot precursor particles in flames," in Soot Formation in Combustion, H. Bockhorn, Ed. Berlin, Germany: Springer-Verlag, 1994.

[17] I. Glassman, Combustion, 3rd ed. San Diego, CA, USA: Academic Press, 1996.

[18] A. Matsson, "Diesel particulate matter emissions: Background, characterization and reduction problems," Licentiate thesis, Dept. Thermo and Fluid Dynamics, Chalmers Univ. of Technol., Göteborg, Sweden, 2000.

[19] U.S. Environmental Protection Agency, "Nonroad diesel emission standards," Staff Technical Paper EPA420-R-01-052, USA, Oct. 2001.

[20] V. Schwarz, "Fuel injection systems for future medium duty and heavy duty low emission diesel engines," in Proc. FISITA World Automotive Congr., Barcelona, Spain, 2004, paper F2004F435.

[21] W. Knecht, "Development trends of heavy-duty diesel engines," Invited lecture, Nat. Tech. Univ. of Athens, Athens, Greece, May 2005.

[22] H. Hiereth and P. Prenninger, Charging the Internal Combustion Engine. Berlin, Germany: Springer-Verlag, 2003.

[23] A. Kokios, "Use of liquefied natural gas as fuel in ocean-going shipping," Diploma thesis, Merchant Marine Academy of Macedonia, Greece, 2003.

[24] Chiyoda Corp., "LNG liquefaction," [Online]. Available: https://www.chiyoda-corp.com/technology/en/lng/liquefaction.html

[25] G. Argyris, "Transportation of liquefied natural gas," Diploma thesis, Merchant Marine Academy, Greece, 2004.

[26] I. Varsamis, "Use of natural gas as ship fuel – bunkering LNG," Diploma thesis, Merchant Marine Academy, Greece, 2014.

[27] V. Pentidis and D. Dinokas, "Two-stroke and four-stroke dual-fuel natural gas–diesel engines," Diploma thesis, Merchant Marine Academy, Greece, 2013.

[28] Caterpillar Inc., “Dual fuel engines,” brochure, 2016. [Online]. Available: https://www.cat.com

[29] MAN B&W, “Dual fuel engines,” brochure, 2016. [Online]. Available: https://marine.man.eu

[30] Wärtsilä Corp., “Dual fuel engines,” brochure, 2015. [Online]. Available: https://www.wartsila.com

[31] B. S. Ahn, Sail on LNG: Reduce Emission at the Source, presented June 13, 2011.

[32] E. E. Attah and R. Bucknall, “An analysis of the energy efficiency of LNG ships powering options using the EEDI,” Ocean Eng., vol. 110, pp. 62–74, 2015.

[33] Wärtsilä Corp., “Wärtsilä to power Mediterranean’s first LNG fuelled passenger ferry,” Press release, Oct. 14, 2016.

[34] Gastrade S.A., “Gastrade official website,” [Online]. Available: http://www.gastrade.gr

[35] Ch. Sarriggiannidis, “Innovative method of marine transportation of natural gas in compressed form (Autonomous compressed natural gas carrier),” in Proc. Annual Meeting on Naval Technology, Hellenic Inst. Marine Technol. (HIMT), Greece, 2016.

[36] McGill et al., “Alternative Fuels for Marine Applications”, IEA Advanced Motor Fuels Implementing Agreement Report, May 2013.

[37] Murakami S. and Baufeld T., “Current Status and Future Strategies of Gas Engine Development”, CIMAC Paper No. 413, CIMAC Congress 2013, Shanghai, China.

[38] Schlick H., “Potentials and challenges of gas and dual – fuel engines for marine application”, 5th CIMAC CASCADES, Busan, 23.10.2014.

[39] Jiehui Li, Bingbing Wu and Gongping Mao, “Research on the performance and emission characteristics of the LNG - diesel marine engine”, Journal of Natural Gas Science and Engineering, Vol. 27, pp. 945 – 954, 2015.

[40] Abdelghaffar W.A., “Performance and emissions of a diesel engine converted to dual diesel-CNG fuelling”, Eur. J. Sci. Res., Vol. 56, pp. 279 - 293, 2011.

[41] Papagiannakis, R.G. and Hountalas, D.T., “Combustion and exhaust emission characteristics of a dual fuel compression ignition engine operated with pilot diesel fuel and natural gas”, Energy Conversion and Management, Vol. 45, pp. 2971 – 2987, 2004.

[42] Christian Klimt-Møllenbach Christian Schack, Thomas Eefsen, Jean De Kat Green Ship of the Future. Vessel emission study: Comparison of various abatement technologies to meet emission levels for ECA [Article] // Technical report. - 2012.

[43] Johan Algell Alexandra Bakosch, Björn Forsman Feasibility Study on LNG Fuelled Short Sea and Coastal Shipping in the Wider Caribbean Region [Article] // International Maritime Organization. - 2012.

[44] SAM AHN BYUNG Sail on LNG. Reduce Emission at the Source [Article] // Wärtsilä. - 2011.

[45] www.bunkerworld.com [Online].

5 Terminology - symbolisms

Symbol / Abbrev.	Description	Units
CN	Cetane number	[-]
cp	Specific heat capacity at constant pressure	[J/kgK]
cv	Specific heat capacity at constant volume	[J/kgK]
k	Boltzmann constant (1.3805×10^{-23})	[J/K]
n	Rotational speed	[rpm]
P	Pressure	[N/m²]
Rmol	Universal gas constant	[J/kmolK]
u	Specific internal energy	[J/kg]
U	Internal energy	[J]
V	Volume	[m³]
$\dot{Q}$	Heat transfer rate	[W]
$\bar{u}$	Mean velocity	[m/s]
a	Refers to air	–
inj	Injection	–
l, L	Liquid	–
st	Stoichiometric	–
μ	Dynamic viscosity	[kg/ms]
ρ	Density	[kg/m³]
λ	Thermal conductivity	[W/mK]
MB	Molecular weight	[kg/kmol]
ν	Kinematic viscosity	[m²/s]
σ	Stefan–Boltzmann constant (5.67×10^{-8})	[W/m²K⁴]
Φeq	Fuel–air equivalence ratio	[-]
BSFC	Brake specific fuel consumption	–

Symbol / Abbrev.	Description	Units
CO	Carbon monoxide	–
EGR	Exhaust gas recirculation	–
EPA	Environmental Protection Agency	–
FTP	Federal test procedure	–
GTL	Gas-to-liquid	–
HC	Unburned hydrocarbons	–
LNC	Lean NOx catalyst	–
LPG	Liquefied petroleum gas	–
NOx	Nitrogen oxides	–
PAH	Polycyclic aromatic hydrocarbons	–
PM	Particulate matter	–
ppm	Parts per million (by volume)	–
SCR	Selective catalytic reduction	–
SMD	Sauter mean diameter	–
SOF	Soluble organic fraction	–
VVA	Variable valve actuation	–
NO	Nitric oxide	–
SOx	Sulfur oxides	–
Re	Reynolds number	–
Pr	Prandtl number	–